Modal Analysis and Synthesis of Broadband Nearfield Beamforming Arrays

P. Thushara D. Abhayapala

B.E. (Hons.) ANU

December 1999

A thesis submitted for the degree of Doctor of Philosophy
of The Australian National University

Telecommunications Engineering Group
Research School of Information Sciences and Engineering
The Australian National University

Declaration

The contents of this thesis are the results of original research and have not been submitted for a higher degree to any other university or institution.

Much of the work in this thesis has been published or has been submitted for publication as journal papers. These papers are:

- R.A. Kennedy, T.D. Abhayapala, and D.B. Ward, "Broadband nearfield beamforming using a radial beampattern transformation," *IEEE Trans. Sig. Proc.*, vol. 46, pp. 2147–2156, Aug. 1998.
- R.A. Kennedy, D.B. Ward, and T.D. Abhayapala, "Nearfield beamforming using radial reciprocity," *IEEE Trans. Sig. Proc.*, vol. 47, pp. 33–40, Jan. 1999.
- T.D. Abhayapala, R.A. Kennedy, and R.C. Williamson, "Nearfield broadband array design using a radially invariant modal expansion," *J. Acoust. Soc. Amer.*, vol. 107, issue 1, pp 392–403, Jan 2000.
- T.D. Abhayapala, R.A. Kennedy, and R.C. Williamson, "Spatial aliasing for nearfield sensor arrays," *Electron. Lett.*, vol. 35, no. 10, pp 764–765, May 1999.
- T.D. Abhayapala, R.A. Kennedy, and R.C. Williamson, "Noise modeling for nearfield array optimization," *IEEE Sig. Proc. Let.*, vol. 6. no. 8, pp 210–212, Aug. 1999.
- T.D. Abhayapala, R.A. Kennedy, and R.C. Williamson, "Nearfield broadband adaptive beamforming for microphone Arrays," *IEEE Trans. Speech and Audio Proc.*, (to be submitted).
- T.D. Abhayapala, R.A. Kennedy, and R.C. Williamson, "Modal space processing for coherent wideband source localization," *IEEE Trans. Sig. Proc.*, (to be submitted).

Papers published in Conference Proceedings, but in some cases containing material overlapping with the above are:

- R.A. Kennedy, T.D. Abhayapala, D.B. Ward, and R.C. Williamson, "Nearfield broadband frequency invariant beamforming," in *Proc. IEEE Int. Conf. Acoust. Speech Sig. Process.*, 1996, vol. 2, pp. 905–908.

- R.A. Kennedy, D.B. Ward, and T.D. Abhayapala, "Nearfield beamforming using nearfield/farfield reciprocity," in *Proc. IEEE Int. Conf. Acoust. Speech Sig. Process.*, vol. 5, pp. 3741–3744, 1997.

- T.D. Abhayapala, R.A. Kennedy, and R.C. Williamson, "Broadband beamforming using elementary shape invariant beampatterns," in *Proc. IEEE Int. Conf. Acoust. Speech Sig. Process.*, vol. 5, pp. 2041–2044, 1998.

- T.D. Abhayapala, R.A. Kennedy, and R.C. Williamson, "Farfield array weight redesign for nearfield beamforming," in *6th IEEE Int. Workshop on Intelligent Signal Processing and Communication Systems*, pp. 537–540, 1998.

- T.D. Abhayapala, R.A. Kennedy, and R.C. Williamson, "Isotropic noise modeling for nearfield array processing," in *Proc. IEEE Workshop on Applications of Signal Processing to Audio and Acoustics (WASSPA99)*, pp. 11–14, October 17-20, 1999.

The research represented in this thesis has been performed jointly with Dr Rodney A. Kennedy, Dr Robert C. Williamson, and Dr Darren B. Ward. The majority, approximately 75%, of this work was my own.

P. Thushara D. Abhayapala
Telecommunications Engineering Group
Research School of Information Sciences and Engineering
The Australian National University
Canberra ACT 0200
Australia

Acknowledgements

The work presented in this thesis would not have been possible without the support of a number of individuals and organizations, and they are gratefully acknowledged below:

- My supervisors Dr Rod Kennedy and Dr Bob Williamson who guided me in producing this research work, gave encouragement, showed enthusiasm, and provided friendship.
- Dr Darren Ward for his collaboration on some of this work.
- My fellow students in the Telecommunication Engineering Group, for their friendship. Ms Maria Davern, administrator of the Telecommunication Engineering Group, for all her assistance.
- The Australian government for the OPRS scholarship and the Australian National University for the PhD scholarship.
- My parents for everything they have provided for me in terms of education, guidance, encouragement, moral and financial support.
- My wife Lalangi and my son Sadeepa, for their unwaivering support, for understanding when I had to spend so much time working and so little time with them.

Abstract

This thesis considers the design of a beamformer which can enhance desired signals in an environment consisting of broadband nearfield and/or farfield sources. The thesis contains: a formulation of a set of analysis tools which can provide insight into the intrinsic structure of array processing problems; a methodology for nearfield beamforming; theory and design of a general broadband beamformer; and a consideration of a coherent nearfield broadband adaptive beamforming problem. To a lesser extent, the source localization problem and background noise modeling are also treated.

A set of analysis tools called *modal analysis techniques* which can be used to a solve wider class of array signal processing problems, is first formulated. The solution to the classical wave equation is studied in detail and exploited in order to develop these techniques.

Three novel methods of designing a beamformer having a desired nearfield broadband beampattern are presented. The first method uses the modal analysis techniques to transform the desired nearfield beampattern to an equivalent farfield beampattern. A farfield beamformer is then designed for a transformed farfield beampattern which, if achieved, gives the desired nearfield pattern exactly. The second method establishes an asymptotic equivalence, up to complex conjugation, of two problems: (i) determining the nearfield performance of a farfield beampattern specification, and (ii) determining the equivalent farfield beampattern corresponding to a nearfield beampattern specification. Using this reciprocity relationship a computationally simple nearfield beamforming procedure is developed. The third method uses the modal analysis techniques to find a linear transformation between the array weights required to have the desired beampattern for farfield and nearfield, respectively.

An efficient parameterization for the general broadband beamforming problem is introduced with a single parameter to focus the beamformer to a desired operating radius and another set of parameters to control the actual broadband beampattern shape. This parameterization is derived using the modal analysis techniques and the concept of the theoretical continuous aperture.

A design of an adaptive beamformer to operate in a signal environment consisting of broadband nearfield sources, where some of interfering signals may be correlated with desired signal is also considered. Application of modal analysis techniques to noise modeling and broadband coherent source localization conclude the thesis.

Glossary of Definitions

$\mathbb{C}$	complex numbers
$\mathbb{Z}$	integers
$\mathbb{Z}^+$	positive integers
a^*	complex conjugate of scalar a
$\boldsymbol{a}^T$	transpose of matrix or vector $\boldsymbol{a}$
$\boldsymbol{a}^H$	conjugate transpose of matrix or vector $\boldsymbol{a}$
$*$	Convolution
$\boldsymbol{A}^\dagger$	matrix pseudo-inverse: $\boldsymbol{A}^\dagger \triangleq [\boldsymbol{A}^H \boldsymbol{A}]^{-1} \boldsymbol{A}^H$
$\otimes$	Kronecker product: $\boldsymbol{a} \otimes \boldsymbol{b} \triangleq [a_1 \boldsymbol{b}, \ldots, a_N \boldsymbol{b}]$, where N is length of $\boldsymbol{a}$
$\lvert a \rvert$	Absolute value of real number a
$\lVert \boldsymbol{a} \rVert$	2-norm of vector $\boldsymbol{a}$
$E\{\cdot\}$	Expectation
diag$(\cdot)$	Form a diagonal matrix with the elements shown in brackets as diagonal elements
sgn$(\cdot)$	signum function: sgn$(a) \triangleq 0$ for $a = 0$, sgn$(a) \triangleq a/\lvert a \rvert$ for $a \neq 0$.
FIR	Finite Impulse Response
DOA	Direction Of Arrival
FFT	Fast Fourier Transform
DFT	Discrete Fourier Transform
SNR	Signal to Noise Ratio

Contents

List of Figures

List of Tables

Chapter 1

Introduction

1.1 Motivation and Scope

Signal reception using an *array* of sensor elements has long been an attractive solution to problems of signal enhancement, detection and estimation [1]. Use of an array of sensor elements to extract useful information from signals carried by propagating waves, is termed as *array signal processing* [2].

The array itself takes on a variety of different geometries depending on the application of interest. The most commonly used configuration is the *linear uniform array*, in which the sensors are uniformly spaced along a straight line. Other common configurations are *circular arrays*, where the sensors are arranged in a circle and *planar arrays*, in which the sensors form a rectangular grid or lie on concentric circles. Other possibilities are nonuniformly spaced and randomly spaced arrays.

Beamforming is the name given to a wide variety of array processing techniques that by some means, focus the array's signal capturing (spatial filtering) capabilities in a particular direction or location [3]. This means that signals from a given spatial region are amplified and signals from other regions are attenuated with the usual objective of estimating a desired signal in the presence of noise and interfering signals. A processor that performs beamforming operations is called a *beamformer*. Thus, a beamformer is used in conjunction with an array of sensors to provide spatial filtering and usually consists of filters or complex weights to combine the sensor signals. Typically a beamformer linearly combines the spatially sampled signal from each sensor to obtain an output signal in the same manner as a FIR filter linearly combines temporally sampled data [4].

A beamformer can be characterized by its *spatial response* in the same way a

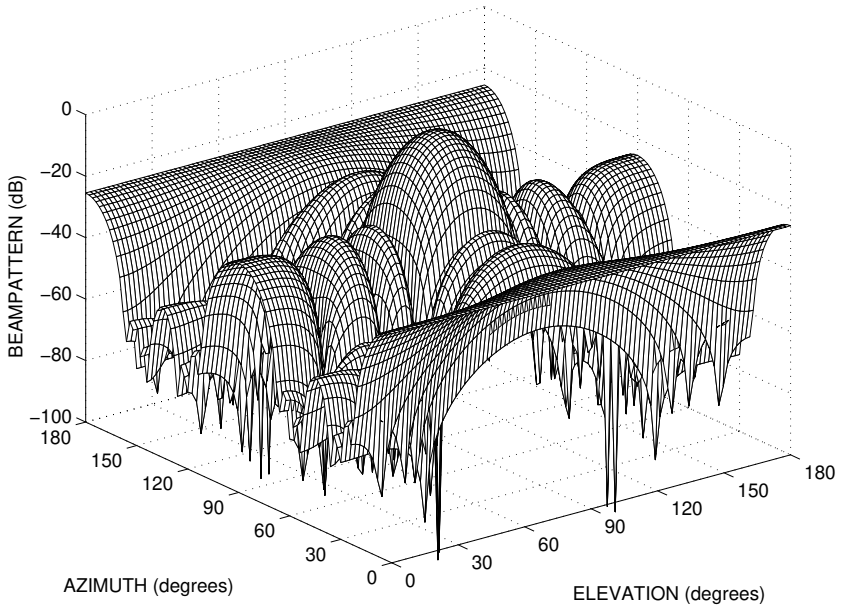

Figure 1.1: An example beampattern

linear time-invariant system is characterized by its frequency response. Mathematically, the spatial response is a function of space variables and the graph of spatial response versus space variables is called the *beampattern* of the beamformer. In the literature, the terms spatial response and beampattern have been used interchangingly. We also use both terms to describe the output response of a beamformer in terms of space variables. Sometimes, the spatial response is expressed only as angular variables, then it is called the *angular response*. An example of a beampattern as a function of azimuth and elevation angles is given in Figure 1.1.

Common applications of beamforming include sonar [5], radar [6], tomography [7], exploration seismology [8], communication systems [9] and speech acquisition systems [10].

In sonar, an array of hydrophones is used to passively detect signals such as ship noise. A transmitting array is used in radar to illuminate an area surrounding the radar site and a receiving array looks for reflections from targets. In tomography, arrays are used to form cross-sectional images of objects from either transmission or reflection data. An array of geophones is used in exploration seismology to receive signals reflected from a region inside the earth with the objective of detecting minerals. Arrays have long been used in High Frequency (HF) communications for signal estimation and detection [11] and more recently their application in personal communications in multiuser environment has also been identified [9]. In speech acquisition systems, electronically steerable microphone arrays are used to cap-

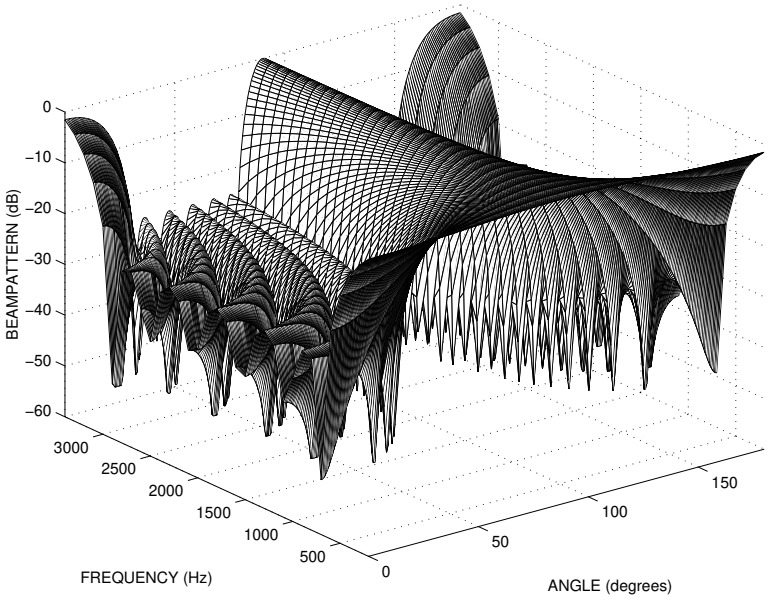

Figure 1.2: Response of a narrowband beamformer over a broad frequency band.

ture high-quality signals from a desired speaker while simultaneously attenuating interfering talkers and ambient noise.

In many applications, the signal of interest covers a wide bandwidth. For example, speech signals typically cover several octaves where the bandwidth of intelligible speech is approximately $200 - 3400$Hz which is roughly 4 octaves[1]. Thus, it is desirable to design beamformers with controllable broadband frequency characteristics. Most of the early array processing literature only considered narrowband or single frequency operation, where the beamformer is designed to have desired spatial response for a particular frequency. In situations where the fractional bandwidth is very wide (a significant fraction of the central frequency of the band), the assumption of a single frequency produces poor results. For example, Figure 1.2 shows the angular response of a narrowband beamformer designed for operation at 1800Hz operated over a bandwidth of $200 - 3400$Hz. At frequencies below 1800Hz the main beam spreads out and spatial resolution is lost. Whereas for frequencies above 1800Hz the main beam becomes narrower until grating lobes begins to appear in the beampattern. Clearly, the spatial resolution varies significantly with frequency; this is unacceptable for broadband applications. Hence, the design of broadband beamformers has been considered as a challenging problem.

The majority of array processing literature deals with the case in which the

[1]One octave is a doubling of frequency, i.e., the frequency range $200 - 400$Hz is one octave and $200 - 800$Hz is two octaves.

source is assumed to be in the *farfield* of the array. That is, the source is assumed to be at an infinite distance from the array and hence the received waveform from a single point source is planar. This significantly simplifies the solution to the beamforming problem. However, in many practical situations, such as use of microphone array to capture speech in an automobile environment, the source is well within the *nearfield* (few wavelengths) of the array, and using the farfield assumption to design the beamformer results in severe degradation in the beampattern. Furthermore, when broadband operation of the beamformer is required, the problem becomes more acute: at low frequencies the source may appear in the nearfield, whereas at high frequencies the same source may appear in the farfield of the array.

Several methods have been suggested to solve the broadband beamforming problem. However, most of these methods are limited in their generality, relying either on specific array geometries (usually uniformly spaced arrays), or specific beampatterns, or assumption of farfield sources.

Thus from the above discussion we have identified a basic question which has not been adequately answered previously. We state it as follows:

> *How can one design a beamformer that can enhance a desired signal in an environment consisting of broadband nearfield and/or farfield sources?*

This general question motivates the work in this thesis, where a general theory for beamforming is developed that can be applied to a wide class of array geometries, allows arbitrary beampatterns, can be used over a large bandwidth and can deal with sources in the nearfield of the array. In developing this theory, we formulate a set of analysis tools which can be used to solve a wider class of array signal processing problems. Whilst the techniques developed are new, the philosophy behind our approach is not; we emphasize:

> The general philosophy of our approach is to analyze the underlying physical and mathematical structure of the array processing problem, and to exploit this knowledge to synthesize solutions to the problem of signal enhancement, detection and estimation. The set of analysis tools we develop called *modal analysis* techniques are based on traditional techniques used to solve the classical wave equation.

Summary of the Thesis:

- The remainder of this chapter reviews related array signal processing literature and lists the contribution of the thesis.
- Chapter 2 presents the theory of modal analysis of beamforming. This chapter serves as the basis of the thesis and the subsequent chapters use modal analysis as a tool to solve various aspects of beamforming and array processing problems.
- Chapter 3 describes a nearfield-farfield beampattern transformation method and presents novel nearfield beamforming techniques using farfield design methods.
- Chapter 4 formulates the design of general broadband beamformers using the modal analysis techniques introduced in Chapter 2.
- Chapter 5 applies the modal analysis theory (Chapter 2) and general beamforming theory (Chapter 4) to the nearfield adaptive broadband beamforming problem.
- Chapter 6 illustrates the application of modal analysis techniques to other related areas such as the problems of nearfield noise modeling and source localization.
- Chapter 7 concludes the thesis and suggests some projects for further research.

1.2 Background Beamforming Concepts

In the previous section, we have outlined the motivation for the work in this thesis, identified a basic question to be answered, and stated the philosophy of our approach. In this section we give some background beamforming theory to set the context for the contributions of the thesis, which are listed at the end of this chapter.

1.2.1 Beamforming and Spatial Filtering

Systems designed to receive propagating signals often encounter interfering signals. If the interference and the desired signal occupy the same temporal frequency band,

then linear temporal filtering cannot be used to separate the desired signal from interference. However, the desired and interfering signals usually originate from different locations in space. Thus, a *spatial filter* can be used to separate the desired signal from the interference originating from a different location. Application of temporal filtering requires processing of data collected over a period of time (temporal aperture). Similarly, application of spatial filtering requires processing of data collected over a region of space which we will refer to as a spatial aperture[2].

The word "beamforming" derives from the fact that early spatial filters were designed to form pencil beams in order to receive a signal radiating from a specific location and attenuate signals from other locations [4]. Spatial filtering can be performed by using either a continuous aperture or discrete aperture (array of sensors). In this thesis, the processor that performs spatial filtering is called a beamformer irrespective of the nature of the aperture. In some literature, it is used only for spatial filtering by an array of sensors [4].

Depending on the bandwidth of the signal environment, a beamformer can be classified as either narrowband or broadband. If the signal bandwidth is more than a significant fraction (say 0.1) of the mid-band frequency, then the signal is said to be broadband. There is no fixed definition for a broadband signal in the literature[3], since, whether one can sufficiently treat the signal as monochromatic[4] depends on a range of other factors associated with the problem. Most of the beamforming literature is concerned with narrowband signals. Dealing with broadband beamforming is more complicated, because of the additional frequency variable. Since the operating frequency is fixed in narrowband beamforming, the frequency can be excluded. Broadband beamforming subsumes or generalizes the narrowband case. In the broadband case, sensor outputs are processed using filters rather than complex scalars (weights).

Beamformers can also be classified as either data independent or data dependent, depending on how the beamformer parameters (filter coefficients or weights) are chosen. The parameters in the data independent beamformer are designed to produce predetermined response regardless of the signal environment. The parameters in a data dependent beamformer are chosen based on the statistics of the array data to optimize the array response according to some design criterion such as maximizing the signal to noise ratio at the beamformer output. The beamforming

[2] An aperture is a region over which energy can be received. Apertures can either be continuous or discrete as in sensor arrays.

[3] A working definition is that if there is a significant (or measurable) difference between the upper and lower frequencies then the signal is broadband.

[4] A signal with one frequency only.

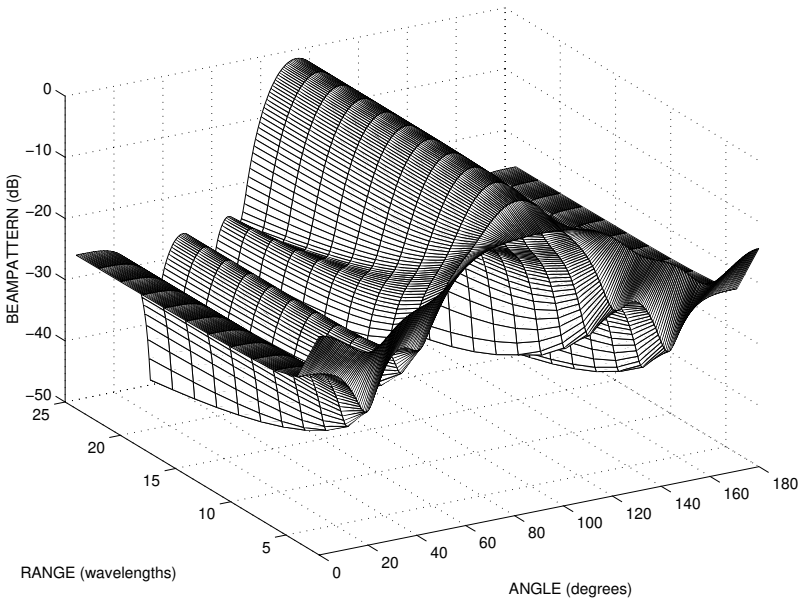

Figure 1.3: Variation of the shape of the angular response of a beamformer designed with farfield assumption with the radial distance (range - expressed in terms of wavelengths). Angular response is normalized at each radial distance , thus amplitude variation versus radial distance is suppressed.

theory developed in this thesis are applicable to both kind of beamformers.

The vast majority of beamforming literature deals only with the situation in which the impinging wavefronts on the array are planar in nature, where all the signals are assumed to be originated from sources in the farfield of the array (an infinite distance from the array). This is called farfield beamforming. A wave propagating from a point source radiates spherically outwards from the source location. If a point source is in the nearfield of the array (suitably close to an array), then the impinging wavefront on the array from that source is spherical. In this situation, use of the farfield assumption to design the beamformer will generally degrade the beamformer spatial response (see Figure 1.3). The common rule of thumb for the approximate distance at which the farfield approximation begins to be valid is $r = 2L^2/\lambda$ (known as *Rayleigh distance*), where r is the distance from an arbitrary array origin, L is the largest array dimension, and λ is the operating wavelength [12]. In the antenna literature, the farfield is called the *Fraunhofer zone* [13, p. 12] and the nearfield is called the *Fresnel zone* [13, p. 10] and they are treated differently. Most of the nearfield designs are based on approximations such as *nearfield compensation* [14] in which a delay correction is used on each sensor to account for the nearfield spherical wavefronts. Even with the simplest array geometries, designs based on nearfield compensation tend only to achieve the

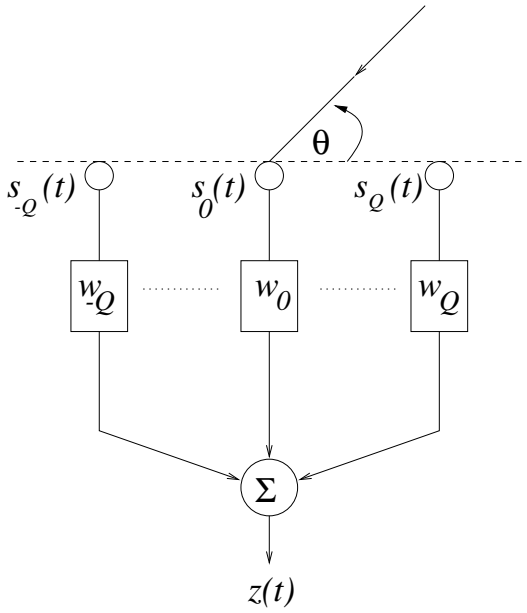

Figure 1.4: A block diagram of a typical narrowband beamformer

desired nearfield beampattern over a limited range of angles because they focus the array to a single point in three dimensional space. *One of the main objective of this thesis is to establish a new theory applicable to both nearfield and farfield beamforming.*

1.2.2 Narrowband Beamformers

In a conventional narrowband beamformer, the output of each sensor is weighted by a complex scalar. All such weighted outputs are summed together to give the beamformer output. A block diagram of a typical narrowband beamformer is shown in Figure 1.4. The output of a narrowband beamformer with $2Q + 1$ sensors at time t is given by

$$z(t) = \sum_{q=-Q}^{Q} w_q \, s_q(t), \tag{1.1}$$

where w_q is the complex weight applied to the qth sensor, and $s_q(t)$ is the signal received at the qth sensor at time t. The basic idea of a narrowband beamformer is to add the outputs of sensors with appropriate weights so that a signal arriving from a desired direction adds up constructively and signals arriving from other directions add destructively (on average).

Nearfield Sources

Suppose the signal environment consists of V nearfield sources located at (r_v, θ_v), $v = 1, \ldots, V$, where r_v is the distance from the sensor origin (assumed to be coincidence with the coordinate origin) to vth source and θ_v is the angle between the array axis (assumed to be along the x-axis) and the line joining the origin and the vth source. Then the received signal at the qth sensor (of a linear double-sided array of $2Q + 1$ sensors) is given by

$$s_q(t) = \sum_{v=1}^{V} \frac{r_v}{d(r_v, \theta_v, x_q)}\, s_v[t - d(r_v, \theta_v, x_q)/c + r_v/c], \tag{1.2}$$

where $s_v(t)$ is the signal received at the sensor origin from vth source, c is the speed of wave propagation and

$$d(r, \theta, x) \triangleq \sqrt{x^2 + r^2 - 2rx\cos\theta)}$$

is the distance between the source at (r, θ) and the sensor at x. Note that the expression (1.2) is normalized for $1/r$ spreading loss and gross delay.

Since we are considering the narrowband operation, assume that all source signals are monochromatic with *radian frequency*[5] ω_0. Then we can write

$$s_v(t) = A_v\, e^{i\omega_0 t}, \tag{1.3}$$

where A_v is the amplitude of the vth source signal. By substituting (1.2) and (1.3) into (1.1), we can write the narrowband beamformer output (1.1) as

$$z(t) = e^{i\omega_0 t} \sum_{v=1}^{V} A_v\, b_{r_v}(\theta_v), \tag{1.4}$$

where

$$b_r(\theta) = \sum_{q=-Q}^{Q} w_q\, \frac{r e^{i(\omega_0/c)r}}{d(r, \theta, x_q)}\, e^{-i(\omega_0/c)d(r,\theta,x_q)}. \tag{1.5}$$

The function $b_r(\theta)$ is known as the *spatial response* or the *beampattern of the beamformer*.

[5]Frequency measured in radians per second, i.e., if f is the frequency in Hz then $\omega = 2\pi f$.

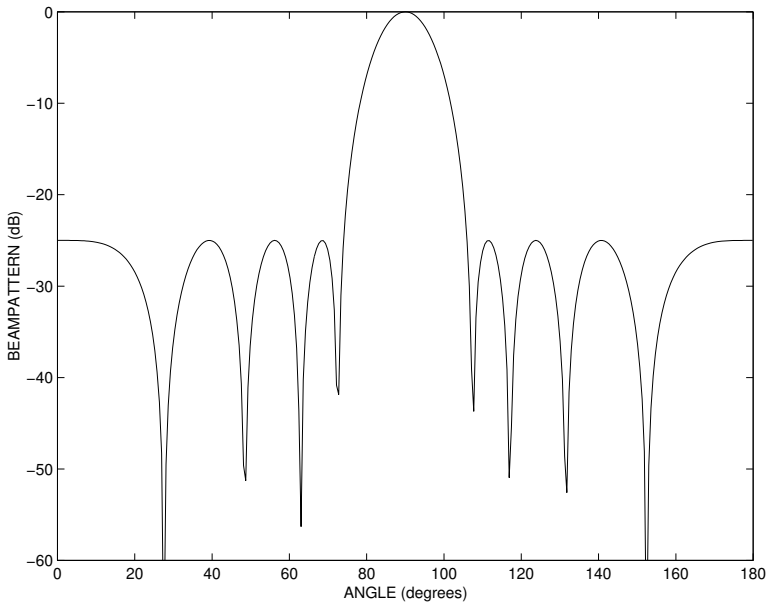

Figure 1.5: Farfield spatial response (beampattern) of a typical narrowband beamformer where 9 sensors are equally spaced at half wavelength spacing. Sensor weights are designed according to Chebyshev method.

Farfield Sources

If the signal environment consists of all farfield sources, impinging wavefronts are planar. In this case $r_v \to \infty$, $v = 1, \ldots, V$ and the farfield spatial response of the narrowband beamformer is given by

$$\begin{aligned} b_\infty(\theta) &= \lim_{r\to\infty} b_r(\theta) \\ &= \sum_{q=-Q}^{Q} w_q \, e^{-i(\omega_0/c)x_q \cos\theta}. \end{aligned} \tag{1.6}$$

Figure 1.5 shows the farfield spatial response (beampattern) of a typical beamformer. By referring to Figure 1.5, some of the features of a beampattern are described as follows. A single main beam, known as the *mainlobe*, is usually directed towards the desired source. The smaller beams are referred to as *sidelobes*. Troughs between beams are called *nulls*, which may be placed in a direction of a strong unwanted signal by designing sensor weights appropriately.

Sensor spacing

Most conventional narrowband beamformers have a uniformly spaced array of sensors. Historically, half a wavelength sensor spacing[6] were used in narrowband arrays to avoid *spatial aliasing*. Similar to the temporal aliasing, which is the effect of undersampling a time domain signal, spatial aliasing is the effect of undersampling in the space domain signal. In both cases, sampling rates need to satisfy the *Nyquist criterion*.

In the array signal processing literature, half a wavelength sensor spacing have been used for both farfield and nearfield beamforming arrays. Simple mathematical analysis shows that half wavelength sensor spacing indeed guarantees no aliasing in the operation of farfield arrays. However, whether half wavelength spacing ensure no spatial aliasing in nearfield arrays does not seem to have been investigated. Another question to be answered in this thesis is *to investigate effects of spatial aliasing for nearfield arrays*.

Use of half a wavelength sensor spacing for farfield arrays simplifies the formula for the beampattern of the narrowband beamformer significantly and enables the use of Fourier techniques to design sensor weights. With half a wavelength ($\lambda/2$) spacing, the beampattern (1.6) reduces to

$$b_\infty(\theta) = \sum_{q=-Q}^{Q} w_q \, e^{-i\pi q \cos\theta}. \tag{1.7}$$

Beam Steering

The main beam of a farfield beampattern may be steered to directions other than broadside of the array by introducing a progressive time delay across the array. Specifically, if the main beam is to be pointed to a angle γ then a phase delay of $x_q(\omega_0/c)\cos\gamma$ should be applied to the qth sensor, where ω_0 is the angular frequency of operation. This is equivalent to delaying the output of the qth sensor by $x_q(\omega_0/c)\cos\gamma$ before summing together to produce the beamformer output. Therefore, this is referred to as *delay and sum beamforming*, which is one of the oldest and simple beamforming techniques. Figure 1.6 shows a spatial response (beampattern) of a steered beamformer.

[6]Known as the $\lambda/2$ rule, where λ is the wavelength.

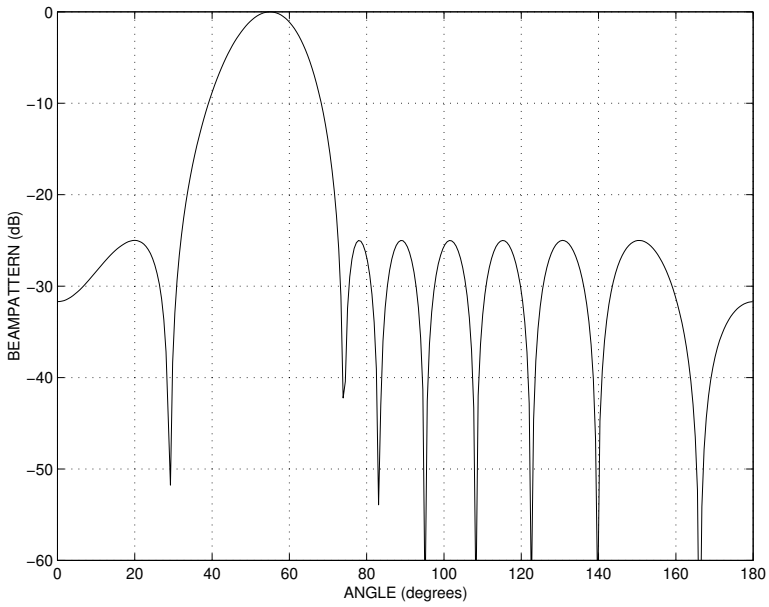

Figure 1.6: Beampattern of a beamformer steered to a direction other than broadside of the array where the unsteered beampattern is given by Figure 1.5.

Narrowband Beamformer Design Methods

For a fixed beamformer design, the spatial response (beampattern) of the beamformer is pre-determined and independent of the actual signal received (array data). For this case, the location of the desired source is assumed to be known. A common approach is first to draft a beampattern specification reflecting the spatial filtering requirement. For example, features like mainlobe width (beam width), sidelobe levels can be used as design specifications, where the beamwidth reflects the resolution required and sidelobe levels can be used to indicate the desired attenuation of undesired signals. The final step is to design a beamformer that achieves the given specifications. Design considerations may involve determining the number of sensors, the sensor separation, the array geometry and the array weights.

Several classical techniques exist in the antenna literature for designing narrowband beamformers. A few methods are briefly outlined below. For a full review, reader is referred to see [12, 15].

The Fourier series method [12, p. 112] can be applied to a narrowband beamforming problem as follows. For a uniformly spaced sensor array (1.6), can be written as

$$b_\infty(u) = \sum_{q=-Q}^{Q} w_q \, e^{-i2\pi q \frac{d}{\lambda} u}, \tag{1.8}$$

where $u = \cos\theta$, d is the inter-sensor spacing and $\lambda = \omega_0/c$ is the wavelength. Equation (1.8) can be considered as a finite Fourier series where w_q are the Fourier coefficients and $b_\infty(u)$ is periodic in u-space with period λ/d. Thus, given the desired beampattern $b_\infty(u)$, weights can be obtain by the Fourier analysis equation as

$$w_q = \frac{d}{\lambda} \int_{-\frac{\lambda}{2d}}^{\frac{\lambda}{2d}} b_\infty(u) e^{i2\pi q \frac{d}{\lambda} u}\, du, \quad q = -Q, \ldots, Q. \tag{1.9}$$

This method provides the least-mean-square-error approximation of the desired beampattern.

The method in [16] expresses (1.8) as a polynomial of degree $2Q+1$,

$$b_\infty(u) = \sum_{q=0}^{2Q+1} w_q\, z^q, \tag{1.10}$$

where $z = e^{-i2\pi \frac{d}{\lambda} \cos\theta}$. The beampattern is synthesized by changing the zero positions of this polynomial. Again this method relies on equal sensor spacing and the farfield assumption.

The Dolph-Chebyshev method [17] equates (1.10) with a Chebyshev polynomial to produce a beampattern with the narrowest mainlobe width for a given constant sidelobe level. Figure 1.5 shows the beampattern of a beamformer designed using Dolph-Chebyshev method with -25dB sidelobe levels.

There are other classical beampattern synthesis methods [18–24] reported in the literature which rely on uniform sensor spacing and farfield assumption.

Introducing nonuniform sensor spacing significantly complicates the beamformer design problem. Most methods that use nonuniform sensor spacing are either iterative [25–27] or use some form of numerical optimization [28]. These methods tend to be more mechanical computational processes with no insight into the structure of the problem, thus they can not be generalized for broadband or nearfield applications. A more fundamental approach was given in [29] where Poisson's summation formula was used to find an analytical solution to the beamformer design problem with nonuniform sensor arrays.

The above classical beampattern synthesis methods are sufficient for traditional farfield narrowband applications such as (most) radar problems, but most of them are not suitable for an increasing range of broadband and/or nearfield applications of arrays. The main theme of this thesis is to design more general beamforming methods that can be applied to process signals from broadband and nearfield

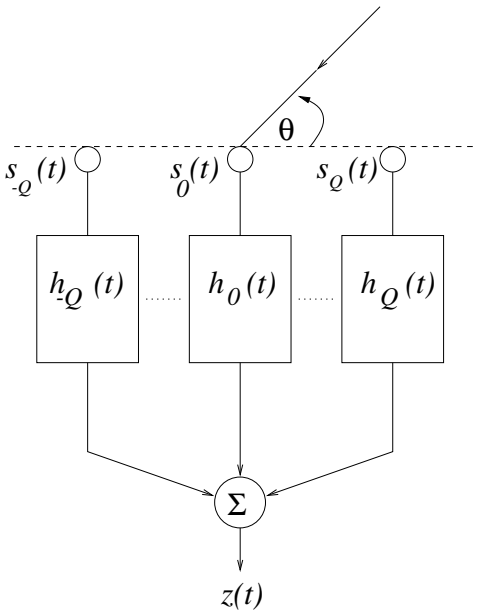

Figure 1.7: Schematic diagram of a broadband beamformer. The functions $h_q(t)$ represent general filters that follow each sensor output.

sources which are valid for arbitrary sensor geometries. In the next section, we outline some of the existing broadband beamformer design methods.

1.2.3 Broadband Beamformers

Narrowband beamforming methods assume that the signal bandwidth is sufficiently narrow to consider only a single frequency. However, the frequency spectrum of many signals of interest have more than one frequency component. As we have already illustrated in Figure 1.2, the use of a narrowband beamformer for a broadband signal degrades the performance of the beamformer. One common approach to this problem is to attach a *temporal filter*[7] to each sensor output instead of a complex weight, before summing them together. Combining these filtered outputs to form a beam is known as *filter and sum beamforming* [3]. Broadband beamforming is said to entail *spatio-temporal filtering* or a *space-time signal processing* problem, since the signal wavefield is sampled and processed in both space and time domains.

Figure 1.7 shows a schematic diagram of a typical beamformer with a filter

[7] A time domain filter; we use this term to distinguish it from a spatial filter which is in the space domain.

attached to each sensor. The broadband beamformer output can be written as

$$z(t) = \sum_{q=-Q}^{Q} h_q(t) * s_q(t), \tag{1.11}$$

where $h_q(t)$ is the impulse response of the filter attached to the qth sensor, $s_q(t)$ is the signal received at the qth sensor and $*$ denotes the continuous time convolution which is defined by [30, p. 97]

$$h_q(t) * s_q(t) = \int_{-\infty}^{\infty} h_q(\tau) s_q(t-\tau)\, d\tau. \tag{1.12}$$

Early beamformers used continuous time filters in beamformers, but almost all modern beamformers use discrete time filters such as FIR filters and are implemented on digital signal processors (DSPs). In order to use a discrete time beamformer, the received signal at each sensor needs to be sampled before filtering it using FIR filters. We can consider (1.11) as the output of a continuous time broadband beamformer. The output of the associated discrete time broadband beamformer is

$$z[n] = \sum_{q=-Q}^{Q} h_q[n] * s_q[n], \tag{1.13}$$

where $h_q[n]$ is the impulse response of the FIR filter and $s_q[n] = s_q(nT)$, where T is a suitable sampling time and $*$ denotes the discrete time convolution given by

$$h_q[n] * s_q[n] = \sum_{m=-\infty}^{\infty} h_q[m] s_q[n-m]. \tag{1.14}$$

Suppose that the signal environment consists of V broadband sources located at (r_v, θ_v), $v = 1, \ldots, V$ where r_v is the distance from the sensor origin to vth source and θ_v is the angle between the array axis and the line joining origin and the vth source. Then the received signal at the qth sensor $s_q(t)$ is given by (1.2) as in the narrowband beamformer. A broadband signal can be considered as a sum of many narrowband signals. Hence, using (1.3) we can write the signal received at the sensor origin from the vth source as

$$s_v(t) = \int_{-\infty}^{\infty} A_v(\omega)\, e^{i\omega t} d\omega, \tag{1.15}$$

where $A_v(\omega)$ is the frequency dependent amplitude of the signal received from the vth source. Observe that $s_v(t)$ and $A_v(\omega)$ form a Fourier transform pair.

Using (1.12), (1.15) and (1.2), the output of the continuous time beamformer can be written as

$$z(t) = \sum_{v=1}^{V} \int_{-\infty}^{\infty} A_v(\omega)\, b_{r_v}(\theta_v;\omega) e^{i\omega t}\, d\omega, \tag{1.16}$$

where

$$b_r(\theta;\omega) = \sum_{q=-Q}^{Q} H_q(\omega)\, \frac{r e^{i\omega r/c}}{d(r,\theta,x_q)}\, e^{-i\omega d(r,\theta,x_q)/c}, \tag{1.17}$$

is the spatial response of a broadband beamformer to a source at (r,θ) and

$$H_q(\omega) = \int_{-\infty}^{\infty} h_q(\tau) e^{-i\omega\tau}\, d\tau, \tag{1.18}$$

is the frequency response of the filter attached to the qth sensor. Observe the similarities between the spatial response of a broadband beamformer (1.17) and that of a narrowband beamformer (1.5). The only difference is that the frequency ω is fixed in the latter case.

The discrete time counterparts of (1.16) and (1.17) can be derived in a similar vein. Specifically, the output $z[n]$ of the discrete time broadband beamformer can be written as follows:

$$\begin{aligned} z[n] &= \sum_{v=1}^{V} \int_{-\infty}^{\infty} A_v(\omega) b_{r_v}(\theta_v;\omega), e^{i\omega nT}\, d\omega, \\ &= \frac{1}{T} \sum_{v=1}^{V} \int_{-\infty}^{\infty} A_v(\frac{\tilde{\omega}}{T}) b_{r_v}(\theta_v;\frac{\tilde{\omega}}{T}), e^{i\tilde{\omega}n}\, d\tilde{\omega}, \end{aligned} \tag{1.19}$$

where T is the sampling time and $\tilde{\omega}$ is the discrete time frequency which is related to the continuous time frequency by $\tilde{\omega} = \omega T$ [31, p. 87]. The spatial response of the discrete time beamformer is same as that of a continuous time beamformer (1.17). However, the frequency response of the discrete filter attached to the qth sensor is given by

$$H_q(\tilde{\omega}) = \sum_{m=0}^{M-1} h_q[m] e^{-i\tilde{\omega}m}, \tag{1.20}$$

where M is the number of filter taps in FIR filter attached to each sensor.

Let $Z_c(\omega)$ be the continuous time Fourier transform of $z(t)$ and $Z_d(\tilde{\omega})$ be the discrete time Fourier transform of $z[n]$; then it can be seen from (1.16) and (1.19) that

$$Z_c(\omega) = 2\pi \sum_{v=1}^{V} A_v(\omega)\, b_{r_v}(\theta_v; \omega), \tag{1.21}$$

where 2π arrives from the inverse Fourier transform, and

$$Z_d(\tilde{\omega}) = \frac{2\pi}{T} \sum_{v=1}^{V} A_v(\frac{\tilde{\omega}}{T}) b_{r_v}(\theta_v; \frac{\tilde{\omega}}{T}). \tag{1.22}$$

In other words, $Z_c(\omega)$ and $Z_d(\tilde{\omega})$ give the output of the continuous and discrete time beamformers respectively. Note the similarity between the two outputs, and recall that earlier we observed the similarity between the spatial response of the two beamformers. Therefore, in this thesis, without loss of generality, we will use (1.17) to write the spatial response and (1.21) to represent output of broadband beamformers, irrespective of whether they are continuous time or discrete time realizations. We prefer this frequency domain representation since most of the theory developed in this thesis is applicable to both continuous time and discrete time beamformers and the theory is naturally formulated in the frequency domain.

Broadband Beamformer Design Methods

In broadband beamformers, the spatial response is also dependent on frequency. Thus, one needs to control the spatial response of the beamformer over the signal bandwidth. This means that a broadband beampattern specification is defined over space and frequency. Figure 1.8 shows a broadband beampattern specified over the elevation angle and frequency (which is defined on a fixed radial distance from the array and no variation with azimuth angle). We now briefly review a few of the existing broadband beamforming techniques.

Frequency Decomposition Method: Most of the techniques described in Section 1.2.2 for narrowband beamformers are not directly applicable to broadband beamformers with a FIR filter attached to each sensor. However, one approach is to use FFT (Fast Fourier Transform) methods to form separate narrowband frequency bins, and perform narrowband beamforming in each frequency bin [32, 33]. Since

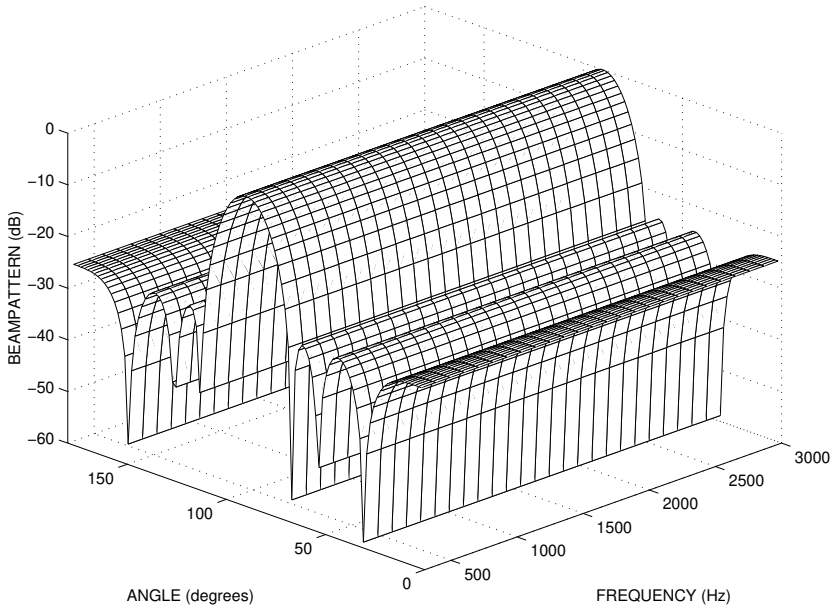

Figure 1.8: A typical broadband beampattern defined over elevation angle and a band of frequency on fixed radius from the array origin with no variation with the azimuth angle.

the broadband received array data are transformed to a set of narrowband array data segments, this method is referred to as frequency decomposition method. One disadvantage of this method over the time domain beamforming is the additional computation required by the FFT operation. Also to avoid spatial aliasing for all frequencies, a highly dense sensor array is needed with sensor spacing of $\lambda_u/2$ where λ_u is the wavelength of the highest frequency of the design band. Obviously, this approach requires a large number of sensors and may not be practical for real applications. Some methods have been suggested recently to reduce the number of sensors using nonuniform sensor spacing [34, 35].

Fourier Transform Method: It has been noted in [36] that, for the case of an equally spaced array, there is a two-dimensional Fourier transform relationship between filter coefficients and the beampattern of a broadband beamformer. This provides a simple means of designing the sensor filters for a desired broadband beampattern. However, to avoid spatial aliasing, as we have mentioned before, a high density uniform spaced array is required.

Least Square Optimization Method: For a general array geometry, the following 2-norm optimization method [37] may be used. Let $\hat{b}_r(\theta, \omega)$ be a desired broadband beamformer response. A response of a discrete time beamformer with

$2Q+1$ sensors and M-tap FIR filters attached to each sensor, can be written using (1.17) and (1.20) as

$$b_r(\theta;\omega) = \boldsymbol{h}^H \boldsymbol{d}_r(\theta,\omega), \tag{1.23}$$

where

$$\boldsymbol{h} = \big[h_{-Q}[0],\ldots,h_Q[0],\ldots,h_{-Q}[M-1],\ldots,h_Q[M-1]\big]^H$$

is the $(2Q+1)M$ vector of filter coefficients, ^{H} denotes the complex conjugate transpose,

$$\boldsymbol{d}_r(\theta,\omega) = \boldsymbol{e}(\omega) \otimes \boldsymbol{a}_r(\theta,\omega)$$

is a $(2Q+1)M$ vector, $\otimes$ denotes the Kronecker product,

$$\boldsymbol{e}(\omega) = \big[1, e^{-i\omega},\ldots,e^{-i\omega(M-1)}\big]^T,$$

is a M dimensional vector and

$$\boldsymbol{a}_r(\theta,\omega) = re^{i\omega r/c}\big[\frac{e^{-i\omega d(r,\theta,x_{-Q})}}{d(r,\theta,x_{-Q})},\ldots,\frac{e^{-i\omega d(r,\theta,x_Q)}}{d(r,\theta,x_Q)}\big]^T$$

is the $2Q+1$ dimensional broadband array response vector. If the desired beampattern $\hat{b}_r(\theta,\omega)$ is sampled at P points (which has to be greater than the product of the number of sensors and number of filter coefficients per each sensor) in (θ,ω) space, then the following well-known over-determined least square minimization problem is obtained:

$$\min_h \|\boldsymbol{D}^H\boldsymbol{h} - \boldsymbol{b}_d\|^2,$$

where $\boldsymbol{D} = [\boldsymbol{d}_r(\theta_1,\omega_1),\ldots,\boldsymbol{d}_r(\theta_P,\omega_P)]$ and $\boldsymbol{b}_d = [b_r(\theta_1,\omega_1),\ldots,b_r(\theta_P,\omega_P)]^T$. The solution to this problem is

$$\boldsymbol{h} = \boldsymbol{D}^\dagger \boldsymbol{b}_d$$

where $\boldsymbol{D}^\dagger$ is the pseudo-inverse[8] of $\boldsymbol{D}$. The above solution exists only if $\boldsymbol{D}$ has full rank, i.e., $\boldsymbol{D}\boldsymbol{D}^H$ is invertible. This is a simple procedure. However, performance

[8] $\boldsymbol{D}^\dagger \triangleq (\boldsymbol{D}\boldsymbol{D}^H)^{-1}\boldsymbol{D}^H$

may be moderate due to rank deficiency of $\boldsymbol{D}$ which may be caused by too closely spaced sensors. Since there are no guidelines to place sensors, spatial aliasing may cause reduced performance. Also, this method provides no insight into the underlying structure of the problem. Nevertheless it can be applied to general geometries.

Harmonic Nesting Method: The method of "harmonic nesting" has often been used for designing microphone arrays for speech acquisition [10, 38, 39]. The basic idea behind this method is that an equally spaced array with an inter-sensor spacing of d exhibits the same beampattern at a frequency ω as an equally spaced array with inter-sensor spacing $d/2$ exhibits at frequency $\omega/2$. The beamformer is composed of a set of nested equally spaced sub-arrays, each of which is a single frequency design (i.e., narrowband design). Bandpass filters are used to combine the sub-array outputs such that the appropriate sub-array is used for each octave. The idea is to reduce the frequency variation to that which would occur in a single octave. However this method also assumes all signal sources are in the farfield of the array; thus it is not the best choice for nearfield applications such as speech acquisition.

There are several variations of the harmonic nesting method. In [40, 41], constraints are imposed on sub-arrays of different octaves. The two sub-arrays are "spaced" an octave apart each other and outputs are combined by two compensation filters, one on each sub-array output. These compensation filters allow two spatial constraints to be maintained over that octave, e.g., a unity constraint at broadside and half power constraint on the main beamwidth. Bandpass filters have been used to apply this techniques over several octaves [42].

Another approach based on harmonic nesting is the frequency sampling method, [43]. Each octave band is divided to K frequencies and the required sensor weights are calculated by taking the inverse discrete Fourier transform of the sampled desired beampattern. An FIR filter is then designed for each sensor to realize the sensor weight at each of the K frequencies. Because of the use of the discrete Fourier transform, this method is restricted to a uniformly spaced array geometry within each octave band and relies on the assumption of farfield sources as well.

Multiple Beamforming: As seen in Figure 1.2 the main width of a narrowband beamformer decreases as frequency increases. If several overlapping beams are simultaneously formed, the width of the resulting multibeam may be kept constant by increasing the steering angle of the outermost beams as the beamwidth

decreases [44, 45].

Space Tapering Method: Doles and Benedict [46] have proposed a method in which the beamformer spatial response has little or no frequency variation over the design bandwidth. The asymptotic theory of unequally spaced arrays [29, 47] is used to derive relationships between beampattern properties (such as peak response, mainlobe width, and sidelobe level) and beamformer design. These relationships are then used to translate beampattern requirements into functional requirements on the sensor spacing and weightings, thereby deriving a broadband design. Although this method provides the desired beampattern over a specified frequency design band, it is based on a linear array and depends on the farfield assumption. However, unlike most other methods, it does allow nonuniformly spaced arrays.

Theoretical Continuous Sensor Approach: Ward *et al.* [34] have taken the above space tapering idea [46] further by developing a frequency invariant beampattern property for a theoretical continuous sensor. The continuous sensor approach is justified from the following observations: to obtain an identical beampattern at K discrete frequencies requires a compound array of K sub-arrays having the self-similarity property as outlined in the harmonic nesting method. Thus, to provide an identical beampattern over a continuous range of frequencies requires an infinite number of sub-arrays, or effectively a continuous sensor. Once the structure of the continuous sensor has been determined, it can be approximated by discrete sensors.

Unlike the earlier described methods, the continuous sensor approach gives a better understanding of the underlying structure of the beamforming problem and this has been exploited to provide improved solutions to broadband adaptive beamforming [48], broadband pattern nulling [49] and broadband direction of arrival estimation [50] problems. However, this method also assumes planar wave propagation (farfield sources), thus lacks the generality that we seek in this thesis. We use some of the ideas presented in this method together with modal analysis techniques (see Chapter 2) to design a general broadband beamformer that can deal with nearfield source signals.

1.2.4 Data Dependent Beamforming Techniques

Conventional fixed beamforming may not provide the amount of interference suppression required in many situations. Better noise suppression is afforded through

statistically optimum techniques. These techniques attempt to choose array weights (in the case of narrowband beamformers) or filter coefficients (in the case of broadband beamformers) such that the desired signal is enhanced and the interfering noise signals are suppressed, based on the statistics of the received array data [1]. If the statistics of the array data are unknown or time dependent, then the optimum solution is estimated from the available data adaptively, which is termed as adaptive beamforming.

Most of the early adaptive array techniques were developed for narrowband applications. However, these methods may be employed for broadband signals by frequency decomposition followed by application of narrowband techniques at each frequency bin. Frost [51] proposed an efficient broadband adaptive algorithm based on the application of linear constraints. An excellent outline of these classical methods is given in [4].

One of the problems that occurs with classical adaptive array techniques is "desired signal cancellation". This is due to interfering signals which can be either delayed versions of the desired signal due to multipath propagation or deliberate jamming signals (The reader is referred to Chapter 5 for more detail). Several methods, which are capable of handling this problem, have been reported [52–56]. However, all of these methods depend on the assumption of farfield sources.

Thus, we have identified another important problem to be investigated. That is, *how to design an adaptive beamformer to enhance a desired signal in a signal environment consisting of nearfield broadband interfering signals that are coherent with the desired signal.* In this thesis we show how to overcome desired signal cancellation by using modal based beamformers.

1.2.5 Source Localization

Estimation of the direction of arrival or localization of the sources present in the signal environment is another important problem in array processing. For example, in passive sonar, the received signals from an array of hydrophones are processed to provide estimates of the direction of sources. There are literally hundreds of papers written on this subject area and it is impossible to review all of them here. Instead we refer [11, 57] for a review of more recently reported techniques.

Source localization procedures may be loosely divided into three general categories [58]: those based upon maximizing the output power of a steered beamformer; techniques adopting high-resolution spectral estimation concepts; and approaches employing time difference of arrival information. The first refers to any

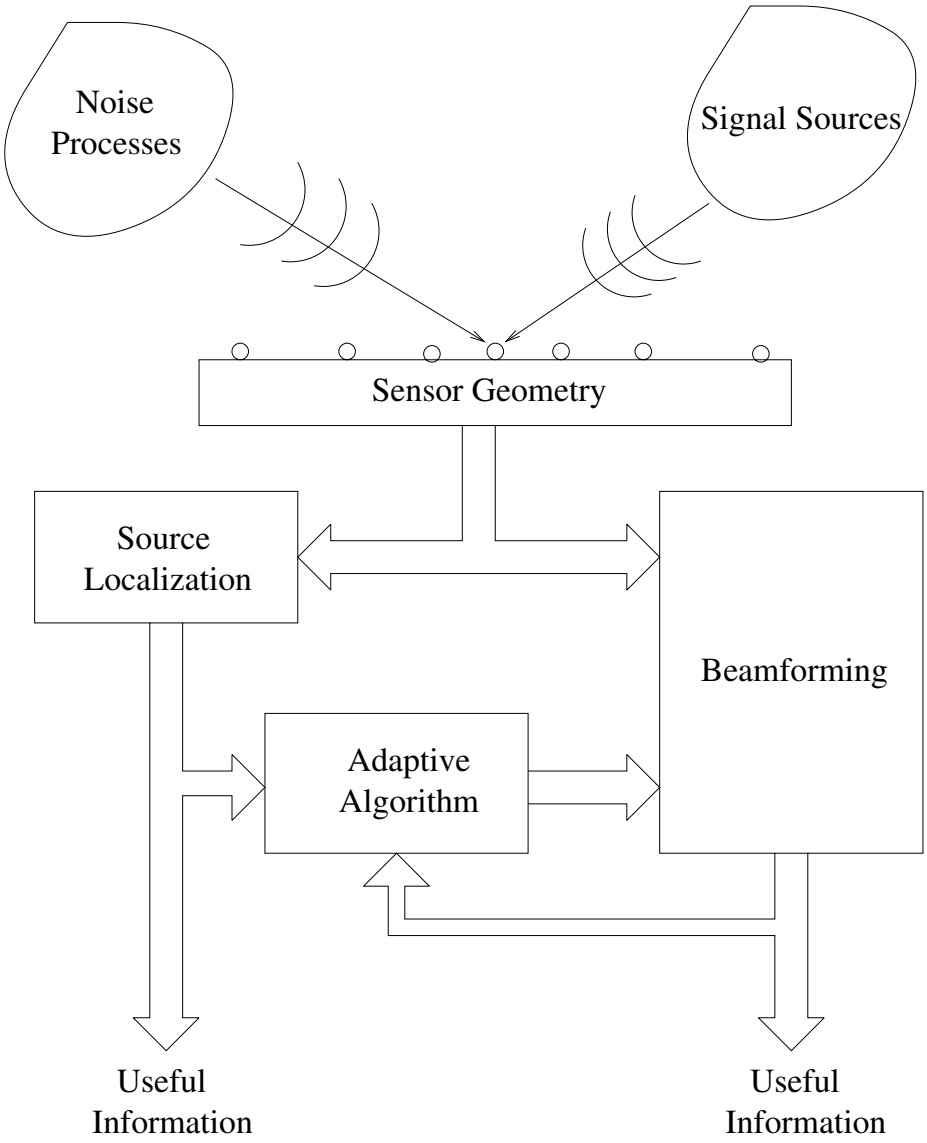

Figure 1.9: A typical array processing system in a block diagram form

situation where the location estimate is derived directly from a filtered, weighted and summed version of the signal data received at the sensors. The second will be used to term any localization scheme relying on application of the signal correlation matrix. The final method calculates source locations from a set of delay estimates measured across various combinations of sensors.

In this thesis, we show that the modal analysis techniques can improve the performance of the first two types of source localization methods described above. Specifically, we consider the problem of broadband source localization in a signal environment with correlated interfering signals.

1.3 Questions to be Answered in this Thesis

In this section we itemize the questions flagged in the previous two sections, which will be answered in the following chapters of this thesis.

- How can one design a beamformer that can enhance a desired signal in an environment consisting of broadband nearfield and/or farfield sources?

- One of the main objectives of this thesis is to establish a set of analysis tools, which are applicable to both nearfield and farfield arrays, to solve a wide variety of array processing problems.

- How does spatial aliasing affect nearfield arrays?, and how can one reduce its effects?

- How can one design an adaptive beamformer to operate in a signal environment consisting of coherent broadband nearfield sources?

1.4 Outline of Thesis

1.4.1 Overview

The primary motivation of this thesis is to design a general broadband beamformer that can deal with signals received from nearfield and/or farfield sources. To develop this beamforming theory, we formulate a set of analysis tools (called modal analysis techniques) which are useful in solving wider class of array signal processing problems.

Figure 1.9 illustrates the various stages of a typical array processing system[9], which includes a set of sensors, a source localization module, a beamforming block and a module containing adaptive algorithms. We claim that most of the problems and issues involved in such a system can be solved using the modal analysis techniques formulated in this thesis. Specifically we make contributions to general beamforming theory, adaptation issues, source localization, background noise modeling and sensor placement issues.

The following subsection reviews what can be found in each of the five technical chapters, 2 to 6. (This discussion is often specific and may be safely skimmed over.)

[9] A practical system may have all or some of these modules depending on the application.

1.4.2 Content and Contribution of Thesis

A summary of the major contributions of this thesis follows.

- **Chapter 2:** establishes the theory of modal analysis of beamforming. We identify the modes as solutions to the classical wave equation, which are orthogonal functions of the spherical coordinates. We show that these modes form a useful basis set to analyze and synthesize arbitrary wavefields, beampattern specifications and spatial response of physical apertures (beamformers). Specifically, we derive a novel representation to express any arbitrary beampattern uniquely based on these modes, which is capable of representing both farfield and nearfield beampatterns. The new modal representation consists of analysis and synthesis equations to decompose a given beampattern to modes and, given the modal decomposition, to construct an arbitrary beampattern respectively. We also devise a Parseval relation to quantify the beampattern error involved by using a finite number of modes in the modal representation. We collectively call these modal representation based results modal analysis techniques and exploit them in the rest of this thesis to solve associated problems in beamforming and array signal processing.

- **Chapter 3:** devises three novel methods of nearfield beamforming by exploiting the modal analysis techniques introduced in Chapter 2 and the concept of a *nearfield-farfield* transformation.

  The first method provides an exact transformation method, which radially transforms a nearfield beampattern specification to a physically equivalent farfield beampattern. A farfield beamformer is then designed for a transformed farfield beampattern which, if achieved, gives the desired nearfield beampattern exactly. Salient features of the new method are: (i) the nearfield patterns can be achieved for all angles, not just the primary look direction, and (ii) general array geometries may be used.

  The second method establishes an asymptotic equivalence, up to complex conjugation, of two problems: (i) determining the nearfield performance of a farfield beampattern specification, and (ii) determining the equivalent farfield beampattern corresponding to a nearfield beampattern specification. Using this reciprocity relationship, we develop a computationally simple procedure to design a beamforming array that achieves a desired nearfield beampattern response. The superiority of this approach to existing methods, both in ease

of design implementation and performance obtained, is analyzed and then illustrated by a design example.

The third and final nearfield beamforming method uses the modal analysis techniques (Chapter 2) to find a linear transformation between the array weights required to achieve the given beampattern for farfield and nearfield, respectively.

- **Chapter 4:** introduces an efficient parameterization for the nearfield (and farfield) broadband beamforming problem with a single parameter to focus the beamformer to a desired operating radius and another set of parameters to control the actual broadband beampattern shape. This parameterization is derived using the modal analysis techniques developed in Chapter 2 and the concept of the theoretical continuous aperture. A set of elementary beamformers are designed for each elementary beampattern and the desired beamformer is constructed by summing the elementary beamformers with frequency and source-array distance dependent weights. An important consequence of our result is that the beamformer can be factored into three levels of filtering: (i) beampattern independent elementary beamformers; (ii) beampattern shape dependent filters; and (iii) radial focusing filters where a single parameter can be adjusted to focus the array to a desired radial distance from the array origin. As an illustration, the method is applied to the problem of producing a practical array design that achieves a frequency invariant beampattern over a frequency range of 1:10 (which is suitable for speech acquisition using a microphone array), and with the array focused either to farfield or nearfield where at the lowest frequency the radial distance to the source is only three wavelengths.

- **Chapter 5:** considers a design of an adaptive beamformer to operate in a signal environment consisting of broadband nearfield sources, where some of the interfering signals may be correlated with desired signal. We extend the general beamforming theory developed in Chapter 4 to propose a novel adaptive beamformer. Specifically, the frequency invariance nature of the beamforming structure (Chapter 4) is used to combat the desired signal cancellation due to correlated interfering signals and the radial focusing capability is used to deal with the nearfield source signals. A simulation example is presented to demonstrate the use of the proposed method in microphone array applications in speech acquisition systems.

- **Chapter 6:** exploits the modal analysis techniques developed in Chapter 2 to analyze and solve related array signal processing problems. We have considered two areas of array processing, namely noise modeling and broadband source localization.

  In the first part of this chapter, an exact series representation for a nearfield spherically isotropic noise model is introduced. The proposed noise model can be utilized effectively to apply well established farfield array processing algorithms for nearfield applications of sensor arrays. A simple array gain optimization is used to demonstrate the use of the new noise model.

  The second part of Chapter 6 shows how to simplify existing broadband source localization techniques using modal analysis techniques (Chapter 2). When received signals from different directions are correlated with each other (e.g., multipath), a common practice is to align the received array data into a single frequency, and then use frequency averaging to reduce the signal correlation and thereby avoid signal cancellation. Usually these frequency alignments are done by either using *focusing matrices* or spatial resampling techniques. By analyzing the received wavefield, we formulate a new set of focusing matrices that, unlike the existing methods, do not require preliminary estimation of source locations and depend only on the array geometry. We also establish a single set of spatial resampling matrices for frequency alignment over the full *field of view* of the array, whereas in the existing techniques, this is done by dividing the field of view of the array into different sectors and using numerical interpolation to find resampling matrices for each sector. Since our intention is only to show how to exploit modal analysis in localization problems, we do not give a detailed study or any example case studies in this chapter.

References

[1] R.A. Monzingo and T.W. Miller, *Introduction to Adaptive Arrays*, John Wiley, New York, 1980.

[2] S. Haykin, Ed., *Array Signal Processing*, Prentice Hall, New Jersey, 1985.

[3] D.H. Johnson and D.E. Dudgeon, *Array Signal Processing*, Prentice Hall, New Jersey, 1993.

[4] B.D. Van Veen and K.M. Buckley, "Beamforming: A versatile approach to spatial filtering," *IEEE Sig. Proc. Mag.*, pp. 4–24, Apr. 1988.

[5] N.L. Owsley, "Sonar array processing," in *Array Signal Processing*, S. Haykin, Ed., New Jersey, 1985, Prentice Hall.

[6] S. Haykin, "Radar array processing for angle of arrival estimation," in *Array Signal Processing*, S. Haykin, Ed., New Jersey, 1985, Prentice Hall.

[7] A.C. Kak, "Tomographic imaging with diffracting and nondiffracting sources," in *Array Signal Processing*, S. Haykin, Ed., New Jersey, 1985, Prentice Hall.

[8] J.H. Justice, "Array processing in exploration seismology," in *Array Signal Processing*, S. Haykin, Ed., New Jersey, 1985, Prentice Hall.

[9] A.J. Paulraj and B. Papadias, "Space time processing for wireless communications," *IEEE Sig. Proc. Mag.*, vol. 14, pp. 49–83, Nov. 1997.

[10] J.L. Flanagan, D.A. Berkeley, G.W. Elko, J.E. West, and M.M. Sondhi, "Autodirective microphone systems," *Acustica*, vol. 73, pp. 58–71, 1991.

[11] H. Krim and M. Viberg, "Two decades of array signal processing research," *IEEE Sig. Proc. Mag.*, vol. 13, pp. 67–94, July 1996.

[12] R.J. Mailloux, *Phased Array Antenna Handbook*, Artech House, Boston, 1994.

[13] B.D. Steinberg, *Principles of Aperture and Array System Design*, Wiley, New York, 1976.

[14] F. Khalil, J.P. Jullien, and A. Gilloire, "Microphone array for sound pickup in teleconference systems," *J. Audio Engineering Society*, vol. 42, pp. 691–700, Sept. 1994.

[15] M.T. Ma, *Theory and Application of Antenna Arrays*, John Wiley and Sons, New York, 1974.

[16] S.A. Schelkunoff, "A mathematical theory of linear arrays," *Bell Sys. Tech. J.*, vol. 22, pp. 80–107, 1943.

[17] C.L. Dolph, "A current distribution for broadside arrays which optimizes the relationship between beam width and side-lobe levels," *IRE*, vol. 34, pp. 335–348, June 1946.

[18] T.T. Taylor, "Design of line-source antennas for narrow beamwidth and low sidelobes," *IRE Trans. Antennas Propagat.*, vol. AP-3, pp. 16–28, Jan. 1955.

[19] A.T. Villeneuve, "Taylor patterns for discrete arrays," *IEEE Trans. Antennas Propagat.*, vol. AP-32, pp. 1089–1093, Oct. 1984.

[20] F.I. Tseng, "Design of array and line-source antennas for Taylor patterns with a null," *IEEE Trans. Antennas Propagat.*, vol. AP-27, no. 4, pp. 474–479, July 1979.

[21] R.S. Elliot, "Design of line source antennas for narrow beamwidth and asymmetric sidelobes," *IEEE Trans. Antennas Propagat.*, vol. AP-23, pp. 100–107, Jan. 1975.

[22] R.S. Elliot, "Design of line source antennas for sum patterns with sidelobes of individually arbitrary heights," *IEEE Trans. Antennas Propagat.*, vol. AP-24, pp. 76–83, Jan. 1976.

[23] P. Woodward, "A method of calculating the field over a plane aperture required to produce a given polar diagram," *J. IEE*, vol. 93, pp. 1554–1558, 1947.

[24] P. Woodward and J. Lawson, "The theoretical precision with which an arbitrary radiation pattern may be obtained from a source of finite size," *J. IEE*, vol. 95, pp. 363–369, 1948.

[25] C.A. Olen and R.T. Compton Jr, "A numerical pattern synthesis algorithm for arrays," *IEEE Trans. Antennas Propagat.*, vol. 38, no. 10, pp. 1666–1676, Oct. 1990.

[26] R.W. Redlich, "Iterative least squares synthesis of nonuniformly spaced linear arrays," *IEEE Trans. Antennas Propagat.*, vol. 21, pp. 106–108, Jan. 1973.

[27] L. Wu and A. Zielinski, "An iterative method for array pattern synthesis," *IEEE J. Oceanic Eng.*, vol. 18, pp. 280–286, July 1993.

[28] B.P. Ng, M.H. E, and C. Kot, "A flexible array synthesis method using quadratic programming," *IEEE Trans. Antennas Propagat.*, vol. 41, no. 11, pp. 1541–1550, Nov. 1993.

[29] A. Ishimaru and Y.S. Che, "Thinning and broadbanding antenna arrays by unequal spacings," *IEEE Trans. Antennas Propagat.*, vol. AP-13, pp. 34–42, Jan. 1965.

[30] A.V. Oppenheim, A.S. Willsky, and S.H. Nawab, *Signals & Systems*, Prentice Hall, New Jersey, 1997.

[31] A.V. Oppenheim and R.W. Schafer, *Discrete Time Signal Processing*, Prentice Hall, New Jersey, 1989.

[32] C. Lieu and S. Sideman, "Digital frequency-domain implementation of optimum broadband arrays," *J. Acoust. Soc. Amer.*, vol. 98(1), pp. 241–246, July 1995.

[33] L.C. Godara, "Application of the fast fourier transform to broadband beamforming," *J. Acoust. Soc. Amer.*, vol. 98(1), pp. 241–246, July 1995.

[34] D.B. Ward, R.A. Kennedy, and R.C. Williamson, "Theory and design of broadband sensor arrays with frequency invariant far-field beampatterns," *J. Acoust. Soc. Amer.*, vol. 97, pp. 1023–1034, Feb. 1995.

[35] T.D. Abhayapala, R.A. Kennedy, and R.C. Williamson, "Nearfield broadband array design using a radially invariant modal expansion," *J. Acoust. Soc. Amer.*, accepted Aug 1998.

[36] S. Haykin and J. Kesler, "Relation between the radiation pattern of an array and the two-dimensional discrete Fourier transform," *IEEE Trans. Antennas Propagat.*, vol. AP-23, no. 3, pp. 419–420, May 1975.

[37] D.B. Ward and R.C. Williamson, "Beamforming for a source located in the interior of a sensor array," *Fifth International Symposium on Signal Processing and Applications, ISSPA99*, vol. 2, pp. 873–876, Aug. 1999.

[38] Y. Grenier, "A microphone array for car environments," *Speech Communication*, vol. 12, pp. 25–39, Mar. 1993.

[39] W. Kellerman, "A self-steering digital microphone array," *Proc. IEEE Int. Conf. Acoust., Speech Signal Processing (ICASSP-91)*, vol. 5, pp. 3581–3584, 1991.

[40] R. Smith, "Constant beamwidth receiving arrays for broad band sonar systems," *Acustica*, vol. 23, pp. 21–26, 1970.

[41] E. Hixson and K. Au, "Broadband constant beamwidth acoustical arrays," Tech. Rep. 19, Acoustics Research Lab, U.T. Austin, 1970.

[42] J. Lardies and J.P. Guilhot, "Realization of a broadband constant beamwidth end-fire line array," *Acoust. Letters*, vol. 10, no. 8, pp. 122–127, 1987.

[43] T. Chou, "Broadband frequency-independent beamforming," M.S. thesis, MIT, Jan. 1995.

[44] M.M. Goodwin and G.W. Elko, "Constant beamwidth beamforming," *Proc. IEEE Int. Conf. Acoust., Speech Signal Processing(ICASSP93)*, vol. 1, pp. 169–172, 1993.

[45] D.G. Tucker, "Arrays with constant beam-width over a wide frequency range," *Nature*, vol. 180, pp. 496–497, Sept. 1957.

[46] J.H. Doles III and F.D. Benedict, "Broad-band array design using the asymptotic theory of unequally spaced arrays," *IEEE Trans. Antennas Propagat.*, vol. 36, pp. 27–33, Jan. 1988.

[47] A. Ishimaru, "Theory of unequally-spaced arrays," *IRE Trans. Antennas Propagat.*, vol. AP-10, pp. 691–702, Nov. 1962.

[48] D.B. Ward, R.A. Kennedy, and R.C. Williamson, "Adaptive broadband beamforming with a dimension-reduction beampattern parameterization," *Int. J. of Adapt. Contr. and Signal Processing*, under review.

[49] P.J. Kootsookos, D.B. Ward, and R.C. Williamson, "Imposing pattern nulls on broadband array responses," *J. Acoust. Soc. Amer.*, vol. 105(6), pp. 3390–3398, June 1999.

[50] D.B. Ward, Z. Ding, and R.A. Kennedy, "Direction of arrival estimation for wideband signals using frequency invariant beamspace processing," *IEEE Trans. Sig. Proc.*, vol. 46, no. 5, pp. 1463–1469, May 1998.

[51] O.L. Frost III, "An algorithm for linearly constrained adaptive array processing," *Proc. IEEE*, vol. 60, pp. 926–936, Aug. 1972.

[52] J.F. Yang and M. Kaveh, "Coherent signal-subspace transformation beamformer," *Proc. IEEE*, vol. 137, pp. 267–275, Aug. 1990.

[53] A. Zeira and B. Friedlander, "Interpolated array minimum variance beamforming for correlated interference rejection," *Proc. IEEE Int. Conf. Acoust., Speech Signal Processing*, pp. 3165–3168, May 1996.

[54] T.S. Lee and T.T. Lin, "Adaptive beamforming with interpolated arrays for multiple coherent interferers," *Signal Processing*, vol. 57, pp. 177–194, 1997.

[55] S. Simanapalli and M. Kaveh, "Broadband focusing for partially adaptive beamforming," *IEEE Trans. Aerosp. Electron. Sys.*, vol. 30, pp. 68–79, Jan. 1994.

[56] D.B. Ward, "Technique for broadband correlated interference rejection in microphone arrays," *IEEE Trans. Speech and Audio Proc.*, vol. 6, pp. 414–417, July 1998.

[57] S. Haykin, Ed., *Advances in Spectrum Analysis and Array Processing*, Prentice Hall, New Jersey, 1991.

[58] M.S. Brandstein, *A Framework for Speech Source Localization Using Sensor Arrays*, Ph.D. thesis, Brown University, May 1995.

Chapter 2

Theory of Modal Analysis of Beamforming

2.1 Introduction

At the physical level, beamforming is characterized by the classical wave equation. The general solution to the wave equation can be decomposed into *modes* which are orthogonal functions of the spatial coordinates. These modes exhibit interesting mathematical properties and form a useful basis set to analyze and synthesize an arbitrary wavefield or a spatial response of a beamformer. In this chapter, we derive expressions for the modes and package them as a set of tools called *modal analysis techniques*. These techniques will be used in subsequent chapters to solve associated problems in beamforming and array signal processing.

In the antenna literature, these modes have been used to synthesize antenna shapes [1, 2], to represent electromagnetic fields radiated by circular antennas [3], and to compute antenna couplings [4]. However, this previous work is limited to specific applications. There does not seem to have been a more general application of classical modal decomposition to array signal processing, especially in the way developed in this thesis.

We preview the contents of this chapter by section. Section 2.2 describes how we represent a space-time signal and the coordinate system we use throughout the thesis. We consider the classical wave equation in Section 2.3 and establish the notion of modes of the wave equation solution. In Section 2.4, we use these modes to find a novel representation for beampatterns, which is valid both in the farfield and the nearfield of the array, and enables us to analyze and synthesize beampatterns. Parseval's relation is used in Section 2.5 to quantify the error involved using a finite

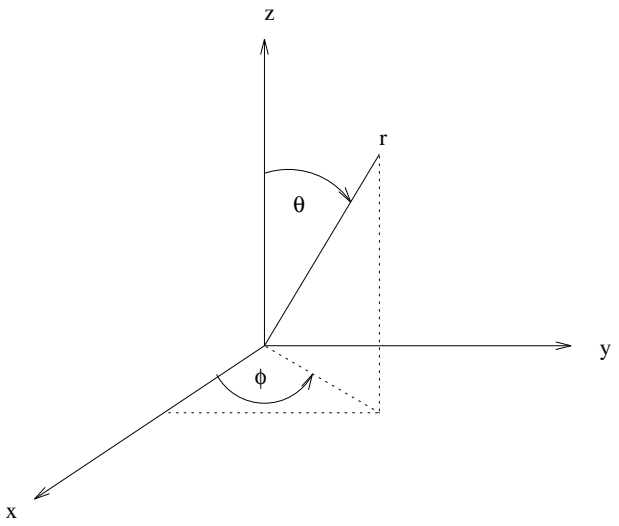

Figure 2.1: Spherical coordinate system.

number of modes in the new representation. In Section 2.6 we analyze the spatial response of an arbitrary aperture using these modes. A summary is included in Section 2.7.

2.2 Coordinate Systems

In this thesis, we use a three-dimensional spherical coordinate system to represent space, with time being the fourth dimension. Here a point in the space is represented by its distance r from the origin, its elevation θ from the vertical axis and azimuth ϕ within an equatorial plane containing the origin (Figure 2.1), and a space-time signal is written as $s(r, \theta, \phi, t)$. The spherical coordinates of a point are related to the (x, y, z) right-handed Cartesian coordinates by the simple trigonometric formulae:

$$\begin{aligned} x &= r \sin\theta \cos\phi \\ y &= r \sin\theta \sin\phi \\ z &= r \cos\theta. \end{aligned}$$

We also use the position vector $\boldsymbol{x}$ to denote the triple of spatial variables (r, θ, ϕ) or (x, y, z). Using this notation we can write a space-time signal as $s(\boldsymbol{x}, t)$. Also

let

$$\hat{\boldsymbol{x}} = \frac{\boldsymbol{x}}{\|\boldsymbol{x}\|} \tag{2.1}$$

be a unit vector in the direction of $\boldsymbol{x}$, where $\|\cdot\|$ denotes the vector 2-norm. We use either (θ, ϕ) or $\hat{\boldsymbol{x}}$ to represent a direction. For example, if there is a function f that depends on θ and ϕ, then we write it as either $f(\theta, \phi)$ or $f(\hat{\boldsymbol{x}})$; both representations are equivalent.

There are other various coordinate systems such as cylindrical and elliptical coordinate systems which may be convenient choices under different circumstances. However, the spherical coordinate system has a special place in this thesis since much of the theory developed is heavily dependent on it. We try to use a coordinate-independent representation $\boldsymbol{x}$ when the relevant theory is independent of the coordinate system.

2.3 Wave Equation

2.3.1 Background

The classical wave equation is one of the fundamental equations in array signal processing. It governs how signals pass from a source radiating energy to a sensor. Array processing algorithms attempt to extract information such as source location from propagating waves. To do this they rely on an accurate characterization of how the medium affects propagation through the wave equation for a given source-medium-sensor situation. Thus, array processing or beamforming algorithms are characterized by the wave equation at the physical level.

Here we study the solution to the wave equation in detail and exploit it to develop *modal analysis techniques* which provide insight into the intrinsic structure of the general broadband beamforming problem highlighted in Chapter 1. In the subsequent chapters, we make use of these modal analysis techniques to solve the various aspects of general array and aperture processing problems.

2.3.2 Reduced Wave Equation

The physics of sound propagation is described by the scalar wave equation given by

$$\nabla^2 s = \frac{1}{c^2}\frac{\partial^2 s}{\partial t^2} \tag{2.2}$$

where ∇^2 is the *Laplacian* which can be expressed in a chosen coordinate system, c is the speed of wave propagation, $s \equiv s(\boldsymbol{x}, t)$ is the scalar wave field (such as sound pressure) at a point $\boldsymbol{x}$ and time t. Conventionally, it is assumed that the wavefield $s(\boldsymbol{x}, t)$ has a time-harmonic dependence [5, p. 48], that is,

$$s(\boldsymbol{x}, t) = b(\boldsymbol{x}; \omega)e^{i\omega t} \tag{2.3}$$

where b is the space dependent part of the wavefield, ω is the radian frequency and $i = \sqrt{-1}$. For broadband signal environment, an arbitrary time dependent solution $s(\boldsymbol{x}, t)$ can be obtained by using the *principle of linear superposition* as

$$s(\boldsymbol{x}, t) = \int_{-\infty}^{\infty} b(\boldsymbol{x}; \omega)e^{i\omega t} d\omega. \tag{2.4}$$

Note that $s(\boldsymbol{x}, t)$ and $b(\boldsymbol{x}; \omega)$ in (2.4) form a Fourier Transform pair.

In the context of this thesis, we are more interested in space-dependent part of the solution $b(\boldsymbol{x}; \omega)$, which we relate to beampatterns and spatial responses of apertures. Substituting (2.3) into the time-dependent wave equation given by (2.2) yields

$$\nabla^2 b + k^2 b = 0 \tag{2.5}$$

which is the time-independent *reduced wave equation* or *Helmholtz equation* [6], where k is the *wavenumber* which is given by

$$k = \frac{\omega}{c} = \frac{2\pi}{\lambda},$$

and λ is the wavelength. We assume that the propagation speed c is independent of frequency, implying k is a constant multiple of radian frequency ω. For this reason, throughout this thesis we will often refer to k as "frequency".

In the following subsection we solve the Helmoltz equation in the spherical coordinate system to obtain the space dependent part of the solution $b(\boldsymbol{x}; \omega)$.

2.3.3 Solution in Spherical Coordinate System

The Helmoltz wave equation (2.5) can be expressed in spherical coordinates as

$$\frac{1}{r^2}\frac{\partial}{\partial r}\big(r^2\frac{\partial b}{\partial r}\big) + \frac{1}{r^2\sin\theta}\frac{\partial}{\partial\theta}\big(\sin\theta\frac{\partial b}{\partial\theta}\big) + \frac{1}{r^2\sin^2\theta}\frac{\partial^2 b}{\partial\phi^2} + k^2 b = 0, \tag{2.6}$$

where $b = b(r,\theta,\phi;k)$ is the wavefield at a point (r,θ,ϕ) for frequency k. The solution of (2.6) is classical [7,8] and a general solution, $b(r,\theta,\phi;k)$, can be written as linear combinations of modes of the form

$$r^{-\frac{1}{2}}\begin{matrix}J_{n+\frac{1}{2}}(kr)\\ N_{n+\frac{1}{2}}(kr)\end{matrix} P_n^m(\cos\theta)\begin{matrix}\cos m\phi\\ \sin m\phi\end{matrix} \tag{2.7}$$

where n and $m\,(n > m)$ are non-negative integers that index the modes, $P_n^m(\cdot)$ is the associated Legendre function; $J_{n+\frac{1}{2}}(\cdot)$ is the half odd integer order Bessel Function of the first kind and $N_{n+\frac{1}{2}}(\cdot)$ is the half odd integer order Neumann Function (or Bessel Function of the second kind) [8]. Note that in (2.7) either the upper or lower function in the r and ϕ portions can be taken, leading to four possibilities. The lack of an option for the θ portion is based on physical grounds related to the associated Legendre functions of the second kind being unbounded for certain arguments [9]. Finally, when $m = 0$ the associated Legendre function is called the Legendre function $P_n(\cdot)$ [8,9].

In this work we use complex combinations of the classical modes (2.7) which leads to a more suitable engineering formulation. We have, equivalent to (2.7),

$$r^{-\frac{1}{2}}\begin{matrix}H^{(1)}_{n+\frac{1}{2}}(kr)\\ H^{(2)}_{n+\frac{1}{2}}(kr)\end{matrix} P_n^{|m|}(\cos\theta)\,e^{im\phi},\ n\in\mathbb{Z},\ m\in\mathbb{Z}\text{ and }n > |m| \tag{2.8}$$

where $|\cdot|$ denotes the absolute value and the radial dependency now comes through the half odd integer order Hankel Functions of the first kind and second kind, respectively

$$H^{(1)}_{n+\frac{1}{2}}(\cdot) \triangleq J_{n+\frac{1}{2}}(\cdot) + i\,N_{n+\frac{1}{2}}(\cdot) \tag{2.9a}$$

$$H^{(2)}_{n+\frac{1}{2}}(\cdot) \triangleq J_{n+\frac{1}{2}}(\cdot) - i\,N_{n+\frac{1}{2}}(\cdot) \tag{2.9b}$$

which form a complex conjugate pair [9].

Note that in (2.8), the half odd integer order Hankel Functions of the first kind are associated with waves propagating away from the origin, whereas the second

kind are associated with waves propagating towards the origin. For the problems considered in this thesis, it is sufficient to consider either waves propagating generally towards the origin or away from the origin; we only consider the waves propagating toward the origin, i.e., the lower mode of (2.8). This option gives us the modes of the solution at a point (r, θ, ϕ) on a surface of an enclosure, where the origin is inside the enclosure and all sources of interest are outside of the enclosure.

For notational convenience, we use the *spherical Hankel function* of the second kind $h_n^{(2)}(kr)$ which is defined as

$$h_n^{(2)}(kr) = \sqrt{\frac{\pi}{2kr}}\, H^{(2)}_{n+\frac{1}{2}}(kr). \tag{2.10}$$

instead of the factor $r^{-\frac{1}{2}} H^{(2)}_{n+\frac{1}{2}}(kr)$ in (2.8).

Another observation regarding (2.8) is that the associated Legendre functions $P_n^{|m|}(\cos\theta)$ and exponential functions $e^{im\phi}$ are two different sets of orthogonal functions. The orthogonality property of the associated Legendre function is [10, p. 117]

$$\int_{-1}^{1} P_n^{|m|}(\cos\theta)\, P_{n'}^{|m|}(\cos\theta) d(\cos\theta) = \frac{2}{2n+1}\frac{(n+|m|)!}{(n-|m|)!}\,\delta_{nn'}, \tag{2.11}$$

and that of exponential functions is

$$\int_0^{2\pi} e^{im\phi}\, e^{-im'\phi}\, d\phi = 2\pi\delta_{mm'}, \tag{2.12}$$

where n, n', m and m' are integers and the *Kronecker symbol*

$$\delta_{mn} \triangleq \begin{cases} 0 & \text{if } m \neq n \\ 1 & \text{if } m = n. \end{cases}$$

Observe that both the associated Legendre and exponential functions are not orthonormal. Therefore, to simplify the beampattern formulation in the next section, we merge these two functions to define the following orthonormal function

$$Y_{nm}(\theta, \phi) \triangleq \sqrt{\frac{2n+1}{4\pi}\frac{(n-|m|)!}{(n+|m|)!}}\, P_n^{|m|}(\cos\theta)\, e^{im\phi} \tag{2.13}$$

for $m = -n, \ldots, n$, $n = 0, 1, 2, \ldots$. Using (2.11) and (2.12), it can be proved that

$$\int_0^{2\pi} \int_{-1}^{1} Y_{nm}(\theta, \phi)\, Y^*_{n'm'}(\theta, \phi)\, d(\cos\theta) d\phi = \delta_{nn'}\,\delta_{mm'} \tag{2.14}$$

where * denotes complex conjugate. In the acoustic literature the functions $Y_{nm}(\cdot)$ are known as *spherical harmonics* [11, p. 121].

We use (2.10), (2.13, and the lower modes of (2.8) to rewrite the basic solution of the Helmoltz wave equation (2.5) as

$$h_n^{(2)}(kr)\, Y_{nm}(\theta, \phi) \tag{2.15}$$

which we refer to as modes of the solution. Now we can write the general solution of the Helmoltz wave equation by combining all possible modes of (2.15) as

$$b(r, \theta, \phi; k) = \sum_{n=0}^{\infty} \sum_{m=-n}^{m} \alpha_{nm}(k)\, h_n^{(2)}(kr)\, Y_{nm}(\theta, \phi) \tag{2.16}$$

where $\alpha_{nm}(k)$ is a set of frequency dependent modal coefficients. Thus (2.16) can be used to write an arbitrary solution to the wave equation in terms of spatial variables r, θ, ϕ and frequency k. In the following section we show how to use this modal representation of the wave equation solution to represent an arbitrary beampattern.

2.4 Beampattern Formulation

2.4.1 Preliminaries

In this section we develop a novel representation for beampatterns using the modes of the solution to the Helmoltz wave equation which we have developed in the previous section. In the engineering literature, this detail of modeling is usually unnecessary as much simpler formulations can be made exploiting the common array geometries (typically equally spaced sensors in a straight line), phasor representations (where the time dependence through the frequency of modulation is not explicitly indicated), and farfield data (facilitating the use of the Fourier Transform). In our work, we find a general representation for a beampattern in terms of the modes (2.15) of the wave equation, and explore it to develop novel beamformers and array processing algorithms. Particularly, we seek a solution to the difficult nearfield broadband beamforming problem, which is one of the the main problems addressed in this thesis, using the beampattern representation developed in this section.

A beampattern can be defined as the spatial response of a beamformer. If the signal processing associated with the beamformer is linear, then the beampattern is

equal to the linearly weighted or filtered sum of the received signals at each sensor (or at each point of the sensor in a case of a distributed sensor[1]) from a point source in space. Since a received signal at a sensor satisfies the wave equation, using the linearity of the wave equation, we can claim that the beampattern of a linear beamformer is also a solution of the Helmoltz wave equation (2.5). Thus we assert that an arbitrary beampattern can be expressed by the general solution of the Helmoltz wave equation (2.16).

2.4.2 Nearfield and Farfield Beampatterns

In the classical beamforming literature, nearfield and farfield operation of beamformers are considered separately [12, p. 57-62], and the beamforming algorithms vary accordingly. In this thesis, our primary aim is to develop general beamforming theory which can be applied to both nearfield and farfield operation of beamformers. Hence we seek a representation of beampatterns that is valid for both nearfield and farfield beamformers.

Observe that the magnitude of each of the modes in (2.15) decays to zero as r approaches infinity. This can be gleaned from the following asymptotic form of the half integer order Hankel Function of the second kind [13, p. 692],

$$h_n^{(2)}(kr) = i^{n+1}\frac{1}{kr}\,e^{-ikr} \quad \text{as } r \to \infty. \tag{2.17}$$

Hence from (2.16) every wave equation solution $b(r,\theta,\phi;k)$ has this property. It is desirable to normalize the modes (2.15) so that we can represent both nearfield (r finite) and farfield (r infinite) beampatterns in one formulation. Hence we define a beampattern through

$$b_r(\theta,\phi;k) \triangleq re^{ikr}b(r,\theta,\phi;k), \tag{2.18}$$

and the normalized modes of the beampattern are given by

$$R_n(r,k)\,Y_{nm}(\theta,\phi), \tag{2.19}$$

where

$$R_n(r,k) \triangleq re^{ikr}\,h_n^{(2)}(kr). \tag{2.20}$$

[1] A distributed sensor can be considered as the limiting case of having an infinite number of discrete sensors (with attached filters) closely packed together.

Now, the magnitude of the normalized modes (2.19) remains finite at infinity, since

$$\lim_{r\to\infty} R_n(r,k) = \frac{i^{n+1}}{k}. \tag{2.21}$$

2.4.3 Analysis and Synthesis Equations

Using (2.16) and (2.18), we write an arbitrary beampattern

$$b_r(\theta,\phi;k) = \sum_{n=0}^{\infty}\sum_{m=-n}^{m} \alpha_{nm}(k)\, R_n(r,k)\, Y_{nm}(\theta,\phi) \tag{2.22}$$

where the complex constants $\alpha_{nm}(k)$ characterize the beampattern. Given a set of modal coefficients $\{\alpha_{nm}(k)\}$, one can synthesis a beampattern (2.22), thus we call it the *synthesis equation*.

Note that we only consider the spherical Hankel function of second kind in the beampattern representation (2.22). This representation is therefore valid on a manifold (typically sphere) that encapsulates but does not penetrate the physical aperture.

Assume that the beampattern $b_r(\theta,\phi;k)$ is given on a sphere of radius r, then we can find an expression for the modal coefficients $\alpha_{nm}(k)$ as follows:
Multiplying (2.22) with $Y^*_{n'm'}(\theta,\phi)\sin\theta$ and integrating with respect to θ and ϕ gives

$$\int_0^{2\pi}\int_0^{\pi} b_r(\theta,\phi;k) Y^*_{n'm'}(\theta,\phi)\sin\theta d\theta d\phi = \sum_{n=0}^{\infty}\sum_{m=-n}^{m} \alpha_{nm}(k)\, R_n(r,k) \int_0^{2\pi}\int_0^{\pi} Y_{nm}(\theta,\phi)\, Y^*_{n'm'}(\theta,\phi)\sin\theta d\theta d\phi.$$

Using (2.14), we can conclude that

$$\alpha_{nm}(k) = \frac{1}{R_n(r,k)}\int_0^{2\pi}\int_0^{\pi} b_r(\theta,\phi;k) Y^*_{n'm'}(\theta,\phi)\sin\theta d\theta d\phi. \tag{2.23}$$

Division by $R_n(r,k)$ is justified by the fact that there is no nonnegative integer n and no real numbers $r > 0$ and $k > 0$ such that $R_n(r,k) = 0$. This result follows from the fact that there are no common zeros for the functions $J_{n+\frac{1}{2}}(r)$ and $N_{n+\frac{1}{2}}(r)$ [14, p. 30].

The equations (2.22) and (2.23) form an orthogonal transform pair which is analogous to the familiar Fourier series and its coefficients. Consequently, they

possess a number of useful properties such as linearity and a Parseval's relation. In Section 2.5, we explicitly give the Parseval's relation which is useful to measure the error associated in a truncated beampattern representation of (2.22).

For a given beamformer, the modal coefficients $\alpha_{nm}(k)$ are dependent on the sensor geometry and the structure of the beamformer. We will derive expressions for $\alpha_{nm}(k)$ in terms of the physical aperture and the associated beamformer structure in Section 2.6.

2.4.4 Elementary Beamshapes

As we have seen by (2.22), any physically realizable beampattern can be constructed by combining modes of (2.19). Inversely, an arbitrary beampattern can be decomposed into modes by (2.23). Therefore, one can consider these modes (2.19) as *elementary beampatterns*. Also note that the shape of the mode (2.19) is determined entirely by the function $Y_{nm}(\theta, \phi)$ and the complex function $R_n(r, k)$ is clearly separated from it. Recognizing the above fact, we denote functions $Y_{nm}(\theta, \phi)$ *elementary beamshapes*. These are elementary because any arbitrary beampattern can be expressed as a linearly weighted sum of elementary beamshapes.

Some examples of the lower order elementary beamshapes $Y_{nm}(\theta, \phi)$ for $m = 0$ (which implies the shape is invariant with ϕ) are illustrated in Figure 2.2 where the magnitude of $Y_{nm}(\theta, \phi)$ is plotted against θ.

2.4.5 Radially Invariant Beampatterns

As a simple illustration of the modal representation (2.22), we now introduce a novel class of beampatterns which are radially invariant with respect to their shape. A radially shape invariant beampattern $b_r(\theta, \phi; k)$ has the following property: For $r_A, r_B > 0$, $\theta \in [0, \pi]$ and $\phi \in [0, 2\pi)$ there exists a complex constant $C \equiv C(r_A, r_B)$ such that

$$b_{r_A}(\theta, \phi; k) = C\, b_{r_B}(\theta, \phi; k). \tag{2.24}$$

One such class of beampatterns can be found excluding all but a single index n in (2.22) as

$$b_r(\theta, \phi; k)_{\text{invariant}} = R_n(r, k) \sum_{m=-n}^{n} \alpha_{nm}(k) Y_{nm}(\theta, \phi), \tag{2.25}$$

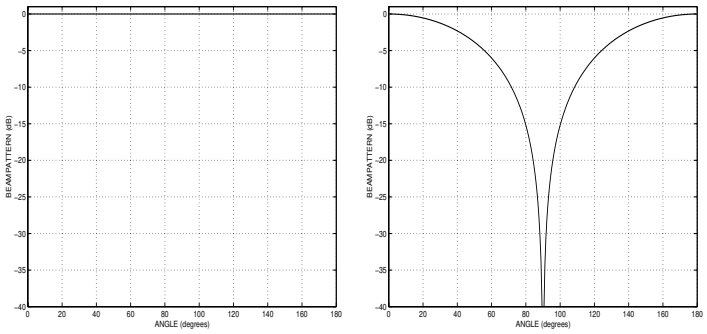

(a) mode: $m = 0, n = 0$ (b) mode: $m = 0, n = 1$

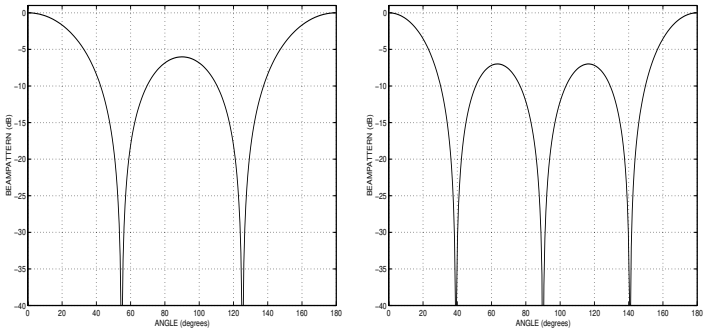

(c) mode: $m = 0, n = 2$ (d) mode: $m = 0, n = 3$

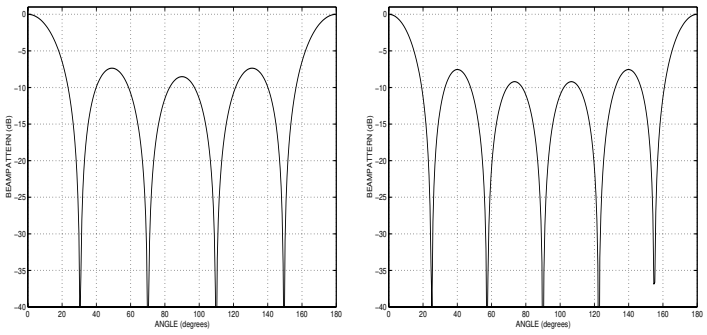

(e) mode: $m = 0, n = 4$ (f) mode: $m = 0, n = 5$

Figure 2.2: Magnitude of few lower order elementary beamshapes $Y_{nm}(\theta, \phi)$ (given by (2.13)) for $m = 0$ plotted against the angle θ.

where, in (2.24), the complex scaling factor $C = R_n(r_A, k)/R_n(r_B, k)$. Here, the shape of the beampattern is fixed with respect to radius r but its amplitude and phase are scaled with the radial distance from the array origin. However, this variation of phase and amplitude is the same for all angles. The beampattern class (2.25) covers only a subset of all possible arbitrary beampatterns (2.22). An example of a beampattern of the form (2.25) is illustrated in Figure 2.3. A drawback of this special class is that all radially invariant beam shapes of the form (2.25) need two-dimensional arrays except those trivial beam shapes such as omni-directional, dipole etc.

Simple design techniques such as the least squares may be applied to design beampatterns such as (2.25) with the resulting beamformer automatically inheriting the radial invariance property if the farfield pattern is accurately realized. We will not proceed how to realize radially invariant beampatterns in this thesis.

Keeping the same beampattern shape in both nearfield and farfield could be a useful solution to such problems such as microphone array design in teleconferencing rooms where the array needs to focus on a nearfield source (the talker) but to attenuate farfield interference (reverberation)[2].

Radially invariant beampatterns are only one of the possible applications of modal representation. In the remainder of this thesis we will illustrate how modal representation can be used to develop theory for more general broadband beamforming.

2.5 Parseval's Relation

The synthesis equation (2.22) usually requires an infinite number of terms to exactly characterize the beampattern. In this section, we establish a Parseval's relation to provide an expression for the error in beampattern power associated with using a finite number of modes in the synthesis equation. Determining the minimum number of modes to accurately model a specific beampattern is an essential component of an efficient numerical procedure.

Rewrite (2.22) and (2.23) as

$$b(\theta, \phi) = \sum_{n=0}^{\infty} \sum_{m=-n}^{n} A_{nm}\, Y_{nm}(\theta, \phi) \tag{2.26}$$

[2]This is referred as the mixed nearfield/farfield problem [15].

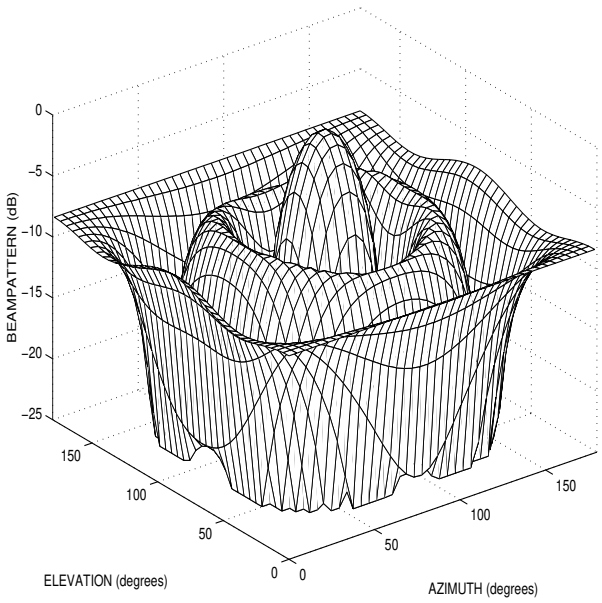

Figure 2.3: An example of a shape invariant beampattern given by (2.25): $n = 4$, $\alpha_{4(4)} = 0.05$, $\alpha_{4(3)} = 0$, $\alpha_{4(2)} = 0.35$, $\alpha_{4(1)} = 0$, $\alpha_{4(0)} = 7.0$, and $\alpha_{4(-m)} = \alpha_{4m}$.

and

$$A_{nm} = \int_0^{2\pi} \int_0^{\pi} b(\theta, \phi) Y_{nm}^*(\theta, \phi) \sin\theta d\theta d\phi \tag{2.27}$$

where $A_{nm} = R_n(r, k)\alpha_{nm}(k)$ and $b(\theta, \phi) = b_r(\theta, \phi; k)$. Although A_{nm} and $b(\theta, \phi)$ are functions of r and k, we suppress this dependence to simplify the notation.

We define the beampattern power on a sphere of radius r and frequency k as

$$\text{Beampattern Power} \triangleq \int_0^{2\pi} \int_{-1}^{1} \left| b(\theta, \phi) \right|^2 d(\cos\theta) d\phi, \tag{2.28}$$

where $b(\theta, \phi)$ is given by (2.26). Then we have the following proposition:

Proposition 2.1 *Let $b(\theta, \phi)$ be a beampattern specification on elevation θ and azimuth ϕ angles. Then,*

$$\int_0^{2\pi} \int_{-1}^{1} \left| b(\theta, \phi) \right|^2 d(\cos\theta) d\phi = \sum_{n=0}^{\infty} \sum_{m=-n}^{n} \left| A_{nm} \right|^2. \tag{2.29}$$

Proof of Proposition 2.1: Multiplying (2.26) by its complex conjugate and

integrating with respect to $\cos\theta$ and ϕ gives

$$\int_0^{2\pi}\int_{-1}^{1}|b(\theta,\phi)|^2 d(\cos\theta)d\phi = \sum_{n=0}^{\infty}\sum_{m=-n}^{n}\sum_{n'=0}^{\infty}\sum_{m'=n'}^{n'} A_{nm}A^*_{n'm'} \times \int_0^{2\pi}\int_{-1}^{1} Y_{nm}(\theta,\phi)Y^*_{n'm'}(\theta,\phi)d(\cos\theta)d\phi.$$

Use of the orthogonality property (2.14) to evaluate the above integral, establishes the result.

□

Given N, we approximate $b(\theta,\phi)$ by a finite series of the form

$$\hat{b}(\theta,\phi) = \sum_{n=0}^{N}\sum_{m=-n}^{n} \hat{A}_{nm}\, Y_{nm}(\theta,\phi), \tag{2.30}$$

where we wish to find the $\hat{A}_{nm}$'s that minimise the integral squared error between the desired beampattern $b(\theta,\phi)$ and the approximate beampattern $\hat{b}(\theta,\phi)$. As for the well known case of a finite Fourier series representation, the minimum squared beampattern error is obtained by setting $\hat{A}_{nm} = A_{nm}$, for $n = 0,\ldots,N$, $m = -n,\ldots,n$, and the residual error is then given by

$$\begin{aligned}\epsilon_N &= \int_0^{2\pi}\int_{-1}^{1} \left|b(\theta,\phi) - \hat{b}(\theta,\phi)\right|^2 d(\cos\theta)\, d\phi \\ &= \int_0^{2\pi}\int_{-1}^{1} \left|b(\theta,\phi)\right|^2 d(\cos\theta)\, d\phi - \sum_{n=0}^{N}\sum_{m=-n}^{n} \left|A_{nm}\right|^2 \\ &= \sum_{n=N+1}^{\infty}\sum_{m=-n}^{n} \left|A_{nm}\right|^2. \end{aligned} \tag{2.31}$$

Thus (2.31) gives the error associated with truncating the synthesis equation (2.26) to a finite number of terms.

The Parseval's relation (2.29) gives some engineering insights into the number of modes with significant power required to get a good beampattern match. In close analogy with frequency domain filter analysis we will see that the lower order modes are the significant ones which give the broad beampattern features (analogous to the lower frequencies in a filter design problem), while the higher order modes give the finer detail (analogous to higher frequencies in a filter design problem). We assert that sensible beampattern specifications should involve only the lower order

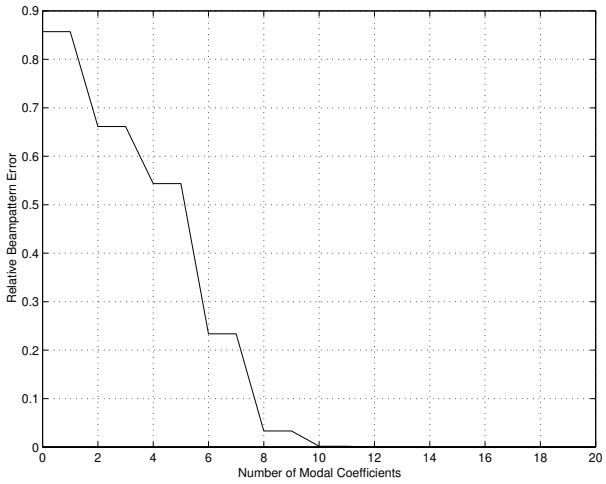

Figure 2.4: Relative beampattern error calculated from (2.31) for the example beampattern shown in Figure 2.5.

modes.

Parseval's Relation Example

We consider the beampattern of a simple narrowband beamformer to demonstrate the utility of the Parseval's relation. Consider a $(2Q+1)$ sensor linear array aligned with the z axis, with inter-sensor spacing of $\lambda/2$ where λ is the wavelength. In this case the beampattern is rotationally symmetric with respect to ϕ and can be expressed as $b(\theta,\phi) = b(\theta)$. The response of this beamformer to a point source in the farfield (farfield beampattern) is given by

$$b(\theta) = \sum_{q=-Q}^{Q} w_q e^{-i\pi q \cos\theta}, \tag{2.32}$$

where w_q is the weight attached to the qth sensor.

In this case, it can be shown that

$$\begin{aligned} \text{Beampattern Power} &= 2\pi \int_{-1}^{1} \left|b(\theta,\phi)\right|^2 d(\cos\theta), \\ &= 4\pi \sum_{q=-Q}^{Q} |w_q|^2. \end{aligned} \tag{2.33}$$

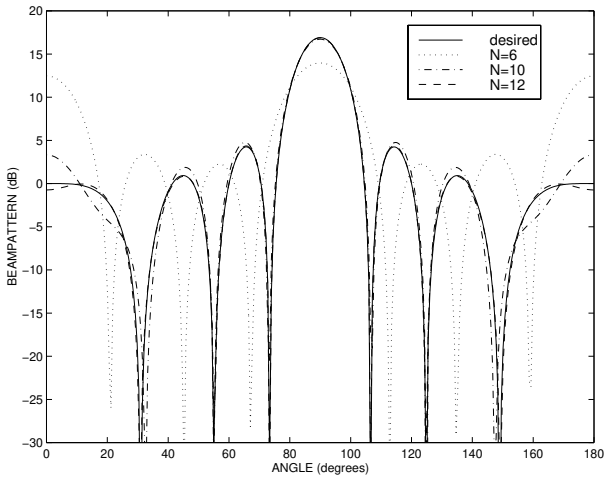

Figure 2.5: Approximate beampatterns of a 7-element linear array calculated from (2.26) for several different values of N. Also shown is the desired beampattern (2.32).

For this special case, $A_{nm} = 0$ for $m \neq 0$ in (2.27) and for $m = 0$

$$A_{n0} = 2\pi \int_0^{\pi} b(\theta) Y_{n0}^*(\theta, \phi) \sin\theta d\theta. \tag{2.34}$$

Generally the integration in (2.34) has to be evaluated numerically, but for the beampattern in this example, it can be done analytically. Using (2.32), (2.48) and (2.11) it can be shown that

$$A_{n0} = 2\sqrt{\pi(2n+1)}\, i^n \sum_{q=-Q}^{Q} w_q j_n(\pi q), \tag{2.35}$$

where $j_n(\cdot)$ is the spherical Bessel function of first kind (see 2.40). Figure 2.4 shows the relative beampattern error ($\triangleq \epsilon_N/(\text{Beampattern Power})$) versus the number of coefficients, calculated from (2.31) for the case of $Q = 3$ and $w_q = 1$ for $q = -Q, \ldots, Q$.

The approximate beampatterns calculated from (2.30) for several different values of N is shown in Figure 2.5. Also shown is the desired beampattern (2.32). Figure 2.4 shows that the use of 8 coefficient should be sufficient to obtain a beampattern with less than 5% beampattern error. This is confirmed by Figure 2.5 where the beampattern with 10 coefficients is almost same as the desired beampattern.

2.6 Modal Analysis of Aperture Response

In the previous sections we have formulated the modal representation to represent arbitrary beampatterns. Up to now we have not considered any beampattern corresponding to a physical aperture. In this section we consider the spatial response (beampattern) of an arbitrarily shaped continuous aperture and a set of arbitrarily located array of sensors. We show that the spatial responses of these physical apertures can also be expressed by the modal representation. Further we derive expressions for modal coefficients $\alpha_{nm}(k)$ in terms of the structure and geometry of the physical aperture. These results will be used in the subsequent chapters to solve the problems identified in the Chapter 1.

2.6.1 Point Source and a Point Sensor

Consider an omnidirectional point source located at a point $\boldsymbol{y} \in \mathbb{R}^3$ and a point sensor located at $\boldsymbol{x} \in \mathbb{R}^3$. Then the received signal at the sensor is given by

$$\bar{s}(\boldsymbol{x}, t) = \frac{\|\boldsymbol{y}\|}{\|\boldsymbol{y} - \boldsymbol{x}\|} \bar{s}_0\big(t - \frac{\|\boldsymbol{y} - \boldsymbol{x}\| - \|\boldsymbol{y}\|}{c}\big), \quad \boldsymbol{x} \neq \boldsymbol{y}, \tag{2.36}$$

where $\|\cdot\|$ denotes the vector 2-norm, and $\bar{s}_0(t)$ is the received signal at the origin of the coordinate system, c is the speed of wave propagation. Let $s_0(k)$ and $s(\boldsymbol{x}; k)$ be the Fourier transform of $\bar{s}_0(t)$ and $\bar{s}(\boldsymbol{x}, t)$, respectively. Then taking the Fourier transform of (2.36) with respect to t, we obtain

$$s(\boldsymbol{x}; k) = \Phi(\boldsymbol{x}, \boldsymbol{y}; k)\, s_0(k), \quad \boldsymbol{x} \neq \boldsymbol{y}, \tag{2.37}$$

where

$$\Phi(\boldsymbol{x}, \boldsymbol{y}; k) = \frac{\|\boldsymbol{y}\|}{\|\boldsymbol{y} - \boldsymbol{x}\|}\, e^{-ik(\|\boldsymbol{y}-\boldsymbol{x}\| - \|\boldsymbol{y}\|)}. \tag{2.38}$$

The function $\Phi(\boldsymbol{x}, \boldsymbol{y}; k)$ can be considered as the normalized transfer function between source and the sensor. It is also a solution of the Helmoltz wave equation (2.5) for a fixed $\boldsymbol{y}$, and is called the *fundamental solution* in the acoustic literature [6, p. 16].

The fundamental solution $\Phi(\boldsymbol{x}, \boldsymbol{y}; k)$ can also be expressed by a weighted sum of modes of the form (2.19). By manipulating some results in [6, p. 30], we can

show that for $\|\boldsymbol{y}\| > \|\boldsymbol{x}\|$

$$\Phi(\boldsymbol{x},\boldsymbol{y};k) = 4\pi(-i)k\|\boldsymbol{y}\|e^{ik\|\boldsymbol{y}\|}\sum_{n=0}^{\infty}\sum_{m=-n}^{n} h_n^{(2)}(k\|\boldsymbol{y}\|)\, j_n(k\|\boldsymbol{x}\|)\, Y_{nm}(\hat{\boldsymbol{y}})Y_{nm}^*(\hat{\boldsymbol{x}}), \tag{2.39}$$

where

$$j_n(r) \triangleq \sqrt{\frac{\pi}{2r}}J_{n+\frac{1}{2}}(r) \tag{2.40}$$

are the *spherical Bessel* functions, $h_n^{(2)}(\cdot)$ are the spherical Hankel functions as defined by (2.10) and $Y_{nm}(\cdot,\cdot)$ are the elementary beamshapes as defined by (2.13). We use (2.20) to write (2.39),

$$\Phi(\boldsymbol{x},\boldsymbol{y};k) = \sum_{n=0}^{\infty}\sum_{m=-n}^{n}\big[-4\pi ik\, j_n(k\|\boldsymbol{x}\|)\, Y_{nm}^*(\hat{\boldsymbol{x}})\big]R_n(\|\boldsymbol{y}\|,k)\, Y_{nm}(\hat{\boldsymbol{y}}), \quad \|\boldsymbol{y}\| > \|\boldsymbol{x}\|, \tag{2.41}$$

as a weighted sum of modes of the form (2.19).

Equation (2.41) takes a special place in this thesis: it will be used to convert any relationship involving the transfer function $\Phi(\boldsymbol{x},\boldsymbol{y};k)$ to modal representation. In the next section, we use it to find the modal representation of the spatial response of a continuous sensor and a set of arbitrarily located sensors.

To derive an alternative expression for (2.41), we use the addition theorem for Legendre functions [16, p. 360] to obtain the following relationship:

$$\sum_{m=-n}^{n} Y_{nm}(\hat{\boldsymbol{y}})Y_{nm}^*(\hat{\boldsymbol{x}}) = \frac{2n+1}{4\pi}P_n(\cos\gamma) \tag{2.42}$$

where γ denotes the angle between $\hat{\boldsymbol{x}}$ and $\hat{\boldsymbol{y}}$. By substituting (2.42) into (2.41) we obtain

$$\Phi(\boldsymbol{x},\boldsymbol{y};k) = \sum_{n=0}^{\infty}\big[-ik(2n+1)\, j_n(k\|\boldsymbol{x}\|)\big]R_n(\|\boldsymbol{y}\|,k)\, P_n(\cos\gamma), \quad \|\boldsymbol{y}\| > \|\boldsymbol{x}\|. \tag{2.43}$$

The expansion (2.43) is preferred over (2.39) when the array is linear[3].

[3]For a linear array aligned with the z axis, only the $m = 0$ modes are non-zero and $\gamma = \theta$ for points on the positive side of the z axis and $\gamma = -\theta$ for points on the negative side of the z axis.

Farfield Behaviour

Here we investigate the behaviour of the normalized transfer function between source and the sensor, $\Phi(\boldsymbol{x}, \boldsymbol{y}; k)$ when the source is in the farfield of the sensor. Let us consider the magnitude and phase of $\Phi(\boldsymbol{x}, \boldsymbol{y}; k)$ separately. Since $\|\boldsymbol{y}\| \gg \|\boldsymbol{x}\|$ for a farfield source, $\|\boldsymbol{y} - \boldsymbol{x}\| \approx \|\boldsymbol{y}\|$; thus from (2.38),

$$\lim_{\|\boldsymbol{y}\|\to\infty} \big|\Phi(\boldsymbol{x}, \boldsymbol{y}; k)\big| = \lim_{\|\boldsymbol{y}\|\to\infty} \frac{\|\boldsymbol{y}\|}{\|\boldsymbol{y} - \boldsymbol{x}\|} = 1. \tag{2.44}$$

On the other hand

$$\begin{aligned} \|\boldsymbol{y} - \boldsymbol{x}\| - \|\boldsymbol{y}\| &\sim \|\boldsymbol{x}\| \cos\gamma \quad \text{as } \|\boldsymbol{y}\| \to \infty \\ &= \boldsymbol{x} \cdot \hat{\boldsymbol{y}} \end{aligned} \tag{2.45}$$

where γ is the angle between $\boldsymbol{x}$ and $\hat{\boldsymbol{y}}$, and $\cdot$ denotes the vector inner product and $\hat{\boldsymbol{y}}$ is a unit vector pointing opposite to the direction of the propagation of waves. Thus, the phase of $\Phi(\boldsymbol{x}, \boldsymbol{y}; k) \to -\|\boldsymbol{x}\| \cos\gamma$ as $\|\boldsymbol{y}\| \to \infty$. Therefore, the normalized transfer function between a farfield source and a sensor is denoted and given by

$$\begin{aligned} \Phi_\infty(\boldsymbol{x}; k) &\triangleq \lim_{\|\boldsymbol{y}\|\to\infty} \Phi(\boldsymbol{x}, \boldsymbol{y}; k) \\ &= e^{-ik\|\boldsymbol{x}\|\cos\gamma} \\ &= e^{-ik\boldsymbol{x}\cdot\hat{\boldsymbol{y}}} \end{aligned} \tag{2.46}$$

From (2.41) and (2.21), the farfield transfer function can be written as

$$\begin{aligned} \Phi_\infty(\boldsymbol{x}; k) &= \sum_{n=0}^{\infty} \sum_{m=-n}^{n} \big[-4\pi i k\, j_n(k\|\boldsymbol{x}\|) Y_{nm}^*(\hat{\boldsymbol{x}}) \big]\, R_n(\infty, k)\, Y_{nm}(\hat{\boldsymbol{y}}) \\ &= \sum_{n=0}^{\infty} \sum_{m=-n}^{n} 4\pi i^n\, j_n(k\|\boldsymbol{x}\|) Y_{nm}^*(\hat{\boldsymbol{x}})\, Y_{nm}(\hat{\boldsymbol{y}}). \end{aligned} \tag{2.47}$$

Similarly, the alternative form (2.43) can be written

$$\begin{aligned} \Phi_\infty(\boldsymbol{x}; k) &= \sum_{n=0}^{\infty} \big[-ik(2n+1) j_n(k\|\boldsymbol{x}\|) \big]\, R_n(\infty, k)\, P_n(\cos\gamma) \\ &= \sum_{n=0}^{\infty} i^n (2n+1) j_n(k\|\boldsymbol{x}\|) P_n(\cos\gamma). \end{aligned} \tag{2.48}$$

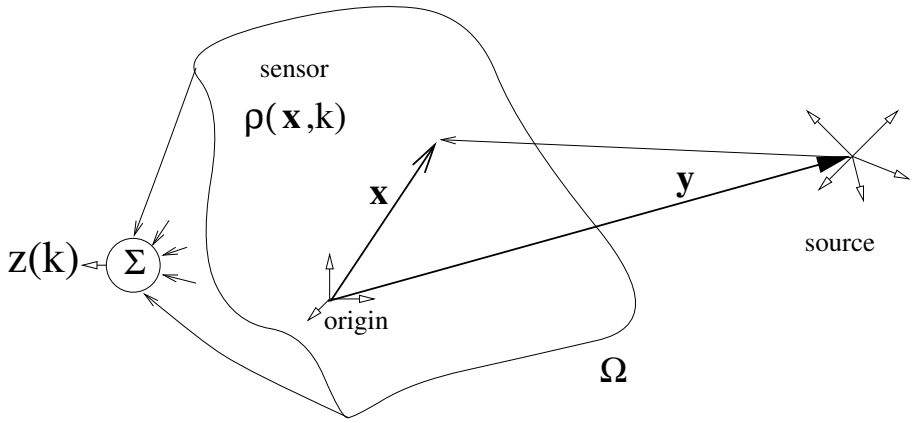

Figure 2.6: A diagram of a theoretical continuous sensor and a point source

In this subsection we have derived the transfer function between a point source and a point on an aperture. We also expressed this transfer function (for both farfield and nearfield sources) as a weighted sum of modes of the form (2.19). As we already highlighted in the Chapter 1, our approach to beamforming and array processing problems is to analyze them using the modal analysis techniques developed in this chapter. Thus, the modal representations (2.41), (2.43), (2.47) and (2.48) will be used throughout this thesis as key analysis tools.

2.6.2 Theoretical Continuous Sensor Response

In this section we express the spatial response of a continuous sensor in the modal representation form (2.22). We determine expressions for the modal coefficients $\alpha_{nm}(k)$ in terms of the physical parameters of the continuous sensor.

Consider a theoretical continuous sensor (see Figure 2.6) with an arbitrary shape and let the sensor be confined to a region $\Omega \subset \mathbb{R}^3$, $\boldsymbol{x} \in \Omega$ be a point on the sensor, and $\rho(\boldsymbol{x}; k) : \mathbb{R} \times \mathbb{R}^+ \to \mathbb{C}$ be the *aperture illumination* function (also called the *sensitivity distribution*). Aperture illumination $\rho(\boldsymbol{x}; k)$ can be interpreted as the sensor gain at point $\boldsymbol{x}$ at frequency k. In other words, we can view the continuous sensor as a distributed filter with filters $\rho(\boldsymbol{x}; k)$ attached to each point $\boldsymbol{x}$ on the sensor.

Let $s(\boldsymbol{x}; k)$ be the Fourier transform of the received signal at point $\boldsymbol{x}$ on the sensor. Then the sensor output in the frequency domain is defined and given by

$$z(k) = \int_{\Omega} \rho(\boldsymbol{x}; k)\, s(\boldsymbol{x}; k)\, d\boldsymbol{x}. \tag{2.49}$$

Suppose, there is a point source at $\boldsymbol{y} \in \mathbb{R}^3 \backslash \mathbb{B}$ where $\mathbb{B} = \{\boldsymbol{x} : \|\boldsymbol{x}\| < a\}$, $a \in \mathbb{R}$ and let $s_0(k)$ be the Fourier transform of the signal received from this source at the origin. Using (2.37) and (2.49) we write the output response of the continuous sensor to a point source at $\boldsymbol{y}$ as

$$z(k) = b(\boldsymbol{y}; k)\, s_0(k), \tag{2.50}$$

where

$$b(\boldsymbol{y}; k) = \int_\Omega \rho(\boldsymbol{x}; k)\, \Phi(\boldsymbol{x}, \boldsymbol{y}; k)\, d\boldsymbol{x}. \tag{2.51}$$

The function $b(\boldsymbol{y}; k)$ can be described as the spatial response or the beampattern of the continuous sensor. We now show that the beampattern $b(\boldsymbol{y}; k)$ can be expressed in the form of modal representation (2.22) using spherical coordinates instead of the vector notation.

By substituting (2.41) into (2.51) and interchanging summation and integration[4], we obtain

$$b(\boldsymbol{y}; k) = \sum_{n=0}^{\infty} \sum_{m=0}^{n} \alpha_{nm}(k) R_n(\|\boldsymbol{y}\|, k) Y_{nm}(\hat{\boldsymbol{y}}) \tag{2.52}$$

where

$$\alpha_{nm}(k) = -i4\pi k \int_\Omega \rho(\boldsymbol{x}; k)\, j_n(k\|\boldsymbol{x}\|) Y^*_{nm}(\hat{\boldsymbol{x}})\, d\boldsymbol{x}. \tag{2.53}$$

Note that if the point $\boldsymbol{y}$ is given by the polar coordinates (r, θ, ϕ), then we can replace $\|\boldsymbol{y}\|$ by r and $\hat{\boldsymbol{y}}$ by (θ, ϕ) in (2.52) to get the modal representation of the beampattern as in (2.22). Equation (2.53) provides us with an expression for the modal coefficients in terms of the physical structure of the aperture $\rho(\boldsymbol{x}; k)$.

2.6.3 Discrete Aperture Response

Consider several omnidirectional point sensors (*ideal sensors*) arbitrary placed in a closed spherical region $\Omega \in \mathbb{R}^3$ with radius a. Let the qth sensor be located at the position $\boldsymbol{x}_q \in \Omega$, $q = 0, \ldots, Q-1$, and let $w_q(k)$ be the complex weight at frequency k or the filter attached to the qth sensor. Then a discrete aperture

[4]The Parseval's relation (2.29) is applicable to the series modal expansion (2.41). Hence, the series (2.41) is uniformly convergent and we can safely interchange the summation and integration.

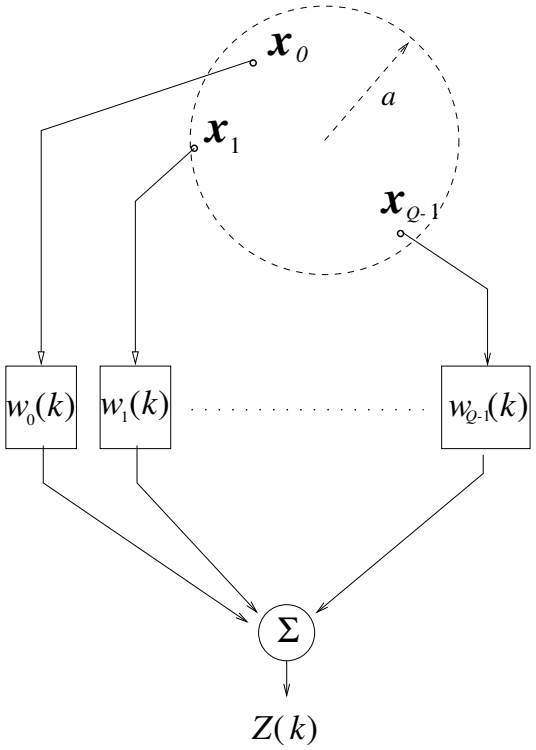

Figure 2.7: Arbitrarily placed set of discrete sensors and associated signal processing.

output is defined to be equal to the sum of filtered outputs of all sensors as shown in Figure 2.7.

Let $s(\boldsymbol{x}_q; k)$ be the Fourier transform of the received signal at the qth sensor. Then the array output is given by

$$z(k) = \sum_{q=0}^{Q-1} w_q(k) s(\boldsymbol{x}_q; k). \tag{2.54}$$

Suppose that there is a point source at $\boldsymbol{y} \in \mathbb{R}^3 \backslash \Omega$ and let $s_0(k)$ be the Fourier transform of the signal received from this source at the sensor origin. Using (2.37) and (2.54) we write the output of the discrete set of sensors to a point source at $\boldsymbol{y}$ as

$$z(k) = b(\boldsymbol{y}; k)\, s_0(k), \tag{2.55}$$

where

$$b(\boldsymbol{y};k) = \sum_{q=0}^{Q-1} w_q(k)\Phi(\boldsymbol{x}_q, \boldsymbol{y};k). \tag{2.56}$$

We can consider (2.56) as the spatial response of the discrete set of sensors. By substituting (2.41) into (2.56) we obtain the modal representation of the spatial response of the discrete aperture as

$$b(\boldsymbol{y};k) = \sum_{n=0}^{\infty} \sum_{m=-n}^{n} \alpha_{nm}(k) R_n(\|\boldsymbol{y}\|,k) Y_{nm}(\hat{\boldsymbol{y}}), \quad \|\boldsymbol{y}\| > a, \tag{2.57}$$

where

$$\alpha_{nm}(k) = -i4\pi k \sum_{q=0}^{Q} w_q(k)\, j_n(k\|\boldsymbol{x}_q\|) Y^*_{nm}(\hat{\boldsymbol{x}}_q), \tag{2.58}$$

and $R_n(\cdot,k)$ is given by (2.20).

Thus, equations (2.57) and (2.58) enable us to write the spatial response of a set of arbitrarily located sensors in form of the modal representation, where the modal coefficients are given in terms of the array geometry and its frequency dependent weights. This is another basic modal analysis result which we will use in the other chapters of this thesis to solve array processing problems.

2.7 Summary and Contributions

A set of modal analysis techniques has been established in this chapter to analyze and synthesize wavefields, beampattern specifications and spatial response of beamformers. These techniques will be exploited in the rest of the thesis to solve a wide class of beamforming and array processing problems.

We itemize some specific contributions made in this chapter:

i. A modal representation was proposed which can be used to represent both farfield and nearfield beampatterns. This includes (1) an analysis equation (2.23) to decompose an arbitrary beampattern (specification) into the modes of the wave equation, and (2) a synthesis equation (2.22) to construct any arbitrary beampattern using the modes.

ii. The notion of elementary beampatterns and elementary beamshapes has been

introduced.

iii. We showed that there is a class of beampatterns that are radially invariant with respect to their shape.

iv. The Parseval's relation was established to quantify the error in beampattern power associated with using a finite number of modes in the synthesis equation.

v. The transfer function between a point source (either in the nearfield or farfield of the aperture) and a point in an aperture was expressed as a weighted sum of modes.

vi. The spatial response of a physical aperture (continuous or discrete) was expressed in the form of a modal representation and an expression for the modal coefficients was derived in terms of the physical aperture structure (its geometry and associated signal processing).

References

[1] R.J. Garbacz and D.M. Pozar, "Antenna shape synthesis using characteristic modes," *IEEE Trans. Antennas Propagat.*, vol. AP-30, pp. 340–350, May 1982.

[2] F.J. Harackiewicz and D.M. Pozar, "Optimum shape synthesis of maximum gain omnidirectional antennas," *IEEE Trans. Antennas Propagat.*, vol. AP-34, pp. 254–258, Feb. 1986.

[3] L.W. Liand M.S. Leong, P.S. Kooi, and T.S. Yeo, "Exact solutions of electromagnetic fields in both near and far zones radiated by thin circular-loop antennas: A general representation," *IEEE Trans. Antennas Propagat.*, vol. 45, no. 12, pp. 1741–1748, Dec. 1997.

[4] A.D. Yaghjian, "Efficient computation of antenna coupling and fields within the nearfield region," *IEEE Trans. Antennas Propagat.*, vol. AP-30, no. 1, pp. 113–128, Jan. 1982.

[5] L.J. Ziomek, *Fundamentals of Acoustic Field Theory and Space-Time Signal Processing*, CRC Press, Boca Raton, 1995.

[6] D. Colton and R. Kress, *Inverse Acoustic and Electromagnetic Scattering Theory*, Springer, New York, 1997.

[7] C.A. Coulson and A. Jeffrey, *Waves: A mathematical approach to the common types of wave motion*, Longman Group Ltd, London, 1977.

[8] G.R. Baldcock and T. Bridgeman, *The Mathematical Theory of Wave Motion*, Ellis Horwood Ltd, Chichester, England, 1981.

[9] M.R. Spiegel, *Mathematical Handbook of Formulas and Tables*, Schaum, McGraw-Hill, New York, 1968.

[10] T.M. MacRobert, *Spherical Harmonics: An Elementary Treatise on Harmonic Functions with Applications*, Pergamon Press, London, 1967.

[11] T. Jonsson and J. Yngvason, *Waves and Distributions*, World Scientific, Singapore, 1995.

[12] J.W. Goodman, *Introduction to Fourier Optics*, McGraw-Hill, San Francisco, 1968.

[13] E. Skudrzyk, *The Foundations of Acoustics*, Springer-Verlag, New York, 1971.

[14] N.W. McLachlan, *Bessel Functions for Engineers*, Oxford University Press, London, 1961.

[15] D.B. Ward and G.W. Elko, "Mixed nearfield/farfield beamforming: A new technique for speech acquisition in a reverberant environment," *Workshop on Applications of Signal Processing to Audio and Acoustics*, Oct. 1997.

[16] E.W. Hobson, *The Theory of Spherical and Ellipsoidal Harmonics*, Cambridge University Press, London, 1955.

Chapter 3

Nearfield Beamforming using Farfield Beamforming Techniques

3.1 Introduction

Nearfield beamforming is a neglected area in the array processing literature. There are several reasons for this neglect. Firstly, nearfield beamformer design is difficult compared to farfield beamformer design, since the impinging wavefront on the array is spherical from nearfield point sources in contrast to the planar wavefronts from farfield sources. Secondly, in traditional applications of array processing such as radar and sonar, sources are effectively in the farfield.

However for applications such as speech acquisition and medical imaging, the source of interest can be in the nearfield of the sensor array, and use of the farfield assumption may considerably degrade the performance of these systems. In this chapter, we use modal analysis techniques developed in Chapter 2 to establish several nearfield beamforming methods.

Since there are well established farfield beamforming methods, it would seem a worthwhile idea to transform a given nearfield beamforming problem to an equivalent farfield problem so that farfield techniques could be applied to solve the nearfield problem. This idea of *nearfield-farfield transformation* is well suited to design data-independent (fixed) nearfield beamformers. The same principle has been used for many years in the radio antenna community for reconstructing farfield antenna patterns from nearfield measurements [1], though these transformations are computationally involved. In this chapter, we propose exact techniques to transform a nearfield beampattern specification to an equivalent farfield beampattern specification.

One common method of nearfield beamforming is *nearfield compensation* (e.g., [2]) in which a delay correction is used on each sensor to account for the nearfield spherical wavefronts. This method depends on the array geometry, and takes its simplest form when the sensors are colinear. Even with the simplest array geometries, designs based on nearfield compensation tend only to achieve the desired nearfield beampattern over a limited range of angles because they focus the array to a single point in three dimensional space. We outline the nearfield compensation method in Section 3.2. Another nearfield compensation method is given in [3], where the curvature of the spherical wavefront is approximated by a quadratic surface over the array aperture. However, designs based on this quadratic compensation method tend only to achieve the desired nearfield beampattern over a limited angles closer to broadside and also ignore the variation of the magnitude with distance and angle. Other nearfield design methods exist that are based on numerical optimization (e.g., [4, 5]), and consequently provide little intuitive insight.

In this chapter, three novel nearfield beamforming methods are proposed in which a desired arbitrary beampattern may be produced using farfield design techniques. In the first method we use modal representation of beampatterns (developed in Chapter 2) to find an exact nearfield-farfield transformation method. The second transformation method, which is computationally simpler than the first, relies on the asymptotic equivalence up to complex conjugation of two transformation problems: (i) determining the nearfield performance of a desired beampattern specification in the farfield, and (ii) determining the equivalent farfield beampattern corresponding to a given desired beampattern specification in the nearfield. As a consequence of this relationship, we show that the computationally difficult nearfield-farfield transformation method may be circumvented by use of a simpler farfield to nearfield determination. Equally importantly we show that farfield techniques may be used directly to solve the nearfield beamformer design problem. Both of above design techniques can be applied to arbitrarily placed sensor geometries. The third and final nearfield design method is also computationally simple but valid only for linear (not necessarily uniformly spaced) arrays. The methodology uses the modal representation of a physical aperture and the concept of a continuous sensor to find a linear transformation between the array weights required to have the given beampattern for farfield and nearfield respectively.

This chapter is organized as follows: Section 3.2 outlines the nearfield compensation method of nearfield beamforming. A nearfield beamforming method based on an exact radial transformation of the beampattern between nearfield and farfield

is proposed in Section 3.3. Section 3.4 proposes a computationally simple nearfield beamforming method based on the radial reciprocity of beampatterns. A method based on a linear transformation between farfield and nearfield array weights is established in Section 3.5. A summary of this chapter is given in Section 3.6.

3.2 Nearfield Compensation Method

In this section, the compensation method [2] is outlined for designing nearfield beamformers based on applying time delays to compensate for the differing propagation delays, assuming spherical propagation.

In order to illustrate nearfield compensation, consider a narrowband linear array of Q sensors aligned with the z axis with a complex weight on each sensor. The normalized spatial response of the array to a signal from a point source at a distance r and angle θ (measured relative to endfire) from the zeroth sensor is (see Figure 2.1)

$$b_r(\theta;k) = \sum_{q=0}^{Q-1} w_q \frac{r}{d(r,\theta,z_q)}\, e^{-ik\left(d(r,\theta,z_q)-r\right)}, \tag{3.1}$$

where w_q is the complex weight on the qth sensor,

$$d(r,\theta,z_q) = \left[r^2 + 2r(z_q - z_0)\cos\theta + (z_q - z_0)^2\right]^{\frac{1}{2}} \tag{3.2}$$

is the distance from the source to the qth element, and z_q is the location of the qth element.

Compare (3.1) with the normalized response of the same array to a farfield source at an angle θ:

$$b_\infty(\theta;k) = \sum_{q=0}^{Q-1} w_q\, e^{-i2\pi k z_n \cos\theta}. \tag{3.3}$$

The goal of nearfield compensation is to transform the nearfield response to the farfield, such that standard farfield techniques can be used to design the array weights.

The compensated nearfield response of method [2] is

$$\hat{b}_r(\theta;k) = \sum_{q=0}^{Q-1} w_q \psi_q \frac{r}{d(r,\theta,z_q)}\, e^{-ik\left(d(r,\theta,z_q)-r\right)},$$

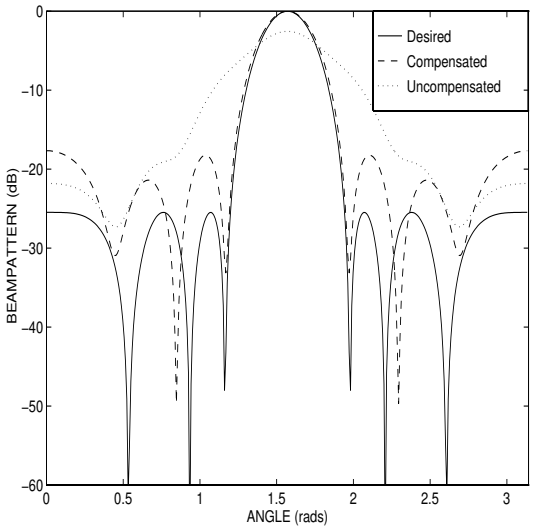

Figure 3.1: Comparison of compensated and uncompensated nearfield beampatterns for a desired Chebyshev 25 dB beampattern at a radius of 3 wavelengths from the centre of a 7-sensor array.

where

$$\psi_q = r^{-1} d(r, \gamma, z_q)\, e^{-ik\left(r - d(r,\gamma,z_q) + z_q \cos\gamma\right)}$$

is the qth compensation term and γ is the desired direction. It is seen that the compensated nearfield response is identical to the farfield response only at $\theta = \gamma$, and is approximately equal for angles close to γ. To design a nearfield beamformer with a desired response, the weights w_q are obtained using standard farfield design techniques. The resulting compensated nearfield response is then approximately equal to the designed farfield response, at least over a range of angles close to γ. This is illustrated in Figure 3.1 which shows a desired Chebyshev 25 dB response and the corresponding compensated nearfield response ($\gamma = \pi/2$) at a radial distance of 3 wavelengths from the centre of a 7-element array. Also shown is the uncompensated nearfield response (farfield design assumption). Clearly, nearfield compensation provides a significant improvement over an uncompensated array, although the compensated response still does not accurately achieve the desired response over all angles.

3.3 Radial Transformation

3.3.1 Preliminary

The nearfield compensation method is relatively straightforward to implement. However, the result achieved may fail to meet the desired design specification (particularly in the sidelobes) since it only achieves the performance in a single direction (see Figure 3.1). The nearfield beamforming method proposed in this section is to radially transform a nearfield beampattern specification to a physically equivalent farfield beampattern and design a farfield beamformer to realize this transformed farfield beampattern. This equivalence, which we establish later in this section, means that we can obtain the desired nearfield response for all angles. We use the modal representation of beampatterns (2.22) developed in Chapter 2 to perform this radial transformation at a given frequency. For broadband beamformer design, this transformation needs to be done for a number of frequencies over the design band.

3.3.2 Design Procedure

For convenience, we restate the synthesis (2.22) and analysis (2.23) equations of the modal representation of a beampattern developed in Chapter 2 as follows:

$$b_r(\theta,\phi;k) = \sum_{n=0}^{\infty} \sum_{m=-n}^{m} \alpha_{nm}(k)\, R_n(r,k)\, Y_{nm}(\theta,\phi), \tag{3.4}$$

$$\alpha_{nm}(k) = \frac{1}{R_n(r,k)} \int_0^{2\pi} \int_0^{\pi} b_r(\theta,\phi;k) Y_{nm}^*(\theta,\phi) \sin\theta d\theta d\phi, \tag{3.5}$$

where the radially dependent function $R_n(r,k)$ is given by (2.20) and the elementary beamshapes $Y_{nm}(\cdot,\cdot)$ are given by (2.13).

Since the modal coefficients $\alpha_{nm}(k)$ in the expansion (3.4) completely characterize the beampattern at all radial distances, the beampattern can be reconstructed for sources at arbitrary points in space. Because of the preferred choice of spherical coordinates, taking a nearfield beampattern specified on a sphere and subsequently transforming to the farfield infinite sphere leads to some computational savings in the above representations.

The utility of the radial beampattern transformation is as follows. Given a beampattern $b_{r_1}(\theta,\phi;k)$ measured at some radius r_1, calculate $\alpha_{nm}(k)$ from (3.5)

with $r = r_1$. The beampattern can now be reconstructed for a source at any radius r_2 by using (3.4) with $r = r_2$.

The method we propose to design a nearfield beamformer is outlined below.

1. Calculate the beampattern coefficients $\alpha_{nm}(k)$ for the desired nearfield beampattern $b_{r_\mathrm{d}}(\theta, \phi; k)$ using (3.5) with $r = r_\mathrm{d}$.

2. Calculate $b_\infty(\theta, \phi; k)$ from (3.4) at $r = \infty$.

3. Design a farfield beamformer to realize this beampattern using classical farfield array design techniques.

A curious feature of this formulation is that the actual array geometry is only of secondary importance. Any array geometry that can realize the resulting transformed farfield pattern may be used. This is important in a practical situation in which the array is mounted on a complex three dimensional manifold, such as a microphone array mounted on the curved dashboard of a car. The question of whether a specific array can realize a specific farfield beampattern is a separate issue and is not addressed in this section.

3.3.3 Nearfield/Farfield Equivalence

Since the solution to the Helmoltz wave equation (2.5) is unique, there is an equivalent farfield beampattern for every nearfield beampattern specification and vice versa. Hence, using the farfield beamformer (obtained in step 3 of Section 3.3.2 above) in the nearfield at $r = r_d$, will produce the desired nearfield beampattern $b_{r_d}(\theta, \phi; k)$. To see this formally, observe that the coefficients in (3.5) are uniquely and completely determined once the beampattern is specified. Using (3.4) and (2.21) in Chapter 2, we obtain the following farfield synthesis equation

$$b_\infty(\theta, \phi; k) = \frac{1}{k} \sum_{n=0}^{\infty} \sum_{m=-n}^{m} \alpha_{nm}(k)\, i^{n+1}\, Y_{nm}(\theta, \phi). \tag{3.6}$$

Equation (3.6) can be used in step 2 of the design procedure given in Section 3.3.2.

3.3.4 Linear Array

Motivation for Special Case

The radial transformation developed in the previous sub-sections is sufficiently general to capture quite arbitrary three-dimensional array geometries. In an attempt

to bring the results into focus and provide a more concrete presentation of the ideas, we examine a linear array aligned with the z axis. In this case, the beampattern is rotationally symmetric with respect to ϕ, and the beampattern can be expressed as $b_r(\theta, \phi; k) = b_r(\theta; k)$.

Radial Transformation

For this special case, the modal coefficients satisfy

$$\alpha_{nm}(k) = 0 \quad \text{for } m \neq 0,$$

that is, only the non-zero components are those for which $m = 0$. Hence we can write (3.4) and (3.5) in the following simplified form:

$$b_r(\theta; k) = \sum_{n=0}^{\infty} \alpha_n(k) R_n(r, k)\, Y_n(\theta) \tag{3.7}$$

and

$$\alpha_n(k) = \frac{2\pi}{R_n(r, k)} \int_0^{\pi} b_r(\theta; k) Y_n(\theta) \sin\theta \, d\theta, \tag{3.8}$$

where $\alpha_n(\cdot) \triangleq \alpha_{n0}(\cdot)$,

$$Y_n(\theta) \triangleq Y_{n0}(\theta, \phi) = \sqrt{\frac{2n+1}{4\pi}} P_n(\cos\theta), \tag{3.9}$$

and $P_n(\cdot)$ is the Legendre function. Using (2.21), the corresponding farfield synthesis equation for a linear array aligned with the z axis is given by

$$b_\infty(\theta; k) = \frac{1}{k} \sum_{n=0}^{\infty} \alpha_n(k)\, i^{n+1} Y_n(\theta). \tag{3.10}$$

Parseval Relation

We have developed the Parseval relation for the modal representation of beampatterns in the Section 2.5. Now we restate it here for the special case of a linear array

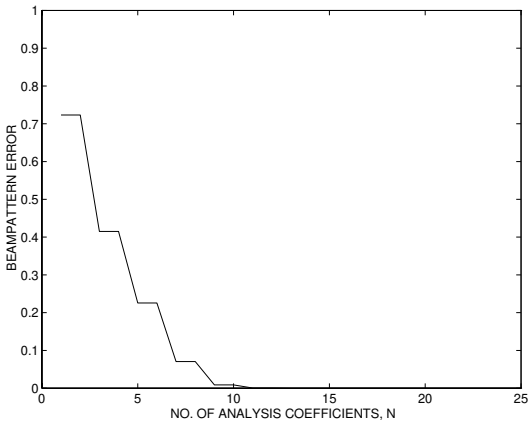

Figure 3.2: Relative beampattern error ϵ_N versus the number of analysis coefficients N, calculated from (3.12) for a Chebyshev 25 dB beampattern at a radial distance of 3 wavelengths.

aligned to the z axis. Specifically, (2.29) reduces to

$$2\pi \int_{-1}^{1} \left|b_r(\theta;k)\right|^2 d(\cos\theta) = \sum_{n=0}^{\infty} \left|R_n(r,k)\right|^2 \left|\alpha_n(k)\right|^2 \tag{3.11}$$

and the integral squared error between the desired beampattern $b_r(\theta;k)$ and an approximation using first $N+1$ terms of the series expansion (3.7) is given by

$$\epsilon_N = 2\pi \int_{-1}^{1} \left|b_r(\theta;k)\right|^2 d(\cos\theta) - \sum_{n=0}^{N} \left|R_n(r,k)\right|^2 \left|\alpha_n(k)\right|^2. \tag{3.12}$$

In the example of Section 3.3.5 to follow, we use (3.12) to quantify the error incurred by using a finite number of terms in (3.7) to approximate a given beampattern specification.

3.3.5 Example

To illustrate the radial beampattern transformation, we revisit our previous example in Section 3.2. The design was for a Chebyshev 25 dB beampattern (the desired beampattern in Figure 3.1) at a radius of $r = 3$ wavelengths.

The squared beampattern error versus the number of modal coefficients is calculated from (3.12) and is shown in Figure 3.2. It is clear from this plot that at least 10 analysis coefficients are required to provide a good approximation to the desired beampattern and 15 coefficients capture essentially all the energy. The

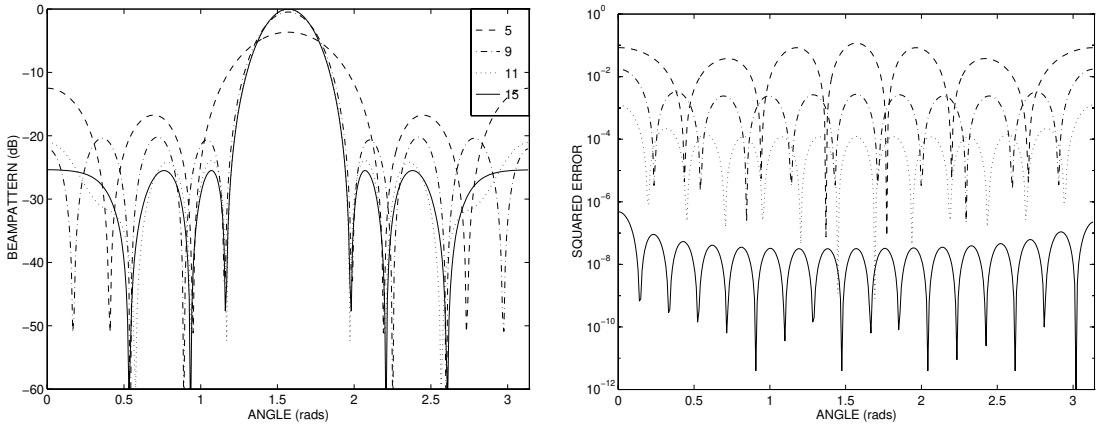

(a) Reconstructed beampatterns.

(b) Squared beampattern error.

Figure 3.3: (a) Reconstructed beampatterns using different numbers of analysis coefficients N for $N = 5, 9, 11, 15$, for a desired Chebyshev 25 dB beampattern at a radial distance of 3 wavelengths. (b) Squared error between the desired and reconstructed beampatterns.

monotonically decreasing property displayed in Figure 3.2 follows directly from (3.12).

To verify that the desired specification has been achieved, we calculated a set of 15 analysis coefficients from (3.8) at a radius of 3 wavelengths, and then reconstructed the nearfield beampattern from (3.7) using different numbers of analysis coefficients. The resulting beampatterns are shown in Figure 3.3, along with the squared error between the desired and reconstructed beampatterns. With 15 coefficients the reconstructed beampattern is indistinguishable from the desired Chebyshev 25 dB beampattern and the squared beampattern error is uniformly less than 10^{-6}.

Using the set of 15 coefficients, we transformed the desired nearfield beampattern to the farfield using (3.10). We then designed a farfield beamformer to achieve this beampattern using a complex-valued least squares design criterion [6]. The resulting beampattern realization for a symmetric linear array with 13 quarter wavelength spaced sensors is shown solid in Figure 3.4. (Note that a quarter-wavelength spaced array was used since we found that it provided a better approximation to the desired beampattern when used in the nearfield than a half-wavelength spaced array[1].) This farfield beamformer was then used in the nearfield at a radial dis-

[1]This is due to the reduction of spatial aliasing in the nearfield; see Appendix A for more detail.

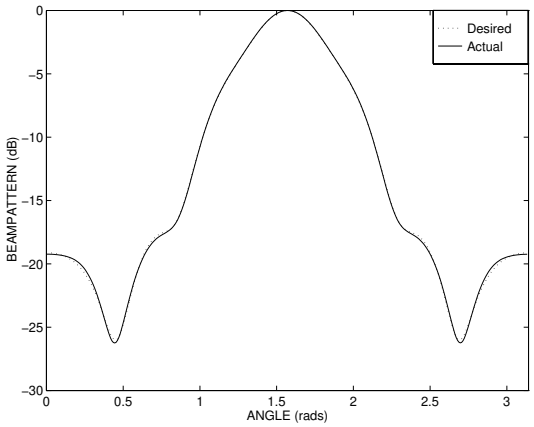

Figure 3.4: Transformed farfield beampattern corresponding to a desired Chebyshev 25 dB beampattern at $r = 3$ wavelengths (dotted), and realization using an array of 13 quarter-wavelength spaced sensors (solid). Phase has not been indicated.

tance of $r = 3$ wavelengths. The corresponding beampattern is shown solid in Figure 3.5, along with the desired nearfield beampattern shown dotted. The proposed nearfield beamforming method provides a very close approximation to the desired beampattern over all angles, not just at angles close to broadside as for the nearfield compensation method.

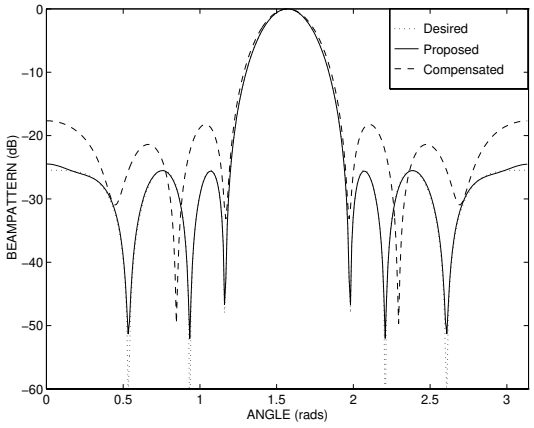

Figure 3.5: Resulting nearfield beampattern (solid) from the proposed nearfield beamforming design technique for a desired Chebyshev 25 dB beampattern (dotted) at a radius of 3 wavelengths. The beampattern of a beamformer designed using nearfield compensation is also shown (dashed) for comparison.

3.4 Radial Reciprocity

3.4.1 Preliminary

In this section, we use the modal analysis techniques developed in Chapter 2 as a theoretical tool to establish the asymptotic equivalence up to complex conjugation of two transformation problems: (i) determining the nearfield performance of a desired beampattern specification in the farfield, and (ii) determining the equivalent farfield beampattern corresponding to a given desired beampattern specification in the nearfield. As a consequence of this relationship, we show that the computationally difficult nearfield-farfield transformation developed in Section 3.3 and [7] may be circumvented, albeit with some approximation, by use of a simpler farfield to nearfield determination. Equally importantly we show that farfield techniques may be used directly to solve the nearfield beamformer design problem.

3.4.2 Radial Transformation and Reciprocity

Problem formulation

The objective is to relate a beampattern specification given on a sphere at one radius r_1 to a beampattern specification at a second radius r_2. This is achieved by beampattern analysis at r_1 (through (3.5)) and resynthesis at r_2 (through (3.4)). The key technical observation we make is that this problem is essentially identical to the problem of beampattern analysis at r_2 and resynthesis at r_1 (for a different solution to the wave equation), up to complex conjugation and an error term which is typically small for problems of interest. This result is far from intuitive and quite non-trivial to derive as we will see. This is exploited later in a nearfield design procedure, given in Section 3.4.3, that permits bypassing the computationally difficult analysis step (calculation of modal coefficients $\alpha_{nm}(k)$ for the desired nearfield beampattern) of the exact design method in Section 3.3.

Asymptotic Equivalence

Given that our key technical development is cast in terms of asymptotic equivalence, we present some concise definitions.

Let $g(x)$ and $f(x)$ be two complex functions of a real variable x within some real domain $\mathcal{D}$ both possessing limits as $x \to x_0$ in $\mathcal{D}$; then we say that $f(x) = O\big(g(x)\big)$ as $x \to x_0$ if there exist positive constants K and δ such that $|f| \leq K|g|$ whenever $0 < |x - x_0| < \delta$.

We say that $f(x)$ is *asymptotically equivalent* to $g(x)$ in the limit as $x \to x_0$ if f and g are such that $\lim_{x\to x_0} f/g = 1$. The notation in this case is $f(x) \sim g(x)$ as $x \to x_0$. As an example of asymptotic equivalence, we can write

$$h_n^{(2)}(kr) \sim i^{n+1} \frac{1}{kr} e^{-ikr} \quad \text{as } r \to \infty \tag{3.13}$$

which follows from (3.20), given later.

Hankel Function Property

Associated with a single mode indexed by n (and independent of m) we have a reciprocity relationship, given next. It is referred to as a reciprocity relationship because the radial behaviour relating an ordered pair of distances (r_1, r_2) for one beampattern problem can be related to the reversed ordered pair (r_2, r_1) of another beampattern problem, after complex conjugation and up to some error term related to the closeness of r_1 and r_2.

Proposition 3.1 *Consider the complex valued function*

$$R_n(r,k) = re^{ikr} h_n^{(2)}(kr) \tag{3.14}$$

where $h_n^{(2)}(\cdot)$ is the spherical Hankel functions of the second kind, n is the modal index, the wave number $k = 2\pi/\lambda$, and λ is the wavelength. Then

$$\frac{R_n(r_1,k)}{R_n(r_2,k)} = \frac{R_n^*(r_2,k)}{R_n^*(r_1,k)} \Big(1 + \epsilon(n, kr_1, kr_2)\Big) \tag{3.15}$$

where

$$\epsilon(n, kr_1, kr_2) = \frac{n(n+1)}{2k^2}\big(\frac{1}{r_2^2} - \frac{1}{r_1^2}\big) + O\big(\frac{1}{k^4 r^4}\big), \ \textit{as } r \to \infty \tag{3.16}$$

with $r = \min(r_1, r_2)$.

□

Proof of Proposition 3.1: The behaviour of $h_n^{(2)}(\cdot)$ is characterized through the recursion [8, p. 693]

$$h_{n+1}^{(2)}(x) = \frac{(2n+1)}{x} h_n^{(2)}(x) - h_{n-1}^{(2)}(x) \tag{3.17}$$

with

$$h_0^{(2)}(x) = \frac{i}{x}\, e^{-ix}.$$

From the recursion (3.17), and after some simplification it follows that

$$h_n^{(2)}(x) = \frac{i^{n+1}}{x} \underbrace{\Big(1 + \sum_{q=0}^{n} \frac{\xi_{q,n}}{(-ix)^q}\Big)}_{p_n(-ix)} e^{-ix} \tag{3.18}$$

for some n real valued coefficients $\xi_{q,n}$. These coefficients can be readily determined in the form

$$p_n(z) = 1 + \sum_{q=0}^{n} \frac{1}{2^q\, q!} \frac{(n+q)!}{(n-q)!} \frac{1}{z^q}, \tag{3.19}$$

leading to the asymptotic representation

$$h_n^{(2)}(x) = \frac{i^{n+1}}{x}\Big(1 + i\frac{1}{2x} n(n+1) - \frac{1}{8x^2}\frac{(n+2)!}{(n-2)!} + O\big(\frac{1}{x^3}\big)\Big)\, e^{-ix}, \tag{3.20}$$

as $x \to \infty$. From (3.14) and (3.18) we can also write

$$R_n(r,k) = \frac{i^{n+1}}{k}\, p_n(-ikr). \tag{3.21}$$

Of interest, in proving the proposition, is the square magnitude of the polynomial portion of the spherical Hankel function which can be written

$$\begin{aligned}\Big|1 + \sum_{q=0}^{n} \frac{\xi_{q,n}}{(-ix)^q}\Big|^2 &\triangleq 1 + \sum_{q=0}^{n} \frac{\eta_{q,n}}{x^{2q}} \\ &= 1 + \underbrace{(\xi_{1,n}^2 - 2\xi_{2,n})}_{\eta_{1,n}} \frac{1}{x^2} \\ &\quad + \underbrace{(\xi_{2,n}^2 + 2\xi_{4,n} - 2\xi_{1,n}\xi_{3,n})}_{\eta_{2,n}} \frac{1}{x^4} + O\big(\frac{1}{x^6}\big),\end{aligned}$$

where $\eta_{q,n}$ are suitable real valued coefficients. Whence, from (3.15),

$$1 + \epsilon(n, kr_1, kr_2) = \big|R_n(r_1,k)\big|^2 \big/ \big|R_n(r_2,k)\big|^2$$

$$
\begin{aligned}
&= \Big(1 + \frac{\eta_{1,n}}{(kr_1)^2} + \frac{\eta_{2,n}}{(kr_1)^4} + O\big(\frac{1}{(kr_1)^6}\big)\Big) \\
&\quad \Big/ \Big(1 + \frac{\eta_{1,n}}{kr_2^2} + \frac{\eta_{2,n}}{(kr_2)^4} + O\big(\frac{1}{(kr_2)^6}\big)\Big) \\
&= \Big(1 + \frac{\eta_{1,n}}{(kr_1)^2} + \frac{\eta_{2,n}}{(kr_1)^4} + O\big(\frac{1}{(kr_1)^6}\big)\Big) \\
&\quad \times \Big(1 - \frac{\eta_{1,n}}{(kr_2)^2} - \frac{\eta_{2,n}}{(kr_2)^4} + \frac{\eta_{1,n}^2}{(kr_2)^4} + O\big(\frac{1}{(kr_2)^6}\big)\Big) \\
&= 1 + \eta_{1,n}\big(\frac{1}{(kr_1)^2} - \frac{1}{(kr_2)^2}\big) + \eta_{2,n}\big(\frac{1}{(kr_1)^4} - \frac{1}{(kr_2)^4}\big) \\
&\quad + \eta_{1,n}^2 \frac{1}{(kr_2)^2}\big(\frac{1}{(kr_2)^2} - \frac{1}{(kr_1)^2}\big) + O\big(\frac{1}{r^6}\big)
\end{aligned}
$$

as $r \to \infty$, where $r = \min(r_1, r_2)$. Using (3.20) the first correction term has coefficient

$$\eta_{1,n} = \xi_{1,n}^2 - 2\xi_{2,n} = \frac{1}{2}n(n+1),$$

and this establishes the result.

□

We make the following observations regarding this result. We can take $r_1 = r < \infty$ and $r_2 = \infty$ to make the reciprocity between the nearfield and the farfield. The quantities in (3.15) are complex. However, the error $\epsilon(n, kr_1, kr_2)$ term is purely real, meaning the error is only in the magnitude or equivalently there is no error in the phase angle. This follows from the property $\arg(z_1/z_2) = \arg(z_2^*/z_1^*)$ where z_1 and z_2 are complex numbers.

Key Reciprocity Relationship

We now show how beampattern specification (analysis) at r_1 and resynthesis at r_2 relates to a conjugate beampattern specification (analysis) at r_2 and resynthesis at r_1, leading to Proposition 3.2 below. While modal techniques are used to establish the result, they are not needed to use the result.

Suppose we need to design a beamformer to have beam shape $b(\theta, \phi)$ specification at radius r_1 and frequency k. Then, using (3.4) and (3.5), we can write

$$b_{r_1}(\theta, \phi; k) = b(\theta, \phi) = \sum_{n=0}^{\infty} \sum_{m=-n}^{n} A_{nm}(b) Y_{nm}(\theta, \phi) \tag{3.22}$$

where

$$A_{nm}(b) = \alpha_{nm}(k)R_n(r,k) = \int_0^{2\pi}\int_0^{\pi} b(\theta,\phi)Y^*_{nm}(\theta,\phi)\sin\theta\, d\theta d\phi. \tag{3.23}$$

Note that $A_{nm}(b)$ depends only on beamshape specification $b(\theta,\phi)$ and not on radius r. Now the resultant beampattern of the above beamformer at distance r_2 is given by

$$\begin{aligned} b_{r_2}(\theta,\phi;k)\big|_{b_{r_1}=b} &= \sum_{n=0}^{\infty}\sum_{m=-n}^{n} \alpha_{nm}(k)\, R_n(r_2,k)Y_{nm}(\theta,\phi) \\ &= \sum_{n=0}^{\infty}\frac{R_n(r_2,k)}{R_n(r_1,k)}\sum_{m=-n}^{n} A_{nm}(b)\, Y_{nm}(\theta,\phi). \end{aligned} \tag{3.24}$$

This equation follows from substituting (3.23) in (3.4).

Compare this with the resulting beampattern at radius r_1 of the beamformer designed to have the complex conjugate beamshape $b^*(\theta,\phi)$ specification at radius r_2:

$$b_{r_1}(\theta,\phi;k)\big|_{b_{r_2}=b^*} = \sum_{n=0}^{\infty}\frac{R^*_n(r_1,k)}{R^*_n(r_2,k)}\sum_{m=-n}^{n} A_{nm}(b^*)\, Y_{nm}(\theta,\phi). \tag{3.25}$$

From (3.23) $A_{nm}(b^*) = A^*_{n(-m)}(b)$. Then taking the complex conjugate of (3.25), by change of variable m in the summation by $-m$, and then using Proposition 3.1 yields

$$\begin{aligned} b^*_{r_1}(\theta,\phi;k)\big|_{b_{r_2}=b^*} &= \sum_{n=0}^{\infty}\frac{R_n(r_1,k)}{R_n(r_2,k)}\sum_{m=-n}^{n} A_{nm}(b)\, Y_{nm}(\theta,\phi) \\ &= b_{r_2}(\theta,\phi)\big|_{b_{r_1}=b}\left(1+O\big(\frac{1}{k^2r_2^2}-\frac{1}{k^2r_1^2}\big)\right) \end{aligned} \tag{3.26}$$

as $r\to\infty$, where $r=\min(r_1,r_2)$ (alternatively for $r_1\to r_2$ this also holds). Thus we have established:

Proposition 3.2 *Let λ be the wavelength and $k=2\pi/\lambda$ the wave number, then*

$$b^*_{r_1}(\theta,\phi)\big|_{b_{r_2}=b^*} = b_{r_2}(\theta,\phi)\big|_{b_{r_1}=b}\left(1+O\big(\frac{1}{k^2r_2^2}-\frac{1}{k^2r_1^2}\big)\right) \tag{3.27}$$

as $r\to\infty$, where $r=\min(r_1,r_2)$.

□

By associating r_1 with the nearfield and r_2 with the farfield, this proposition establishes an asymptotic equivalence, up to complex conjugation, of two problems: (i) determining the nearfield performance of a farfield beampattern specification, and (ii) determining the equivalent farfield beampattern corresponding to a nearfield beampattern specification. We make the following observations:

(i) If $r_2 = \infty$ then this result is saying that a nearfield problem can be solved approximately by solving a related farfield problem.

(ii) Consider the tradeoff between operating at a distance (measured in wavelengths) sufficiently large to ensure the dominant error term in (3.16) to be small. (For analysis purposes we take $r_1 = r$ and $r_2 = \infty$.) This requires, after taking the square root,

$$\sqrt{\frac{n(n+1)}{8\pi^2}} \ll \frac{r}{\lambda}, \tag{3.28}$$

whereas for the first order term in the asymptotic expansion of $R_n(r,k)$, (3.21), to be small (see (3.20)) requires

$$\frac{n(n+1)}{4\pi} \ll \frac{r}{\lambda}. \tag{3.29}$$

This shows that asymptotic reciprocity holds much better than might be expected by taking the naive approach of operating at a distance with r/λ large enough such to guarantee that the asymptotic form (3.13) can be used as an approximation. Further, the true dominant error term (3.28) grows linearly with n relative to r/λ versus the naive condition (3.29) which grows quadratically (and hence more quickly) with n relative to r/λ.

(iii) The reciprocity holds whenever the dominant error term can be made small, which implies that either the beampattern is low-pass in character, i.e., most of the energy is in the lower order modes (small n, which generally holds), or that the difference in the radial distances, $r_1 - r_2$, is small enough. The meaning of the former condition will be fleshed out later in Section 3.4.5.

3.4.3 Nearfield Design Procedure

The exact nearfield design given in Section 3.4.2 can be implemented by transforming the nearfield specification $b(\theta, \phi)$ defined on a sphere of radius r to the farfield.

This method requires in the analysis step (3.5) multi-dimensional numerical integrations to be performed which must contend with numerical issues. The advantage of the radial reciprocity technique defined in this section, although only asymptotically exact, is that *no analysis step or modal synthesis needs to be performed.* This leads to a sequence of computationally straightforward signal processing steps to achieve a high quality nearfield design.

Novel Design using Reciprocity

The reciprocity relationship (3.27) with $r_1 = r$ and $r_2 = \infty$, leads to the corollary of Proposition 3.2:

Proposition 3.3 *The farfield beampattern corresponding to a desired nearfield beampattern specification $b_r(\theta, \phi) = b(\theta, \phi)$ satisfies the asymptotic equivalence*

$$b_\infty(\theta, \phi)\big|_{b_r = b} \sim b_r^*(\theta, \phi)\big|_{b_\infty = b^*}, \quad as\ r \to \infty. \tag{3.30}$$

□

By assuming (3.30) holds with equality we have the following approximate design procedure:

Nearfield Design Procedure

Step 0) Specify the desired nearfield beampattern $b(\theta, \phi)$ at distance r.

Step 1) Synthesize the farfield beampattern $b^*(\theta, \phi)$ at $r_2 = \infty$, i.e., $b_\infty(\theta, \phi) = b^*(\theta, \phi)$.

Step 2) Using the sensor weights of Step 1 evaluate the resultant nearfield beampattern $a(\theta, \phi)$ at r, i.e., $a(\theta, \phi) = b_r(\theta, \phi)\big|_{b_\infty = b^*}$.

Step 3) Synthesize a farfield beampattern $a^*(\theta, \phi)$ at $r_2 = \infty$. These weights will produce the desired beampattern $b(\theta, \phi)$ at distance r.

This procedure requires a nearfield beampattern determination from farfield data sandwiched between two farfield designs.

The farfield design in Step 1 may be implemented as follows. Determine Q sensor weights $\{w_q\}$, using standard farfield techniques, to synthesize the response

using

$$b^*(\theta,\phi) = \sum_{q=0}^{Q-1} w_q e^{-ik(x_q \sin\theta\cos\phi + y_q \sin\theta\sin\phi + z_q\cos\theta)}, \tag{3.31}$$

where (x_q, y_q, z_q) is the location of the qth sensor—this is a well studied design procedure and can be effected by using least squares techniques.

Step 2 requires determination of the nearfield response from the farfield design. The response can be computed using the weights and array geometry used in Step 1, i.e.,

$$a(\theta,\phi) = C\sum_{q=0}^{Q-1} w_n \frac{d_0(r,\theta,\phi)}{d_q(r,\theta,\phi)} e^{-ik\left(d_q(r,\theta,\phi) - d_0(r,\theta,\phi)\right)} \tag{3.32}$$

where $d_q(r,\theta,\phi)$ is the distance from a point at (r,θ,ϕ) to the qth sensor and C is some normalizing complex constant. Note that in (3.32) we use the propagation model where magnitude attenuates like the reciprocal of distance and the phase is proportional to distance. This type of response determination, (3.32), which requires explicit sensor locations and weights can be contrasted with the more general methods given in Section 3.4.2 which do not require any array geometry information (but do require the determination of the modal coefficients (3.5)).

The final step, Step 3, is to determine the $\widetilde{Q}$ sensor weights $\widetilde{w}_q$ to give the farfield response:

$$a^*(\theta,\phi) = \sum_{q=0}^{\tilde{Q}-1} \widetilde{w}_q\, e^{-ik(\tilde{x}_q \sin\theta\cos\phi + \tilde{y}_q \sin\theta\sin\phi + \tilde{z}_q\cos\theta)} \tag{3.33}$$

where $(\widetilde{x}_q, \widetilde{y}_q, \widetilde{z}_q)$ is the location of the qth sensor. Note that this array geometry need not necessarily be the same as in Step 1, but should correspond to the actual array. A typical design procedure is illustrated in the next section.

The primary utility in the procedure is the circumvention of the computationally difficult transformation from a desired nearfield beampattern to the equivalent farfield beampattern requiring numerical integration, and the direct use of farfield design procedures.

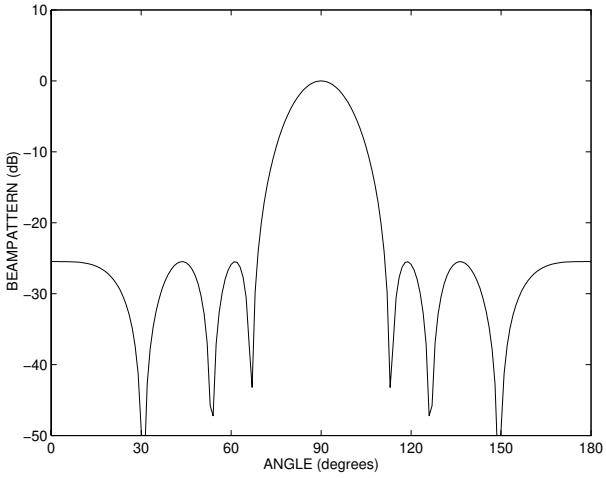

(a) Desired nearfield Chebyshev 25 dB beampattern. The phase is flat at zero radians. (Steps 0 and 1 of Nearfield Design Procedure).

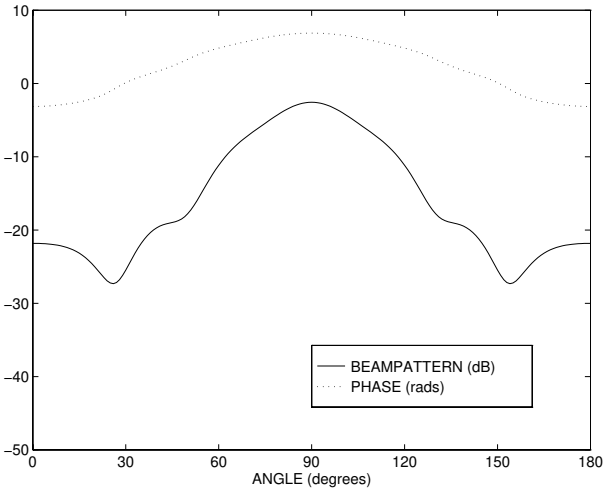

(b) Result of using a Chebyshev 25 dB farfield beamformer in the nearfield at a radius of 3 wavelengths (Step 2 of Nearfield Design Procedure).

Figure 3.6: Demonstration of Steps 0, 1, and 2 of the Nearfield Design Procedure using Nearfield/Farfield Reciprocity.

3.4.4 Design Example and Analysis

Application of Parseval Relation

We have developed a Parseval relation in Section 2.5 for modal representation of beampatterns. It will be essential later in assessing the novel design using reciprocity by determining the distribution of power across the modal components for a given beampattern specification on a sphere of arbitrary radius. An observation regarding the $A_{nm}(b)$ in (3.23) is that these represent modal amplitudes and depend only on the shape of the beampattern and not on the radius of the sphere on which the beampattern is given, e.g., the computation is identical whether the beampattern is nearfield or farfield.

As indicated in the following example, whenever such a "low pass" beampattern specification is used, the novel design procedure using reciprocity has been observed to work extremely well. The analysis that follows the example corroborates these claims.

Linear 1D Array Example

The following example shows the result of the nearfield design procedure of Section 3.4.3 in comparison with the nearfield compensation technique [2] outlined in Section 3.2. The objective was to realize a seventh-order zero-phase Chebyshev 25 dB beampattern, shown in Figure 3.6(a), in the nearfield at a radius of 3 wavelengths—this is Step 0 of the nearfield design procedure. The array sensors are co-linear and aligned along the z axis.

Step 1 of the nearfield design procedure required a design to realize the complex conjugate of this Chebyshev beampattern in the farfield. This is a classical design problem [9], and the weights for a 7 sensor half-wavelength spaced farfield array are easily calculated. The resultant designed farfield beampattern is identical to that shown in Figure 3.6(a). This is $b^*(\theta, \phi)$ in the design procedure, i.e., the complex conjugate of the objective beampattern.

The response of this farfield beamformer was then evaluated in the nearfield at the required radius of 3-wavelengths according to (3.32). Figure 3.6(b) shows the resulting beampattern. This is $a(\theta, \phi)$ in Step 2 of the nearfield design procedure.

Step 3 of the nearfield design procedure required designing a farfield beamformer to realize $a^*(\theta, \phi)$. We used a weighted complex-valued least-squares design method [6] to realize $a^*(\theta, \phi)$ with a quarter-wavelength spaced array. Thirteen elements, corresponding to a 3 wavelength aperture, were used to achieve an adequate match

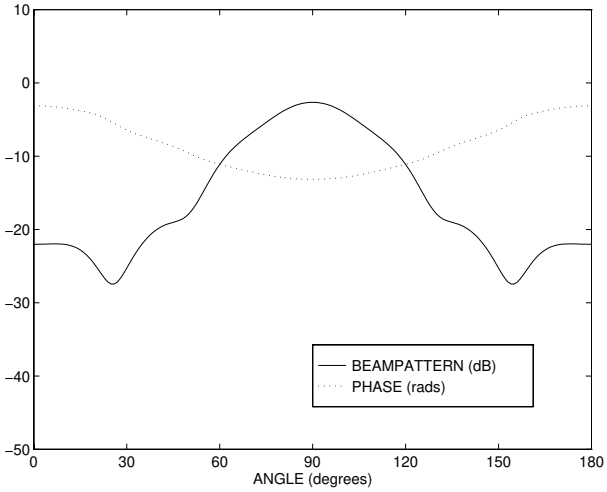

(a) Farfield realization of conjugate beampattern using least square design for a 13 element quarter-wavelength spaced array (Step 3 of Nearfield Design Procedure).

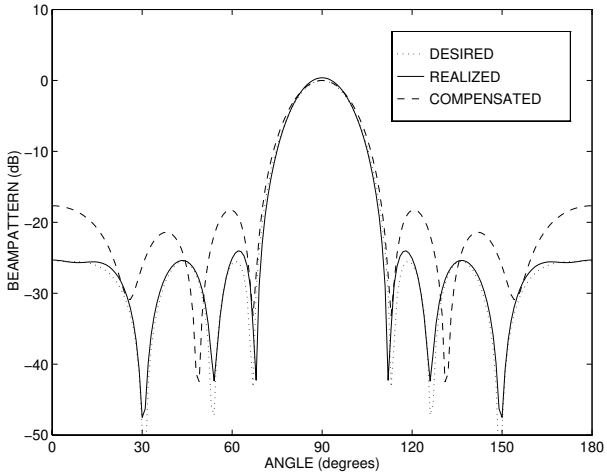

(b) Result of using 13 sensor farfield beamformer in the nearfield (solid curve) compared with the design specification which is the dotted curve. For comparison, the compensated design technique in [2] (outlined in Section 3.2) is given (dashed curve).

Figure 3.7: Demonstration of Step 3 of the Nearfield Design Procedure using Nearfield/Farfield Reciprocity.

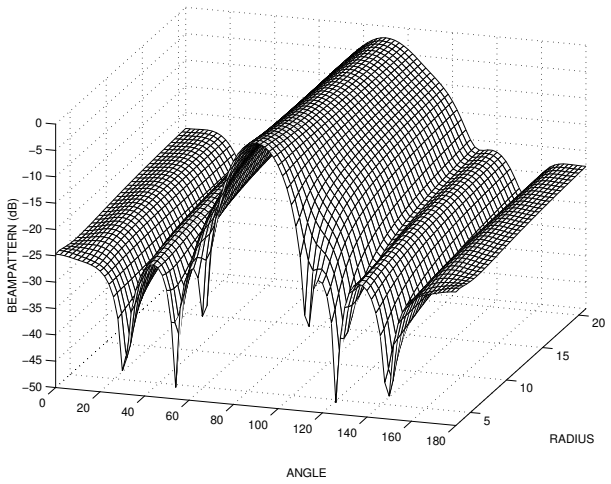

Figure 3.8: Performance of the beamformer design magnitude as a function of angle (degrees) and radial distance (wavelengths). The phase response is not shown.

to the desired beampattern. Angles outside the range 70°–110° were weighted more heavily so that the sidelobe region of the desired Chebyshev beampattern would be accurately approximated. The resulting farfield realization is shown in Figure 3.7(a).

Finally, to verify the design objectives had been met, this beamformer was simulated in the nearfield at a radius of 3 wavelengths; the nearfield beampattern shown solid in Figure 3.7(b) resulted. Also shown is the desired Chebyshev 25 dB beampattern (dotted), and the response of the nearfield compensation method in Section 3.2 (dashed). We note that the proposed nearfield design technique provides a very close realization of the desired beampattern over all angles, not just at angles close to broadside as for the nearfield compensation method in Section 3.2. Figure 3.8 shows the performance of the beamformer versus angle (degrees) and distance (wavelengths). It shows the desired beampattern at 3 wavelengths (near edge) and the variation with distance as we move towards the farfield (far edge).

This example highlights the main feature of our proposed nearfield beamforming procedure: when the reciprocity relation holds, it is only necessary to use well-established farfield beamformer design techniques in the design of a nearfield beamformer.

3.4.5 Modal Analysis of the Example

Since the array sensors are aligned along the z axis, only the $m = 0$ modes are potentially nonzero, i.e., only the $A_{n0}(b)$ coefficients, (3.23), can be nonzero. Further,

Table 3.1: Power and Errors versus Modal Coefficients for Example 1

n	$A_{n0}(b)$	$\lvert\epsilon(n, 6\pi, \infty)\rvert$	$\lvert A_{n0}(b)\rvert^2$	% Pow	% Err
0	0.748830	0.000000	0.560746	27.7	0.0
2	-0.790121	0.008443	0.624291	30.8	0.3
4	0.619535	0.028145	0.383824	18.9	0.5
6	-0.560184	0.059104	0.313806	15.5	0.9
8	0.353918	0.101321	0.125258	6.2	0.6
10	-0.129829	0.154796	0.016855	0.8	0.1
12	0.029584	0.219529	0.000875	0.0	0.0
14	-0.004547	0.295520	0.000021	0.0	0.0
16	0.000504	0.382769	0.000000	0.0	0.0
18	-0.000042	0.481276	0.000000	0.0	0.0
20	0.000003	0.591040	0.000000	0.0	0.0
22	0.000000	0.712063	0.000000	0.0	0.0
24	0.000000	0.844343	0.000000	0.0	0.0
Sum	n/a	n/a	2.025676	100.0	2.5

since the phase is zero for this example, the $A_{n0}(b)$ coefficients are purely real, and because the beampattern is symmetric the odd coefficients are zero.

In order to determine the validity of the reciprocity relation (3.27), we analyze the modal expansion for this example. The results are summarized in Table 3.1 and Figure 3.9. Table 3.1 shows a decomposition of the beampattern as a modal expansion indexed by n.

A conservative check can first be made by seeing whether (3.28) is satisfied for all significant terms used in the beampattern synthesis equation (3.22). The Parseval relation (2.29) identifies the power contained in each $(m = 0)$ mode with $\left|A_{n0}(b)\right|^2$. In this way we can see the error measured in beampattern power associated with using a finite number of analysis coefficients in the synthesis equation (3.22) and also see which are the dominant modes. Using this Parseval expression, we calculated the power in each mode in the fourth column of Table 3.1. In Figure 3.9 we have plotted the cumulative beampattern power versus n. Clearly, only the even terms up to $n = 10$ are significant. Substituting $n = 10$ into the error bound (3.28) gives

$$\frac{\sqrt{55}}{2\pi} \approx 1.068 \ll \frac{r}{\lambda},$$

which can be compared with our design for $r = 3$ wavelengths. Note that for this

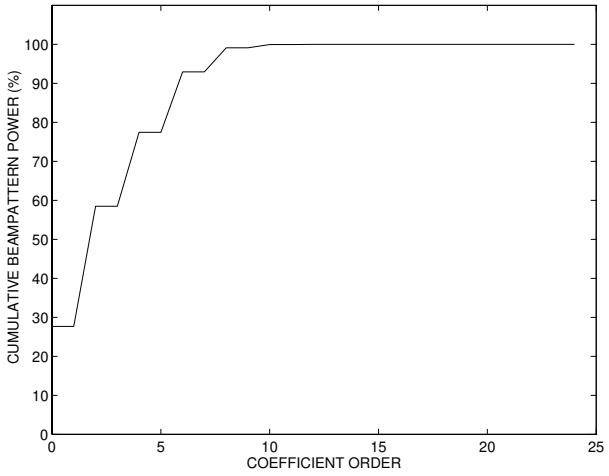

Figure 3.9: Number of terms required in (3.22) to accurately model a seventh-order Chebyshev 25 dB beampattern. There is insignificant power beyond the tenth order mode.

distance, $kr = 6\pi$ and we take $r_1 = r$ and $r_2 = \infty$.

A more detailed examination of the modal expansion shows that the lower-order modes (small n) dominate the power, but it is these modes that contribute the least asymptotic error in (3.16). From (3.16), for the parameters in this example, we have

$$\left|\epsilon(n, 6\pi, \infty)\right| = \frac{n(n+1)}{72\pi^2} \tag{3.34}$$

which is computed in the third column of Table 3.1. However, to better gauge the overall error this causes to the reciprocity condition (3.27) we weight these error magnitudes by the power in the corresponding mode and the result is sixth column of Table 3.1 which is provided as a guide only. So it can be seen that an upper bound on the approximate accuracy of the reciprocity is at most of the order of 2.5% in error.

3.5 Farfield Array Weight Redesign

3.5.1 Preliminary

In this section, we present yet another new method for nearfield array beamforming, exploiting the modal analysis techniques developed in Chapter 2. Unlike the methods in Section 3.3 and Section 3.4, this method is developed only for linear

arrays. Generalization of this method to arbitrary array geometries is a possibility but is not considered in this thesis.

Here we devise a linear transformation to obtain a set of array weights that achieves the desired beampattern for sources in the nearfield, given another set of array weights that achieves the same beampattern for farfield sources. The design methodology relies on three key ideas: 1) a relationship between nearfield response and farfield response of a given theoretical continuous sensor based on modal expansion; 2) a Fourier transform relationship between the farfield beampattern and a continuous aperture function; and 3) an expression for the modal coefficients of a beampattern in terms of the farfield array weights. Using these ideas, we redesign the farfield array weights using a linear transformation to produce the desired beampattern in the nearfield.

3.5.2 Problem Formulation

Suppose there exists a linear array of $(2M+1)$ sensors with array weight vector

$$\boldsymbol{W}^{(\infty)} = [w_{-M}^{(\infty)}, \ldots, w_{M}^{(\infty)}]^T$$

aligned to the z axis, such that the response to plane waves from a farfield source, impinging at an angle θ to the array axis, is

$$a(\theta) = \sum_{m=-M}^{M} w_m^{(\infty)} e^{-ikz_m \cos\theta} \tag{3.35}$$

where z_m is the distance to the mth source. Suppose

$$\boldsymbol{W}^{(r)} = [w_{-Q}^{(r)}, \ldots, w_{Q}^{(r)}]^T$$

are the weights of a linear array of $(2Q+1)$ sensors that achieve the desired beampattern specification $a(\theta)$ for a nearfield source at an angle θ and distance r from the array origin. Hence,

$$a(\theta) = \sum_{q=-Q}^{Q} w_q^{(r)} \frac{r}{d(r,\theta,z_q)} e^{-ik(d(r,\theta,z_q)-r)}, \tag{3.36}$$

where

$$d(r,\theta,z) \triangleq (r^2 - 2rz\cos\theta + z^2)^{1/2}$$

is the distance from the source to a sensor position z in the array axis.

The problem we consider is determining the "farfield-nearfield" transformation matrix $\boldsymbol{A}$ such that

$$\boldsymbol{W}^{(r)} \approx \boldsymbol{A}\boldsymbol{W}^{(\infty)} \tag{3.37}$$

and identify the nature of the approximation in (3.37).

3.5.3 Theoretical Continuous Aperture

In Chapter 2, we have shown how to write the aperture response using the modal representation. In this section we use those results for a linear aperture to derive the desired transformation $\boldsymbol{A}$.

Nearfield Response

Consider a linear continuous aperture aligned to the z axis with an aperture illumination function $\rho(z;k)$. Then the response of the sensor to a source at an angle θ and distance r from the array origin is

$$b_r(\theta) = \int_{-\infty}^{\infty} \rho(z;k)\, \frac{re^{ikr}}{d(r,\theta,z)}\, e^{-ikd(r,\theta,z)} dz, \tag{3.38}$$

provided that the function $d(r,\theta,z) \neq 0$ (which is the distance from the source to a point z in the sensor). Also we assume that $\rho(z;k) \approx 0$ for $|z| > r$. Under these mild conditions, we can use (2.43) to write

$$\frac{re^{ikr}}{d(r,\theta,z)} e^{-ikd(r,\theta,z)} = \sum_{n=0}^{\infty} \big[-ik(2n+1) j_n(kz) \big] R_n(r,k) P_n(\cos\theta), \quad \text{for } |z| < r$$

where $P_n(\cdot)$ are the Legendre functions and $j_n(\cdot)$ is the spherical Bessel function (2.40) and $h_n^{(1)}(\cdot)$ is the Hankel functions of first kind (2.10). By substituting the above expansion in (3.38) and integrating the series term by term, we obtain the nearfield sensor response as

$$b_r(\theta) = \sum_{n=0}^{\infty} \alpha_n(k)\, R_n(r,k)\, P_n(\cos\theta), \tag{3.39}$$

where

$$\alpha_n(k) \triangleq (-i)k(2n+1) \int_{-\infty}^{\infty} \rho(z;k) j_n(kz) dz. \tag{3.40}$$

Farfield Response

The response of the same continuous sensor $\rho(z;k)$ to a farfield source at an angle θ can be written from (3.39) as

$$b_\infty(\theta) = \sum_{n=0}^{\infty} \alpha_n(k)\, R_n(\infty, k)\, P_n(\cos\theta), \tag{3.41}$$

where $\alpha_n(k)$ is given by (3.40) as for the case of the nearfield response. Note that, (3.41) is the equivalent farfield beampattern of the nearfield beampattern (3.39).

Modal Coefficients

We can also evaluate the coefficients $\alpha_n(k)$ of the series (3.39) for a fixed frequency k using the orthogonality property of Legendre functions (2.11) as

$$\alpha_n(k) = \frac{1}{R_n(r,k)} \int_{-1}^{1} b_r(\theta) P_n(\cos\theta) d(\cos\theta). \tag{3.42}$$

Suppose that the response $b_r(\theta)$ of the continuous sensor is equal to the desired beampattern specification $a(\theta)$. Hence, we can substitute (3.35) into (3.42) and interchange the integration and summation to obtain

$$\alpha_n(k) = \frac{1}{R_n(r,k)} \sum_{m=-M}^{M} w_m^{(\infty)} \int_{-1}^{1} e^{-ikz_m u} P_n(u)\, du,$$

where $u = \cos\theta$. The integral of the above equation can be evaluated using (2.48) and the orthogonality property of Legendre functions (2.11) to get

$$\alpha_n(k) = \frac{2i^n}{R_n(r,k)} \sum_{m=-M}^{M} w_m^{(\infty)}\, j_n(kz_m). \tag{3.43}$$

Thus we have established an expression relating the modal coefficients $\alpha_n(k)$ of a beampattern to its farfield array weights.

In summary, the modal coefficients $\alpha_n(k)$ may be related by either: 1) the aperture illumination function $\rho(z;k)$ in (3.40); 2) the equivalent beampattern

$b_r(\theta)$ at distance r in (3.42); or, 3) the linear array weights (3.43) which realize the desired beamshapes in the farfield.

Aperture Illumination

In order to derive an expression for the aperture function $\rho(z;k)$ in terms of the array weights, we write the response of $\rho(z;k)$ to a farfield source at an angle θ as

$$\tilde{b}_\infty(u) = \int_{-\infty}^{\infty} \rho(z;k)\, e^{-ikuz}\, dz \tag{3.44}$$

where $u = \cos\theta$ and $\tilde{b}_\infty(u) \triangleq b_\infty(\cos^{-1} u) = b_\infty(\theta)$. Note that (3.44) is the standard Fourier transform relating a farfield aperture response $\tilde{b}_\infty(u)$ to the aperture illumination function $\rho(z;k)$ for frequency k. Thus the inverse Fourier transform corresponding to (3.44) is given by

$$\rho(z;k) = \frac{k}{2\pi} \int_{-1}^{1} \tilde{b}_\infty(u)\, e^{ikuz}\, du. \tag{3.45}$$

Using the series expansion (2.48), we may write

$$e^{ikzu} = \sum_{n=0}^{\infty} (-i)^n (2n+1) j_n(kz)\, P_n(u). \tag{3.46}$$

Since (3.41) is the modal representation of the farfield response of the continuous sensor $\rho(z;k)$, we substitute (3.41) and (3.46) into (3.45), and interchange integration and summation to get an exact expression for the aperture illumination

$$\rho(z;k) = \frac{k}{\pi} \sum_{n=0}^{\infty} (-i)^n R_n(\infty,k)\, \alpha_n(k)\, j_n(kz). \tag{3.47}$$

For practical purposes, we assume that there are only $N+1$ significant terms in the infinite series expression (3.47) for the continuous sensor $\rho(z;k)$. From (3.43), (2.21), and a truncated series (3.47) we get

$$\rho(z;k) = \frac{2}{\pi} \sum_{n=0}^{N} \frac{i^{n+1}}{R_n(r,k)}\, j_n(kz) \sum_{m=-M}^{M} w_m^{(\infty)}\, j_n(kz_m), \tag{3.48}$$

which relates the continuous aperture function required to produce the beampattern $a(\theta)$ for a nearfield source to the weights of a linear array of sensors which produce the same beampattern $a(\theta)$ for a farfield source. In the following section,

we truncate and discretize this continuous aperture to obtain the desired transformation matrix between farfield and nearfield weights.

3.5.4 Transformation Matrix

It can be shown that the Fourier transform of the aperture illumination (3.48) $\rho(z;k)$ with respect to z is bandlimited by k. This implies that we can represent $\rho(z;k)$ by its samples if the sampling distance is less than $\lambda/2\,(=\pi/k)$. Further, we have assumed that $\rho(z;k) \approx 0$ for $|z| > r$; hence we can approximate the integral in (3.38) by a finite summation to obtain

$$b_r(\theta) \approx \sum_{q=-Q}^{Q} g_q\, \rho(z_q;k)\, \frac{r}{d(r,\theta,z_q)} e^{-ik(d(r,\theta,z_q)-r)}, \tag{3.49}$$

where $[z_{-Q},\ldots,z_Q]$ is a possible set of sampling points (sensor locations) and g_q depends on the sensor separations. By comparing (3.36) with (3.49) we can observe that

$$w_q^{(r)} \approx g_q \rho(z_q;k) \;\text{ for }\; q = -Q,\ldots,Q$$

so that

$$\boldsymbol{W}^{(r)} \approx \begin{bmatrix} g_{-Q}\rho(z_{-Q};k) \\ \vdots \\ g_Q\rho(z_Q;k) \end{bmatrix}. \tag{3.50}$$

By combining (3.50) and (3.48) we can obtain the following matrix equation,

$$\boldsymbol{W}^{(r)} \approx \boldsymbol{D}_1\boldsymbol{J}_1\boldsymbol{D}_2\boldsymbol{J}_2^T\boldsymbol{W}^{(\infty)},$$

where

$$\boldsymbol{D}_1 = \begin{bmatrix} g_{-Q} & 0 & \ldots & 0 \\ 0 & \ddots & & \vdots \\ \vdots & & \ddots & 0 \\ 0 & \ldots & 0 & g_Q \end{bmatrix}$$

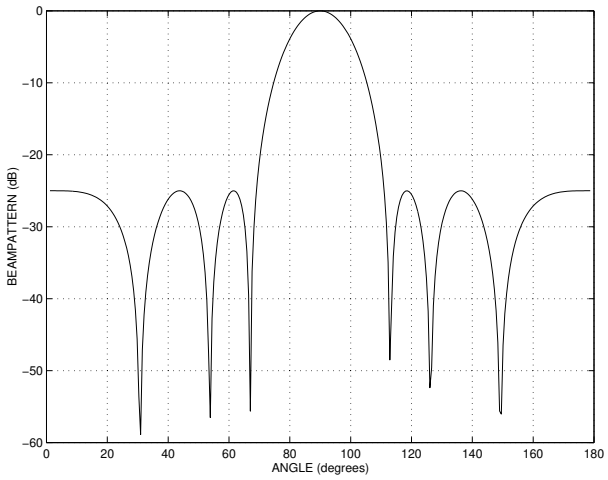

Figure 3.10: Desired nearfield beampattern.

is a $(2Q+1)\times(2Q+1)$ diagonal matrix,

$$\boldsymbol{J}_1 = \begin{bmatrix} j_0(kz_{-Q}) & \dots, & j_N(kz_{-Q}) \\ \vdots & & \vdots \\ j_0(kz_Q) & \dots, & j_N(kz_Q) \end{bmatrix}$$

is a $(2Q+1)\times(N+1)$ matrix,

$$\boldsymbol{D}_2 = \frac{2}{\pi}\begin{bmatrix} \frac{i^{0+1}}{R_0(r,k)} & 0 & \dots & 0 \\ 0 & \ddots & & \vdots \\ \vdots & & \ddots & 0 \\ 0 & \dots & 0 & \frac{i^{N+1}}{R_N(r,k)} \end{bmatrix}$$

is a $(N+1)\times(N+1)$ diagonal matrix, and

$$\boldsymbol{J}_2 = \begin{bmatrix} j_0(kz_{-M}) & \dots, & j_N(kz_{-M}) \\ \vdots & & \vdots \\ j_0(kz_M) & \dots, & j_N(kz_M) \end{bmatrix}$$

is a $(2M+1)\times(N+1)$ matrix. Hence we can conclude that the farfield-nearfield transformation matrix is given by

$$\boldsymbol{A} = \boldsymbol{D}_1\boldsymbol{J}_1\boldsymbol{D}_2\boldsymbol{J}_2^T.$$

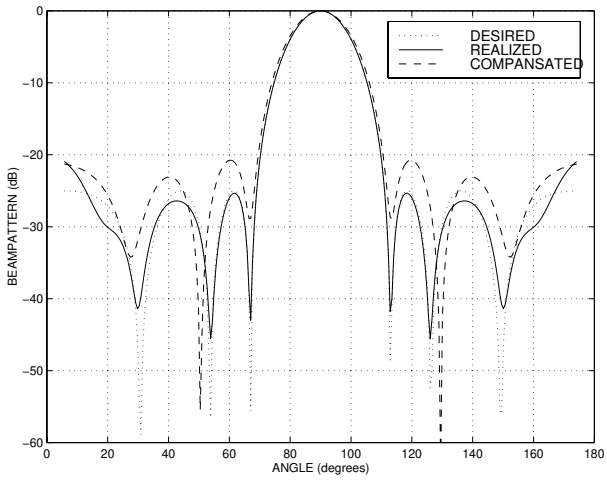

Figure 3.11: Resulting beamformer performance in the nearfield at a distance of 3 wavelengths from the array origin. The desired beampattern (dotted) and the response of the beamformer designed using nearfield quadratic compensation method (dashed) are also shown for comparison.

3.5.5 Weight Redesign Example

The following example illustrates the use of the above transformation technique for nearfield beamforming in comparison with the nearfield quadratic compensation technique in [3, p. 36]. We wish to design a nearfield beamformer having the response in Figure 3.10 at a distance of 3 wavelengths from the array origin.

A set of weights for a linear array of 7 ($Q = 3$) half wave-length spaced sensors was designed according to [9] to produce the required beampattern in the farfield. For the actual array for nearfield operations, we chose 13 ($M = 6$) sensors with uniform sensor separation of half a wavelength. Then we calculated the transformation matrix $\boldsymbol{A}$ with the maximum number of modes $N = 15$ for this example. Next we evaluated the corresponding nearfield weight vector using (3.37). The resulting beamformer response was evaluated in the nearfield and the response is depicted (solid) in Figure (3.11). Also shown is the desired beampattern (dotted), and the response of the nearfield method [3] (dashed). We note that the proposed nearfield design technique provides a close realization of the desired beampattern over all angles, not just at angles close to broadside as for the nearfield method of [3].

3.6 Summary and Contributions

Three methods of nearfield beamforming have been presented exploiting the modal analysis techniques developed in Chapter 2. Based on the results of this chapter, we can make two conclusions: 1) a nearfield beamforming can be effectively performed by using farfield design techniques after obtaining a relationship between the nearfield beampattern specification and its equivalent farfield beampattern, 2) modal analysis techniques are useful in establishing these nearfield-farfield beampattern relationships.

We itemize some specific contributions made in this chapter:

i. The concept of nearfield-farfield beampattern transformation was introduced to design data-independent nearfield beamformers.

ii. An exact nearfield-farfield beampattern transformation method was developed for nearfield beamforming using modal analysis techniques developed in the Chapter 2. This method involves the radial transformation of a nearfield beampattern to a physically equivalent farfield beampattern and the subsequent design of a farfield beamformer to realize this transformed beampattern.

iii. We established an asymptotic equivalence between two transformation problems: (i) determining the nearfield performance of a desired beampattern specification in the farfield, and (ii) determining the equivalent farfield beampattern corresponding to a given desired beampattern specification in the nearfield. This result was used to propose a computationally simple nearfield beamformer design procedure based on farfield design techniques.

iv. A direct linear matrix transformation was obtained between the array weights required to achieve the given beampattern specification in the farfield and nearfield.

References

[1] A.C. Ludwig, "Calculation of scattered patterns from asymmetrical reflectors," Tech. Rep. 32-140, Jet Propulsion Laboratory, California institute of Technology, Pasadena, California, Feb. 1970.

[2] F. Khalil, J.P. Jullien, and A. Gilloire, "Microphone array for sound pickup in teleconference systems," *J. Audio Engineering Society*, vol. 42, pp. 691–700, Sept. 1994.

[3] B.D. Steinberg, *Principles of Aperture and Array System Design*, Wiley, New York, 1976.

[4] M.F. Berger and H.F. Silverman, "Microphone array optimization by stochastic region contraction," *IEEE Trans. Sig. Proc.*, vol. 39, pp. 2377–2386, Nov. 1991.

[5] S. Nordebo, I. Claesson, and S. Nordholm, "Weighted Chebyshev approximation for the design of broadband beamformers using quadratic programming," *IEEE Sig. Proc. Lett.*, vol. 1, pp. 103–105, July 1994.

[6] B.D. Van Veen and K.M. Buckley, "Beamforming: A versatile approach to spatial filtering," *IEEE Sig. Proc. Mag.*, pp. 4–24, Apr. 1988.

[7] R.A. Kennedy, T.D. Abhayapala, and D.B. Ward, "Broadband nearfield beamforming using a radial beampattern transformation," *IEEE Trans. Sig. Proc.*, vol. 46, pp. 2147–2156, Aug. 1998.

[8] E. Skudrzyk, *The Foundations of Acoustics*, Springer-Verlag, New York, 1971.

[9] C.L. Dolph, "A current distribution for broadside arrays which optimizes the relationship between beam width and side-lobe levels," *IRE*, vol. 34, pp. 335–348, June 1946.

Chapter 4

General Broadband Aperture/ Array Design

4.1 Introduction

In this chapter, we develop a systematic procedure for the design of a general broadband beamformer using the modal analysis techniques developed in Chapter 2 and the concept of a theoretical continuous sensor.

We identify a set of *elementary aperture functions* indexed by modes, where each elementary aperture function realizes the corresponding elementary beamshape introduced in Chapter 2. By linearly combining these elementary aperture functions an arbitrary broadband beampattern, can be realized. Then we approximate the resulting aperture by a set of discrete sensors to obtain a realizable broadband beamformer. The proposed beamformer structure has three major processing blocks: (i) a beampattern independent filtering block consisting of elementary beamformers; (ii) a beampattern shape dependent filtering block; and (iii) a radial focusing filter block, where a single parameter can be adjusted to focus the array to different radial distances from the array-origin. Hence, this design provides an efficient parametrization for adaptive beamformers (Chapter 5), where only the beampattern shape dependent filters and a radial distance dependent parameter need to be adapted.

This chapter is organized as follows: Section 4.2 establishes a relationship between the modal coefficients of an arbitrary broadband beampattern specification and the aperture illumination function required to realize this beampattern at a given distance from the sensor origin. Explicit expressions for elementary aperture functions for linear and spherical apertures are derived in Section 4.3. Section 4.4

shows how to approximate the theoretical continuous sensor by a practical discrete array of sensors. Guidelines for choosing the non-uniformly spaced sensor locations and the consequence of spatial sampling are addressed in Section 4.5. We conclude with an example broadband beamformer, which can be focused to either nearfield or farfield, in Section 4.6.

4.2 Broadband Continuous Sensor

4.2.1 Background

A broadband continuous aperture can be viewed as a limiting case of a closely packed set of discrete sensors with a temporal filter attached to each sensor. That is, the aperture illumination of a broadband continuous sensor is a function of frequency. The concept of such a theoretical aperture has been used previously [1], to design farfield frequency invariant beamformers. We also use a similar approach, since mathematical relationships between the functional requirements of the broadband beampattern specification and the beamformer structure are simple to derive using a theoretical continuous aperture. Once the relevant beamforming structure is developed, it can be approximated by a set of discrete sensors to realize a practical implementation.

4.2.2 Continuous Aperture for Farfield

Even though the problem addressed in this chapter is to design a general broadband beamformer, first we consider a problem of designing a farfield beamformer. In the following section we generalize the results of this section to accommodate general broadband beamforming.

Suppose the desired farfield broadband beampattern is specified by the modal representation (2.22) as

$$b_\infty(\hat{\boldsymbol{y}}; k) = \sum_{n=0}^{\infty} \sum_{m=-n}^{n} \alpha_{nm}(k)\, R_n(\infty, k)\, Y_{nm}(\hat{\boldsymbol{y}}), \;\; k \in [k_\mathrm{l}, k_\mathrm{u}] \tag{4.1}$$

where the integers $n \geq 0$, $m \in \{-n, -(n+1), \ldots, n\}$ index the modes, $Y_{nm}(\cdot)$ is the elementary beamshape (2.13), k_l and k_u are the lower and upper frequencies of

the design band,

$$R_n(\infty, k) \triangleq \lim_{r\to\infty} R_n(r,k) = \frac{i^{n+1}}{k}, \tag{4.2}$$

$R_n(r,k)$ is defined in (2.20), and $\alpha_{nm}(k)$ are the modal coefficients. (Recall that an arbitrary beampattern can be uniquely specified by the modal coefficients $\alpha_{nm}(k)$ for each frequency k.) Now we seek a theoretical sensor that gives the spatial response (4.1) to a farfield point source.

Consider a continuous sensor confined to a bounded region $\Omega \subset \mathbb{R}^3$ with broadband aperture illumination $\rho(\boldsymbol{x}; k)$, $\boldsymbol{x} \in \Omega$. From the development in Chapter 2, the angular response of a this aperture to planar waves (i.e., those generated by a farfield point source) impinging from an angle (θ, ϕ) can be written using (2.51) and (2.46) as

$$b_\infty(\hat{\boldsymbol{y}}; k) = \int_\Omega \rho(\boldsymbol{x}; k) e^{-ik\boldsymbol{x}\cdot\hat{\boldsymbol{y}}} d\boldsymbol{x}, \tag{4.3}$$

where $\hat{\boldsymbol{y}} = (\sin\theta\cos\phi, \sin\theta\sin\phi, \cos\theta)$, is a unit vector pointing opposite to the direction of the propagation of waves. Observe that (4.3) is a three-dimensional Fourier Transform relating the farfield beampattern to aperture illumination for a frequency k. The three-dimensional inverse Fourier transform corresponding to (4.3) is given by

$$\rho(\boldsymbol{x}; k) = \frac{k}{2\pi} \int_{\mathbb{B}} b_\infty(\hat{\boldsymbol{y}}; k) e^{jk\boldsymbol{x}\cdot\hat{\boldsymbol{y}}} d\hat{\boldsymbol{y}} \tag{4.4}$$

where the three-dimensional integration is over the unit sphere and $\mathbb{B} = \{\hat{\boldsymbol{y}} \in \mathbb{R}^3 : \|\hat{\boldsymbol{y}}\| = 1\}$.

Suppose the continuous sensor response (4.3) is equal to the desired beampattern (4.1). We substitute (4.1) into (4.4) and rearrange to obtain the aperture illumination function as

$$\rho(\boldsymbol{x}; k) = \sum_{n=0}^{\infty} \sum_{m=-n}^{n} \alpha_{nm}(k)\, R_n(\infty, k)\, \varrho_{nm}(\boldsymbol{x}; k), \tag{4.5}$$

where

$$\varrho_{nm}(\boldsymbol{x}; k) \triangleq \frac{k}{2\pi} \int_{\mathbb{B}} Y_{nm}(\hat{\boldsymbol{y}})\, e^{jk\boldsymbol{x}\cdot\hat{\boldsymbol{y}}} d\hat{\boldsymbol{y}}. \tag{4.6}$$

That is, the given farfield beampattern (4.1), can be achieved by a beamformer

(theoretical sensor) with the aperture illumination (4.5). Observe the similarities in mathematical form between the farfield beampattern (4.1) and the corresponding aperture illumination (4.5). In (4.1), an arbitrary farfield beampattern is represented by the weighted sum of elementary beamshapes $Y_{nm}(\cdot)$ with the frequency dependent weights are given by $\alpha_{nm}(k)R_n(\infty, k)$. Whereas in (4.5), the aperture illumination required to produce the beampattern (4.1) for a farfield source is given by weighted sum of functions $\varrho_{nm}(\cdot)$ where the weights are same as in (4.1). In recognition of this similarity, we name the functions $\varrho_{nm}(\cdot)$ *elementary aperture illumination* functions.

Note that (4.6) could be directly used to find the elementary aperture illumination $\varrho_{nm}(\cdot)$ for each elementary beamshape $Y_{nm}(\cdot)$. Since these elementary aperture functions act as a functional basis they are independent of the specific beampattern, and can be calculated beforehand in a practical situation. That is, a beampattern specification, in this case in the farfield, can be reduced to a constructible set of frequency dependent weights (filters).

4.2.3 Nearfield Equivalence

In the previous subsection we introduced a technique to obtain a continuous aperture illumination function $\rho(\boldsymbol{x}; k)$ that realizes a given broadband farfield beampattern. In this section, we generalize this result to establish the aperture illumination function needed to realize a given broadband beampattern at any radial distance from the array origin. We make use of the modal analysis techniques introduced in Chapter 2 to derive the desired result.

Theorem 4.2.1 *Let $b(\theta, \phi; k)$ be an arbitrary broadband beampattern specification. Suppose that a continuous sensor is contained inside a ball centred at the origin with radius r_0; then the aperture illumination, $\rho_r(\boldsymbol{x}; k)$ of the continuous sensor that realizes the beampattern $b(\theta, \phi; k)$ at a radius $r > r_0$ from the sensor origin is given by*

$$\rho_r(\boldsymbol{x}; k) = \sum_{n=0}^{\infty} \sum_{m=-n}^{n} A_{nm}(k) \, \frac{R_n(\infty, k)}{R_n(r, k)} \, \varrho_{nm}(\boldsymbol{x}; k), \tag{4.7}$$

where the elementary aperture illumination functions $\varrho_{nm}(\boldsymbol{x}; k)$ are given by (4.6), $R_n(\cdot, \cdot)$ is given by (2.20) and

$$A_{nm}(k) = \int_0^{2\pi} \int_0^{\pi} b(\theta, \phi; k) Y_{nm}^*(\theta, \phi) \sin\theta \, d\theta d\phi. \tag{4.8}$$

Proof of Theorem 4.2.1: Let $a_r(\theta,\phi;k)$ be the beampattern (spatial response) of the continuous sensor $\rho_r(\boldsymbol{x};k)$ for a source at (r,θ,ϕ). Then we use the modal representation (2.22) to write,

$$a_r(\theta,\phi;k) = \sum_{n=0}^{\infty}\sum_{m=-n}^{n} \alpha_{nm}(k) R_n(r,k) Y_{nm}(\theta,\phi), \quad r > r_0, \tag{4.9}$$

where the constraint $r > r_0$ comes from the fact that the modal representation (2.22) is valid on a manifold that encapsulates the aperture. Using (2.23) we can write

$$A_{nm}(k) = \alpha_{nm}(k) R_n(r,k) = \int_0^{2\pi}\int_0^{\pi} a_r(\theta,\phi;k)\, Y_{nm}^*(\theta,\phi)\sin\theta\, d\theta d\phi. \tag{4.10}$$

Since $a_r(\theta,\phi;k) = b(\theta,\phi;k)$,

$$A_{nm}(k) = \int_0^{2\pi}\int_0^{\pi} b(\theta,\phi;k)\, Y_{nm}^*(\theta,\phi)\sin\theta\, d\theta d\phi. \tag{4.11}$$

The farfield beampattern equivalent to a_r is given by

$$a_\infty(\theta,\phi;k) = \sum_{n=0}^{\infty}\sum_{m=-n}^{n} \alpha_{nm}(k) R_n(\infty,k) Y_{nm}(\theta,\phi). \tag{4.12}$$

From (4.5) the aperture illumination function corresponding to this farfield pattern is

$$\rho_r(\boldsymbol{x},k) = \sum_{n=0}^{\infty}\sum_{m=-n}^{n} \alpha_{nm}(k) R_n(\infty,k) \varrho_{nm}(\boldsymbol{x};k), \quad r > r_0. \tag{4.13}$$

Finally, substituting (4.10) into (4.13) completes the proof.

□

Comments:

1. The theorem provides a method to achieve a desired beampattern response at any radius $r > r_0$ from the array origin by a single parameter r adjustment of the continuous sensor $\rho_r(\boldsymbol{x};k)$. This has practical implications, shown later, for easily being able to focus the array.

2. When $r \to \infty$ then the theorem gives the result for the farfield. That is, an arbitrary broadband beampattern can be realized at the farfield by the

aperture illumination

$$\rho_\infty(\boldsymbol{x};k) = \sum_{n=0}^{\infty} \sum_{m=-n}^{n} A_{nm}(k)\, \varrho_{nm}(\boldsymbol{x};k),$$

where $A_{nm}(k)$ is given by (4.8).

4.3 Elementary Aperture Functions

In the previous section, we derive the aperture illumination required to realize a given broadband beampattern specification at any radial distance from the aperture origin. In doing so, we expressed the aperture illumination (4.7) as a (frequency dependent) weighted sum of elementary aperture functions (4.6). However, (4.6) is a integral equation and falls short of providing complete insight into the structure of the continuous aperture. In this section, to get a better structural insight, we derive closed-form expressions for the elementary aperture functions $\varrho_{nm}(\cdot)$ (4.6) and consider specific aperture geometries which are of interest in practical implementations.

Theorem 4.3.1 *Consider a continuous sensor confined to a bounded region $\Omega \subset \mathbb{R}^3$ and let $\hat{\boldsymbol{x}}$ be a unit vector directed to a point $\boldsymbol{x} \in \Omega$ on the sensor, then the elementary aperture function $\varrho_{nm}(\boldsymbol{x};k)$ is given by*

$$\varrho_{nm}(\boldsymbol{x};k) = 2k(-i)^n\, j_n(k\|\boldsymbol{x}\|)\, Y_{nm}(\hat{\boldsymbol{x}}), \tag{4.14}$$

where $j_n(\cdot)$ are the spherical Bessel functions (2.40) and $Y_{nm}(\cdot)$ are the elementary beamshapes given by (2.13).

Proof of Theorem 4.3.1: The complex conjugate of (2.47) is given by

$$e^{ik\boldsymbol{x}\cdot\hat{\boldsymbol{y}}} = 4\pi \sum_{n=0}^{\infty} \sum_{m=-n}^{n} (-i)^n j_n(k\|\boldsymbol{x}\|)\, Y_{nm}(\hat{\boldsymbol{x}}) Y^*_{nm}(\hat{\boldsymbol{y}}). \tag{4.15}$$

By substituting (4.15) into (4.6), interchanging integration and summation, we obtain

$$\varrho_{nm}(\boldsymbol{x};k) = 2k \sum_{n'=0}^{\infty} \sum_{m'=-n'}^{n'} (-i)^n j_{n'}(k\|\boldsymbol{x}\|) Y_{n'm'}(\hat{\boldsymbol{x}}) \int Y_{nm}(\hat{\boldsymbol{y}})\, Y^*_{n'm'}(\hat{\boldsymbol{y}}) d\hat{\boldsymbol{y}}.$$

We use the result (2.14) to evaluate the integration to complete the proof.

□

Now Theorem 4.2.1 and Theorem 4.3.1 provide the complete mathematical formulation for the theoretical broadband continuous sensor (beamformer) which realizes a given broadband beampattern at a given radius from the aperture origin.

Linear Continuous Sensor

The broadband array theory developed in the previous sections is sufficiently general to capture quite arbitrary three-dimensional sensor geometries. In an attempt to bring the result into focus and provide a more concrete presentation of the ideas, we examine a linear sensor aligned with the z axis. Suppose the origin is at the centre of the linear sensor. In this case, the beampattern is rotationally symmetric with respect to ϕ, and a beampattern can be expressed as $b_r(\theta;k) = b_r(\theta,\phi;k)$.

By rotational symmetry about the z axis, the only non-zero components of the modal representation (2.22) are those for which $m = 0$. Thus we obtain

$$\begin{aligned} b_r(\theta;k) &= \sum_{n=0}^{\infty} \alpha_{n0}(k)\, R_n(r,k) \sqrt{\frac{2n+1}{4\pi}}\, P_n(\cos\theta) \\ &= \sum_{n=0}^{\infty} A_n(k)\, P_n(\cos\theta), \end{aligned} \tag{4.16}$$

where

$$A_n(k) \triangleq \sqrt{\frac{2n+1}{4\pi}}\, \alpha_{n0}(k)\, R_n(r,k) \tag{4.17}$$

$$= \frac{2n+1}{2} \int_0^{\pi} b_r(\theta;k) P_n(\cos\theta) \sin\theta d\theta, \tag{4.18}$$

and $P_n(\cdot) = P_n^0(\cdot)$ is the Legendre function of order n. The linear continuous aperture illumination (4.7) that realizes the beampattern (4.16) at a radius $r > r_0$ from the array origin is given by

$$\rho_r(z;k) = \sum_{n=0}^{\infty} A_n(k) \sqrt{\frac{4\pi}{2n+1}}\, \frac{R_n(\infty,k)}{R_n(r,k)}\, \varrho_{n0}(z;k), \tag{4.19}$$

where r_0 is chosen such that $\rho_r(z;k) = 0$, $\forall |z| > r_0$.

We can use the Theorem 4.3.1 to write the elementary aperture functions for

this special case as

$$\varrho_{n0}(z;k) = (-i)^n k \sqrt{\frac{2n+1}{\pi}}\, j_n(k|z|) \begin{cases} P_n(1) & \text{if } z > 0 \\ P_n(-1) & \text{if } z < 0. \end{cases} \tag{4.20}$$

To further simplify (4.20), we use some properties of the Bessel and Legendre functions.

The Bessel functions of the first kind have the following property [2, p. 75]

$$J_v(-t) = e^{i\pi v} J_v(t), \tag{4.21}$$

where $v \in \mathbb{R}$, $t \in \mathbb{R}$ and $J_v(\cdot)$ is the Bessel function of first kind. Using (4.21) and (2.40), we can derive that

$$j_n(-t) = (-1)^n j_n(t). \tag{4.22}$$

Now we use (4.22) and the following results [3, p. 688]

$$P_n(t) = (-1)^n P_n(t)$$
$$P_n(1) = 1,$$

to write (4.20) as

$$\varrho_{n0}(z;k) = (-i)^n\, k \sqrt{\frac{2n+1}{\pi}}\, j_n(kz). \tag{4.23}$$

Now we state the following theorem regarding a linear continuous broadband aperture (beamformer) as a special case of Theorem 4.2.1:

Theorem 4.3.2 *Let $b(\theta;k)$ be an arbitrary broadband beampattern specification (rotationally symmetric around z axis). Then the aperture illumination, $\rho_r(z;k)$ of a linear continuous aperture, aligned with the z axis, that realizes this beampattern at a radius $r > r_0$ from the aperture origin is given by*

$$\rho_r(z;k) = \sum_{n=0}^{\infty} A_n(k)\,(-i)^n 2k\, \frac{R_n(\infty,k)}{R_n(r,k)}\, j_n(kz), \tag{4.24}$$

where

$$A_n(k) = \frac{2n+1}{2} \int_0^{\pi} b(\theta;k) P_n(\cos\theta) \sin\theta\, d\theta, \tag{4.25}$$

and r_0 is chosen such that $\rho_r(z;k) = 0$, $\forall |z| > r_0$.

Comments:

1. The above theorem provides a foundation to design a linear sensor array for broadband beamforming, which will be considered in the next section.

2. We need to comment on the condition $r > r_0$ in Theorem 4.3.2 which somewhat restricts the application of Theorem 4.3.2 in the nearfield of the aperture. Naturally, $\rho_r(z;k)$ in (4.24) is infinite in length, since the spherical Bessel functions $j_n(t)$ is defined for $t \in \mathbb{R}$. However, we have noticed in Chapter 3 that a "reasonable" beampattern specification can be represented by a finite number of modal coefficients. Suppose the given beampattern specification $b(\theta;k)$ can be accurately modeled by first $N+1$ coefficients, i.e., $A_n(k) = 0$, for $n > N$. Therefore, we only need to consider first $N+1$ terms of the series expansion (4.24). We also note from [3, p. 692] that for $kz \gg n$,

$$\begin{aligned} j_n(kz) &= \frac{1}{kz} \cos\big(kz - \frac{n+1}{2}\pi\big), \\ &= 0 \quad \text{as } kz \to \infty. \end{aligned} \tag{4.26}$$

   Therefore we can claim that for a specific design condition, i.e., signal bandwidth and beampattern specification, $\rho_r(z;k)$ is effectively equal to zero for z greater than some number r_0.

Spherical Continuous Sensor

Another aperture geometry that may have practical significance is a spherical aperture[1]. For example in [4], a set of microphones were flush-mounted on the surface of 19mm diameter rigid nylon sphere to have a steerable, first order differential microphone array.

Consider a spherical continuous sensor with radius r' and let a point on the sensor $\boldsymbol{x} = \boldsymbol{x}(r', \theta', \phi')$ in spherical coordinates where the centre of the sensor is located at the origin. Then the elementary aperture functions (4.14) for this special case is given by

$$\varrho_{nm}(\boldsymbol{x}(r', \theta', \phi'); k) = 2kj_n(kr')\, Y_{nm}(\theta', \phi'). \tag{4.27}$$

[1] This can be a rigid ball or a shell, where the surface of the sphere is considered as the aperture.

Unlike the linear aperture, the spherical aperture has finite dimensions. However, in this thesis, we will not proceed with any further developments on the spherical aperture.

4.4 Broadband Discrete Array Design

4.4.1 Background

We now show how to exploit the above ideas for broadband array design. An array is a finite set of identical, discrete, omni-directional broadband sensors arranged in a regular geometric fashion. We will only consider one-dimensional linear sensor arrays, although the results can be generalized to two and three dimensions. We consider a double sided linear array aligned to the z axis. There are a few techniques discussed in the literature [5,6] for discretization of a continuous sensor; we closely follow the procedure given in [1].

4.4.2 Approximation

An array of sensors can only approximate the continuous aperture distribution described by (4.24). In our formulation this reduces to a numerical approximation of the following integral representation, which gives the continuous sensor output

$$Z(k) = \int_{-\infty}^{\infty} \rho_r(z;k)\, S(z;k)\, dz, \tag{4.28}$$

where $S(z;k)$ is the Fourier Transform of the received signal at point z on the sensor. We use the well-known Trapezoidal integration method as used in [1] to approximate (4.28) by

$$\widetilde{Z}(k) = \sum_{q=-Q}^{Q} g_i\, \rho_r(z_q;k)\, S(z_q;k), \tag{4.29}$$

where $\{z_q\}_{q=-Q}^{Q}$ is a set of $2Q+1$ discrete sensor locations and g_q is a spatial weighting term which is used to account for the (possibly) nonuniformly spaced sensor locations. The role of the g_q is better understood at the end of Section 4.5, where the g_q are expressed in terms of sensor locations. The above approximation introduces two kind of errors: (i) the physical array is finite in extent and thus an infinite length integral has been replaced by a finite length summation; (ii) two spa-

tially continuous functions $\rho_r(z;k)$ and $S(z;k)$ are replaced by their corresponding spatially discrete counterparts and, hence, there is a possibility of spatial aliasing errors.

4.4.3 Beamformer Structure

We can consider $\rho_r(z_q;k)$ in (4.29) as the frequency response of a filter attached to the sensor at point z_q. By combining (4.24) and (4.29) we write,

$$\widetilde{Z}(k) = \sum_{q=-L}^{L} g_q\, S(z_q;k) \sum_{n=0}^{\infty} A_n(k)\, G_n(r;k)\, F_n(z_q;k), \tag{4.30}$$

where

$$F_n(z_q;k) \triangleq 2(-i)^n\, j_n(kz_q) \tag{4.31}$$

$$G_n(r;k) \triangleq k\,\frac{R_n(\infty,k)}{R_n(r,k)}. \tag{4.32}$$

We will call $F_n(z_q;k)$ the *elementary filters* (consistent with terminology of elementary beamshapes and elementary aperture functions). As in the case of elementary aperture functions, these elementary filters can be considered a common element of all beamformers; thus they are useful in developing an effective parameterization for adaptation of beampatterns (see Chapter 5). Figure 4.1 illustrates the magnitude of the frequency response of the elementary filters of the first six modes versus the product of the wavenumber k and the distance z to the associated sensor. Note that all but the mode zero elementary filters are bandpass in nature. This fact will be used in Section 4.5 to find the best possible sensor locations, i.e., to derive the nonuniform spacings naturally afforded by this design method to deal the broadband signals.

We now demonstrate an important result regarding the elementary filters as a consequence of (4.31). Note that in (4.31), $F_n(z_q;k)$ is a symmetric function of the spatial variable z_q and of the frequency variable k. Thus, these elementary filters are related through a frequency *dilation property*:

Theorem 4.4.1 *All elementary filter responses $F_n(z_q;k)$ of the same mode n at different sensor locations z_q are identical up to a frequency dilation. That is,*

$$F_n(z_q;k) = F_n(z_0;\frac{z_q}{z_0}k), \tag{4.33}$$

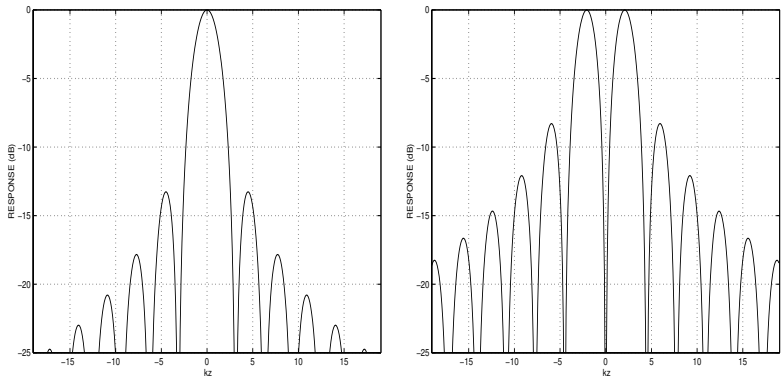

(a) mode: $n = 0$ (b) mode: $n = 1$

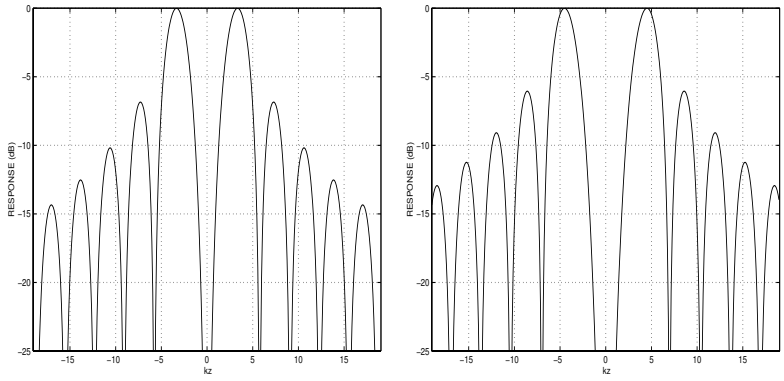

(c) mode: $n = 2$ (d) mode: $n = 3$

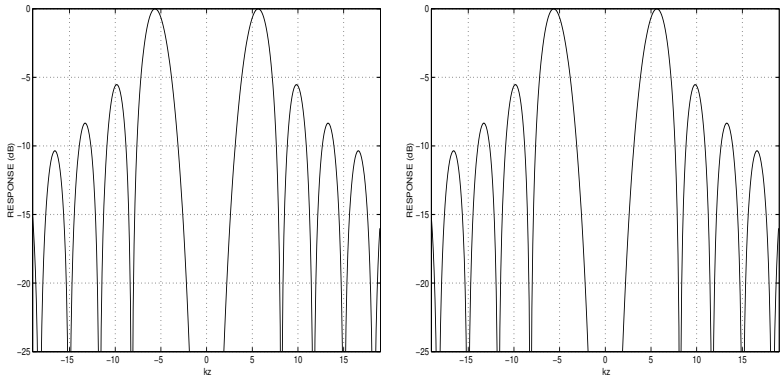

(e) mode: $n = 4$ (f) mode: $n = 5$

Figure 4.1: Magnitude response of elementary filters $F_n(z;k)$ for $n = 0, 1, 2, 3, 4$ and 5, plotted against the product of the wavenumber k and the distance z to the associated sensor.

where z_0 is a reference sensor location.

Proof of Theorem 4.4.1: Let $F_n(z_0;k)$ and $F_n(z_q;k)$ be the frequency response of two elementary filters of the same mode n and associated with sensors at $z_0 \neq 0$ and z_q, respectively. Then from (4.31),

$$\begin{aligned} F_n(z_q;k) &= 2\, j_n(kz_q) \\ &= 2\, j_n(k\frac{z_q}{z_0}z_0) \\ &= F_n(z_0;\frac{z_q}{z_0}k), \end{aligned} \tag{4.34}$$

which is a dilation in the frequency domain.

□

With the output of the double-sided one-dimensional broadband array as defined in (4.30) and the dilation property of the elementary filters (4.34), we are led to a block diagram of a general linear broadband beamformer (4.30) as shown in Figure 4.2.

Regarding the beamformer structure we can make following comments:

1) The proposed general beamformer has three levels of filtering associated with it. The first level consists of elementary beamformers, which are shown inside the dashed-line boxes in Figure 4.2. Each of the elementary beamformers consists of elementary filters of the same mode which are connected to different sensors but are related by the dilation property. As a consequence, we have a set of unique beamformers for each and every mode n. In other words, the elementary beamformer of mode n produces the elementary beamshape of the mode n. Further, the elementary beamformers are independent of the required beampattern specifications.

2) The coefficients $A_n(k)$ form the second level of filtering. Since the $A_n(k)$ determine the shape of the beampattern, we call them *beam shape filters.*

3) The final set of filters $G_n(r;k)$ are independent of sensor locations but dependent on the operating radius r and the mode, and can be simplified using (4.32), (2.20) and (2.17) to obtain

$$G_n(r;k) = \frac{2(-i)^{n+1}}{re^{ikr}h_n^{(2)}(kr)}. \tag{4.35}$$

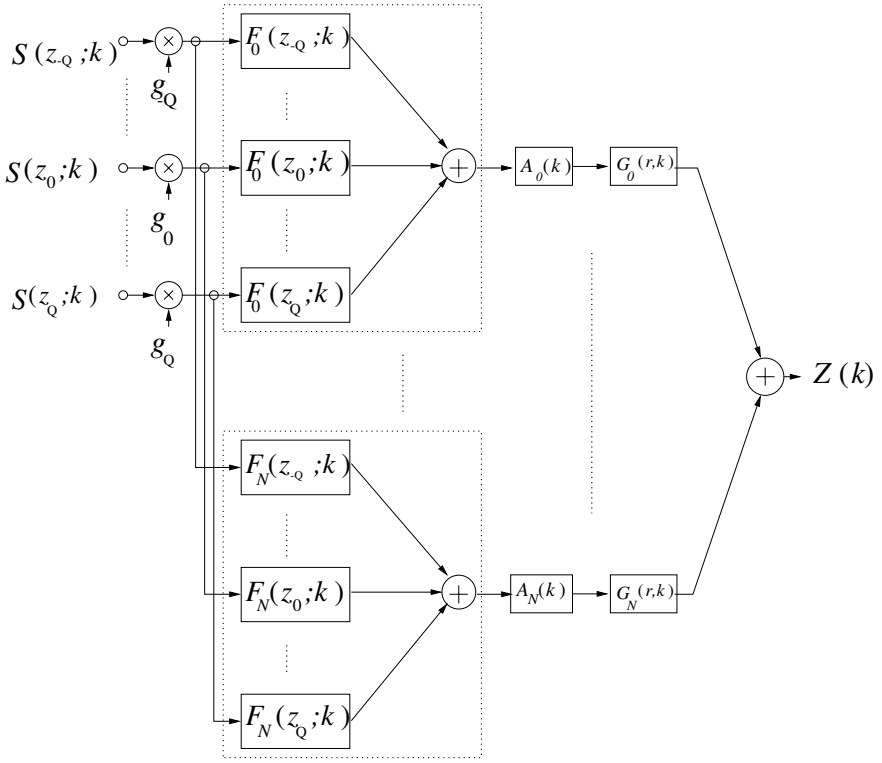

Figure 4.2: Block diagram of a general one-dimensional broadband beamformer described by (4.30) where $F_n(z_q, k)$ are the elementary filters, $G_n(r; k)$ are the radial focusing filters and $A_n(k)$ are the beam shape filters.

By adjusting the parameter r in $G_n(r;k)$, the beamformer can be focused to a particular operating radius r either in nearfield or farfield. To highlight this important property we call the filters $G_n(r;k)$ *radial focusing filters*.

4) In Section 4.2.2 we showed that an arbitrary beampattern can be decomposed into a weighted sum of elementary beamshapes, where the weights are the modal coefficients. Since each elementary beamformer produces an elementary beamshape, an arbitrary beamformer can be implemented by adding them together with the beamshape filter $A_n(k)$ and the focusing filters $G_n(r;k)$. Because of these properties, our design is readily convertible to adaptive implementations, where only the beam shape filters and radial focusing filters need to be adapted (see Chapter 5).

5) Finally, we will give some remarks about the general beamforming structure for two and three dimensional arrays. We can generalize the one dimensional beamforming structure (4.30) to higher dimensions:

$$\widetilde{Z}(k) = \sum_q g_q \, S(\boldsymbol{x}_q;k) \sum_{n=0}^{\infty} G_n(r;k) \sum_{m=-n}^{n} A_{nm} \, F_{nm}(\boldsymbol{x}_q;k), \tag{4.36}$$

where q is an integer, $F_{nm}(\cdot;\cdot)$ are appropriately defined elementary filters of mode n and submode m and the sensors are placed at points $\{\boldsymbol{x}_q\}$ in 3-dimensional space. Let us assume that $\alpha_{nm}(k) = 0$ for $n > N$, where N is a positive integer. Then, there will be $N(N+2)$ elementary beamformers whose outputs are connected to the shape filters $\alpha_{nm}(k)$. Compared with the one-dimensional beamformer (Figure 4.2), there are additional summing points before the radial focusing filters $G_n(r;k)$ which add the outputs from the $(2n+1)$ shape filters A_{nm} of the same mode n but different m values.

4.4.4 Frequency Invariant Beamforming

In many applications it is desirable for a broadband beamformer to have spatial resolution that is constant over the entire bandwidth of the source signals. For examples, in speech acquisition with a microphone array, it might be desirable that the spatial resolution remain constant over the entire speech bandwidth, which covers approximately four octaves. Signals with a bandwidth of several octaves are also encountered in sonar applications. A beamformer that maintains a constant spatial response over an arbitrarily wide bandwidth is called a *frequency invariant beamformer* [7].

In this section we consider the design of frequency invariant beamformers as a special case of the general beamforming theory developed in this chapter. This method generalizes the previous work [1].

An arbitrary beampattern over an arbitrary bandwidth can be expressed by (4.16). It can be seen from (4.16) that if the coefficients $A_n(k)$ are independent of frequency k for a range of frequencies $k \in [k_\mathrm{l}, k_\mathrm{u}] \subset (0, \infty)$, i.e., if

$$A_n(k) = \alpha_{n0} R_n(r, k) = A_n \quad \forall k \in [k_\mathrm{l}, k_\mathrm{u}], \tag{4.37}$$

where $\{A_n\}$ are set of complex scalars, then the beampattern is frequency invariant over $k \in [k_\mathrm{l}, k_\mathrm{u}]$. This simplifies the general beamformer structure in Figure 4.2, where the set of shape dependent filters becomes a set of scalars.

If the beamshape specification $b(\theta)$ is given then the set of scalars $\{A_n\}$ can be determined using (4.17) where $b_r(\theta, k) = b(\theta)$.

4.5 Choice of Sensor Locations

As an engineering problem, it is desirable to minimize the number of sensors required whilst maintaining acceptable performance. The major factor determining the minimum number of sensors possible is *spatial aliasing*. It is well known from the array literature [8] that a sensor spacing of $\lambda/2 = \pi/k$ is needed to avoid spatial aliasing for a narrowband array operating at frequency k. For a broadband array, the upper limit of the design band frequency k_u must be used to avoid spatial aliasing in all frequencies, which suggests that a uniformly spaced array with π/k_u spacing is needed. However, such an array will give a smaller effective aperture for lower frequencies and larger aperture for a high frequencies, which is undesirable. We will now show how to overcome this problem.

In Section 2.5, it was shown that the lower-order modes are the significant ones that give the broad beampattern features, whereas the higher-order modes give the finer detail. We assert that sensible beampattern specifications should involve only the lower order modes. Hence, for most practical beampatterns, the coefficients $A_n(k)$ can be taken as zero for larger n (typically $n > 15$ or so). Let us assume $A_n(k) = 0$ for $n > N$, and thus we need to consider only modes up to N, which limits the number of elementary filters required.

We observe from Figure 4.1 that all the elementary filters tend to have the characteristics of a bandpass filter except the $n = 0$ mode filter which has low-pass characteristics. Due to the dilation property of the elementary filters (see

Theorem 4.4.1), the bandwidth and the cut-off frequencies of elementary filters are scaled with the location of the sensor to which they are connected. Therefore, as we move away from the origin, sensors become relatively inactive at higher frequencies. This means that the sensor spacings can be increased according to the highest frequency for which that sensor is effectively active. Consequently we can minimize the number of sensors as well as avoid the spatial aliasing.

For a given sensor location, the effective cut-off frequency of these filters increases as mode n increases (see Figure 4.1). Let a_n be the product of the upper cut-off frequency $k_{\mathrm{c},n}$ of the mode n filter and the distance z to the associated sensor from the origin (i.e., $a_n = k_{\mathrm{c},n} z$), where $k_{\mathrm{c},n}$ is defined as the first zero crossing point above the passband[2]. Table 4.1 lists the a_n of the first 16 elementary filters. Clearly the upper cut-off frequencies of elementary filters are related by $k_{\mathrm{c},1} < k_{\mathrm{c},2} < \ldots < k_{\mathrm{c},N}$. Therefore to make a sensor inactive for a given frequency k, it is sufficient to have $k_{\mathrm{c},N} < k$.

mode (n)	$a_n = k_{\mathrm{c},n} z$	mode (n)	$a_n = k_{\mathrm{c},n} z$
0	3.142	8	12.79
1	4.493	9	13.91
2	5.763	10	15.03
3	6.988	11	16.14
4	8.183	12	17.25
5	9.356	13	18.35
6	10.51	14	19.44
7	11.05	15	20.54

Table 4.1: Upper cut-off frequencies of the first 16 elementary filters as a product of sensor location z and cut-off frequency $k_{\mathrm{c},n}$.

We can now give complete guidelines for choosing discrete sensor locations. Here we consider a double-sided array and begin with a sensor located at the array origin. Initially, to avoid spatial aliasing we need a sampling distance of

$$d_{k_{\mathrm{u}}} = \lambda_{\mathrm{u}}/2 = \pi/k_{\mathrm{u}}. \tag{4.38}$$

As long as the cut-off frequency k_q of the sensor located at z_q (which is equal to the cut-off frequency $k_{\mathrm{c},N}$ of the highest mode elementary filter attached to that sensor) is greater than the upper design frequency k_{u}, we need to maintain the

[2]Note that these elementary filters are not ideal bandpass filters and other definitions for cut-off frequencies such as half power point can be used.

above sampling distance. In this central portion of the array, the cut-off frequency of the qth sensor from either side of the origin is given by

$$k_q = \frac{a_N}{|q|\pi} k_{\mathrm{u}} \qquad \text{for } 0 < |q| \leq Q,$$

where Q is the number of uniformly spaced sensors in one side of the array. As we move further away from the origin, i.e., as q grows, k_q decreases and will become less than k_{u}. The number of uniformly spaced sensors Q required to satisfy this constraint is given by

$$Q = \lceil \frac{a_N}{\pi} \rceil, \tag{4.39}$$

where $\lceil \cdot \rceil$ is the ceiling function. At this point, we can increase the sampling distance, just to avoid spatial aliasing at k_Q. Since the cut-off frequency k_{Q+1} of the $(Q+1)^{th}$ sensor is less than that of Q^{th} sensor, the sampling distance can be further increased for the next location. This process can be continued until the cut-off frequency of the last sensor becomes less than the lower design frequency k_{l}. Therefore the location of the q^{th} sensor relative to the origin is given by

$$z_q = \begin{cases} \frac{q\pi}{k_{\mathrm{u}}} & \text{for } |q| \leq Q \\ \frac{Q\pi}{k_{\mathrm{u}}} \left(1 + \frac{\pi}{a_N}\right)^{|q|-Q} & \text{for } Q < |q| \leq L \ , \end{cases} \tag{4.40}$$

where L is the total number of sensors in one side of the array. Using the fact that the cut-off frequency of the last sensor has to be less than or equal to the lower design frequency k_{l}, the number of minimum sensors per one side required to implement a broadband array over the design band is

$$L = Q + \lfloor \frac{\log\left(\frac{a_N k_{\mathrm{u}}}{Q\pi k_{\mathrm{l}}}\right)}{\log\left(1 + \frac{\pi}{a_N}\right)} \rfloor, \tag{4.41}$$

where $\lfloor \cdot \rfloor$ is the floor function. Note that we need a total of $2L+1$ sensors altogether to have a double-sided array.

Spatial Weights

In order to complete the guidelines for a practical realization of the beamformer given by (4.30), we now consider the spatial weighting term g_q introduced in (4.29). Recall that the Trapezoidal rule has been used to approximate the integral in

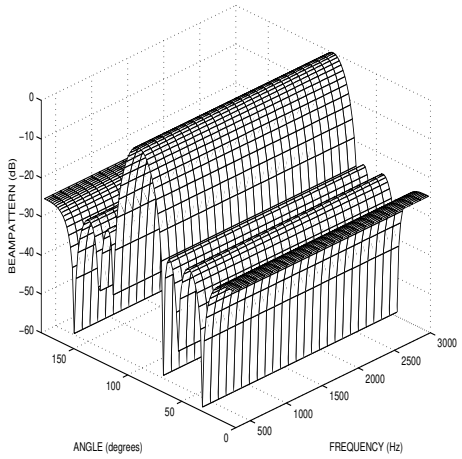

Figure 4.3: Desired beamformer response used in the example in Section 4.6: 25dB Chebyshev beampattern over $300 - 3000$Hz.

equation (4.28) by the summation in (4.29), hence the spatial weighting term g_q is given by (possibly) non-uniform sensor locations (4.40) as

$$g_q = \begin{cases} \frac{1}{2}(z_{q+1} - z_{q-1}) & \text{if } |q| < L \\ \frac{1}{2}(z_L - z_{L-1}) & \text{if } |q| = L. \end{cases} \tag{4.42}$$

Note that any other integral approximation method can be used instead of the Trapezoidal rule and the spatial weighting term g_q needs to be determined appropriately.

4.6 Design Example

We now consider an example of broadband beamforming design using the techniques introduced above.

Suppose we wish to design a one-dimensional microphone array for operation in the air at sea level so $c = 345\text{ms}^{-1}$. Suppose that the desired design frequency range is $300 - 3000$ Hz, which is suitable for speech applications. Let us limit the maximum mode index, N, to 15 as suggested in Section 4.5; thus we assume all beampatterns of our interest can be approximately decomposed to the first 16 modes. Now we can determine the sensor locations and 16 elementary filters, which are independent of the desired response once the design band and the number of modes are decided. From Table 4.1, the product of cut-off frequency $k_{c,n}$ and the sensor location z of the highest (15th) mode elementary filter is $a_N = 20.54$. Next

the sensors are placed according to (4.40) and it is found from (4.41) that the total number of sensors required is 41 and the length of the double sided array is 4.9m. The sensor locations are given in Table 4.2 and the frequency responses of the elementary filters are given by (4.31).

Now we consider an example beampattern which is for a beamformer having a constant Chebyshev 25 dB beampattern (shown in Figure 4.3) over the frequency range $300 - 3000$ Hz. The example chosen is a frequency invariant beampattern, although we stress that our design method is not restricted to frequency invariant beamformers. For this case, the beampattern is characterized by the scalar coefficients A_n and we have calculated them for $n = 0, 1, \ldots, 15$ using (4.18).

For the sake of efficient implementation, all the filters are collapsed into one filter per sensor. This is possible, since the proposed beamformer structure (Figure 4.2) consists of linear combinations of various filters.

q	z_q/λ_u	q	z_q/λ_u
0	0.0	11	6.2
1	0.5	12	7.1
2	1.0	13	8.2
3	1.5	14	9.5
4	2.0	15	10.9
5	2.5	16	12.6
6	3.0	17	14.5
7	3.5	18	16.7
8	4.0	19	19.3
9	4.6	20	22.3
10	5.4		

Table 4.2: Locations z_q of the q^{th} sensor of the example double sided symmetric array in Section 4.6 (given in terms of the upper design wavelength λ_u).

The resulting beamformer is focused at the farfield by setting the parameter $r = 100\lambda_l$ in the focusing filter $G_n(r;k)$. The response of the beamformer to a farfield source is given in Figure 4.4(b), which is close to the desired response. The response of the same farfield focused beamformer to a nearfield source at a radius $3\lambda_l$ is given Figure 4.4(a). It is evident from this figure that the farfield design is inadequate for the desired nearfield performance. Next we focus the same beamformer to the nearfield by simply adjusting the variable r in the focusing filter $G_n(r;k)$ to $3\lambda_l$. The resulting beamformer is simulated in the nearfield and

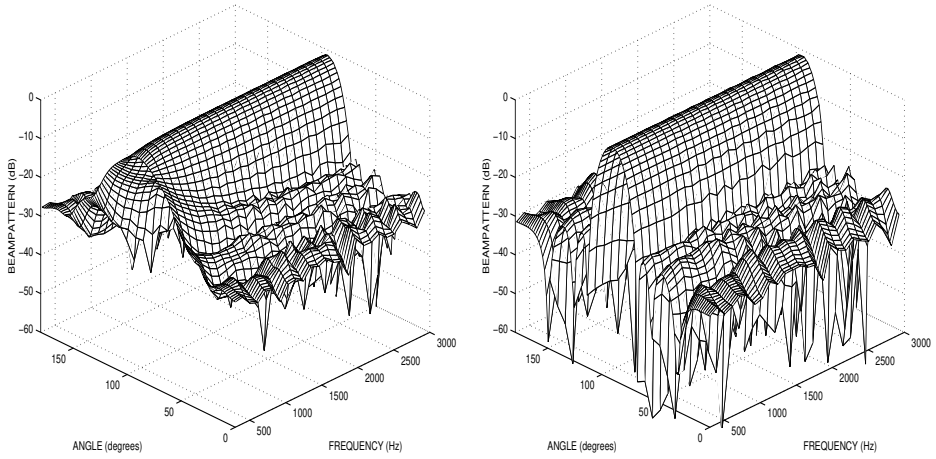

(a) nearfield response at a radius $3\lambda_l$

(b) farfield response

Figure 4.4: Response of the farfield focused (by setting $r = 100\lambda_l$ in the focusing filter $G_n(r;k)$) beamformer (see Figure 4.2) with 25dB Chebyshev beampattern to (a) a nearfield source at a radius $3\lambda_l$ (b) a farfield source at $100\lambda_l$. This figure demonstrates that the farfield design is inadequate for the desired nearfield performance.

we observe an improved response in Figure 4.5(a). The focused array response is close to the desired response with negligible variation in the main beam and slight ripples in the side lobes. We conclude that the approximation involved in discretizing and truncating the continuous sensor was sufficiently accurate. For completeness, we find the response of nearfield focused beamformer to a farfield source and show this in Figure 4.5(b).

The similar appearance of Figure 4.4(a) and Figure 4.5(b) (also the pair Figure 4.4(b) and Figure 4.5(a)) can be explained by the results in Section 3.4 and our work [9] on radial reciprocity, which established the asymptotic equivalence of two transformation problems: (i) determining the nearfield performance of a farfield beampattern specification, and (ii) determining the equivalent farfield beampattern corresponding to a nearfield beampattern specification. We can view Figure 4.5(b) and Figure 4.4(a) as the result of problem (i) and (ii), respectively, with beampattern specification given in Figure 4.3 for both cases.

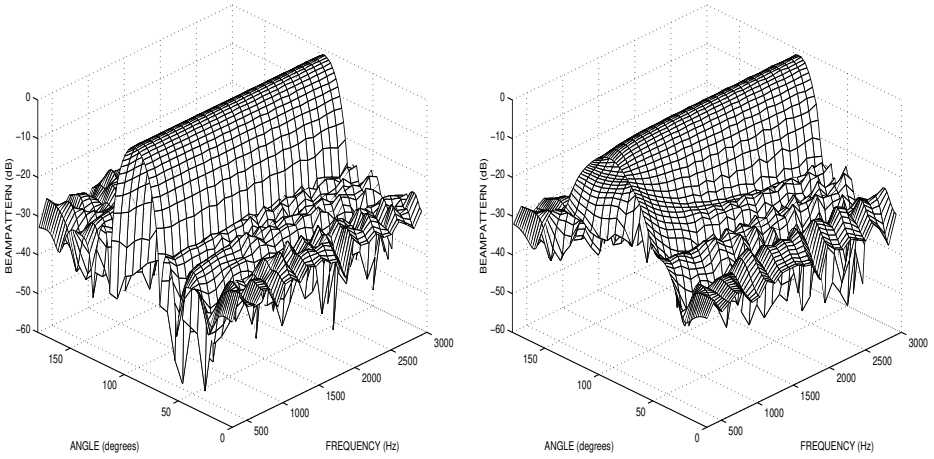

(a) nearfield response at $3\lambda_l$ (b) farfield response

Figure 4.5: Response of the nearfield focused (by setting $r = 3\lambda_l$ in the focusing filter $G_n(r;k)$) beamformer (see Figure 4.2) with 25dB Chebyshev beampattern to (a) a nearfield source at a radius $3\lambda_l$ (b) a farfield source at $100\lambda_l$.

4.7 Summary and Contributions

A new method of general broadband beamforming covering farfield and nearfield operations has been proposed in this chapter. The efficient parameterization afforded by this technique enables the beamformer to be focused to a desired radial distance using a single parameter and the shape of the beampattern can be controlled by another set of parameters. These properties make it potentially useful for adaptive beamformer design.

We itemize some specific contributions made in this chapter:

i. We have established an expression for the continuous aperture illumination required to realize a given farfield broadband beampattern in terms of modal coefficients of the given beampattern.

ii. The above result was generalized to obtain a continuous aperture, which can realize an arbitrary beampattern at a radius r from the origin, i.e., the aperture can be focused to a desired radius. The only restriction that applies is that the aperture must be inside a sphere with the radius r.

iii. The concept of elementary aperture functions indexed by modes, was introduced. Each elementary aperture function corresponds to the elementary beamshape of the same mode. Thus, given a beampattern specification in its

modal representation, the required continuous aperture can be constructed by linearly combining elementary aperture functions with appropriate weights which depend on the modal coefficients of the desired beampattern.

iv. We also obtained exact expressions for the elementary aperture functions for linear and spherical aperture geometries.

v. A general discrete linear beamformer was obtained by approximating the theoretical continuous aperture by a set of discrete sensors. The resulting beamformer structure can be factored into three levels of filtering: (i) beampattern independent elementary beamformers; (ii) beampattern shape dependent filters; and (iii) radial focusing filters where a single parameter can be adjusted to focus the array to a desired radial distance from the array origin.

vi. We also gave guidelines on how to place sensors in a nonuniform fashion to minimize the number of sensors required.

References

[1] D.B. Ward, R.A. Kennedy, and R.C. Williamson, "Theory and design of broadband sensor arrays with frequency invariant far-field beampatterns," *J. Acoust. Soc. Amer.*, vol. 97, pp. 1023–1034, Feb. 1995.

[2] G.N. Watson, *A Treatise on the Theory of Bessel Functions*, Cambridge University Press, London, 1958.

[3] E. Skudrzyk, *The Foundations of Acoustics*, Springer-Verlag, New York, 1971.

[4] G.W. Elko and A.N. Pong, "A steerable and variable first-order differential microphone array," *Proc. IEEE Int. Conf. Acoust., Speech Signal Processing(ICASSP97)*, pp. 223–226, 1997.

[5] R.S. Elliott, "On discretizing continuous aperture distributions," *IEEE Trans. Antennas Propagat.*, vol. AP-25, pp. 617–621, Sept. 1977.

[6] C.F. Winter, "Using continuous aperture illumination discretely," *IEEE Trans. Antennas Propagat.*, vol. AP-25, No. 5, pp. 695–700, Sept. 1977.

[7] D.B. Ward, *Theory and Application of Broadband Frequency Invariant Beamforming*, Ph.D. thesis, Australian National University, Canberra, Australia, 1996.

[8] J.L. Flanagan, "Beamwidth and useable bandwidth of delay-steered microphone arrays," *AT&T Technical Journal*, vol. 64, pp. 983–995, Apr. 1985.

[9] R.A. Kennedy, D.B. Ward, and T.D. Abhayapala, "Nearfield beamforming using radial reciprocity," *IEEE Trans. Sig. Proc.*, vol. 47, no. 1, pp. 33–40, Jan. 1999.

Chapter 5

Nearfield Adaptive Beamforming

5.1 Introduction

In this chapter, we consider the design of an adaptive beamformer to operate in a signal environment consisting of broadband nearfield sources, where some of the interfering signals may be correlated with the desired signal.

Conventional adaptive beamformers such as the Frost beamformer [1] and Generalized Sidelobe Canceller (GSC) [2] are found to be effective in strong interference as long as the interferers are uncorrelated with the desired source and the assumption of plane wave propagation is met. In some cases, due to coherent interference, conventional beamformers break down as a result of signal cancellation of the desired source. This problem arises in hands-free speech acquisition using a microphone array, where the correlated interference is due to reflections of the desired signal [3]. Remedies have been proposed to reduce the effect of signal cancellation due to correlated interference by spatial averaging [4] for narrowband signals and by interpolating arrays or spectral averaging [3, 5–7]. However, all of the above pieces of work are based on the assumption of farfield sources. In this chapter, we use the general broadband beamforming theory developed in Chapter 4 to propose a novel adaptive beamformer that overcomes coherent signal cancellation and works well for the sources in the nearfield of the array.

There appears to be little work in the literature on nearfield adaptive beamforming. In [8], the Frost algorithm and another method have been used to suppress uncorrelated interference speech sources. However, they assumed that plane waves are incident on the array and the issue of coherent interference was not addressed. In [9], spatial filtering is employed in the blocking matrix of a beamformer based on the GSC structure [2] to control the desired signal cancellation, and the adaptation

takes place only when the speaker is silent in order to avoid signal cancellation due to speaker correlated interference. The few other related works we are aware of dealing with adaptive microphone array can be found in [10–12].

In this chapter, a nearfield broadband adaptive beamformer is proposed by extending the results in Chapter 4, where a general broadband beamformer is introduced using modal analysis tools introduced in Chapter 2. It provides an efficient parameterization for the nearfield broadband beamforming problem with a single parameter to focus the beamformer to a desired operating radius, and another set of parameters to control the actual broadband beampattern shape. In this chapter, the frequency invariant nature of the above beamforming structure is used to combat signal cancellation due to correlated interference and the radial focusing capability is used to deal with the nearfield source signals.

5.2 Problem formulation

5.2.1 Background

The objective of broadband adaptive beamforming is to preserve a chosen frequency response for a desired signal arriving from a given source while minimizing the contribution from interfering sources. This is often achieved by minimizing the beamformer output power while maintaining the chosen frequency response in the look direction.

Several different performance measures can be adopted to govern the adaptation process that adjusts the parameters (e.g., sensor weights or filter coefficients) of the beamformer. The four popular performance measures for obtaining the optimum solution are based on minimum mean square error (MSE), maximum signal to noise ratio (SNR), maximum likelihood (ML), and minimum variance (MV) criteria. In this chapter we use the last criterion, specifically the linearly constrained minimum variance (LCMV) beamformer.

There are two general methods of beamforming for broadband signals: time-domain beamforming and frequency-domain beamforming. In time-domain beamforming, a transversal filter (FIR filter) is used on each sensor. For an array with $2Q+1$ sensors, each feeding a L-tap FIR filter, there are $(2Q+1) \times L$ parameters to be adapted. The popular Frost algorithm [1] solves the broadband time-domain minimum variance beamforming problem.

In frequency-domain beamforming, the data received by each sensor is separated into narrowband frequency bins and the data in each frequency bin is processed

separately using narrowband techniques. For an array with $(2Q+1)$ sensors, with M frequency bins in the bandwidth of interest, there are $(2Q+1)\times M$ parameters to be adapted. Frost's algorithm can also be used in frequency-domain beamforming [13] where in each frequency bin one of the parameters is used to maintain a look direction constraint, and the remaining parameters minimize the output power.

A discussion on the trade-off between frequency- and time-domain processors is found in [14, 15]. Since our proposed nearfield adaptive beamformer is naturally formulated in the frequency-domain, we will only consider frequency domain processing in this thesis.

5.2.2 Array Model

Consider V broadband signals impinging on a linear double-sided array of $2Q+1$ sensors from sources at $(r_1,\theta_1),\ldots,(r_V,\theta_V)$ where r_v is the distance to the vth source from the array origin and θ_v is measured relative to the array axis. One of these signals is from the desired source at known location (r_1,θ_1), and the remaining signals are treated as interference. We assume that the desired source location is known exactly. Otherwise, derivative constraints [16] could be included to provide robustness for look direction mismatch.

In the farfield array processing literature, the received signal from a source at each sensor is expressed as a time delay or advance of the received signal at the sensor origin from the corresponding source. In this paper, we follow the same convention.

The received signals are discretized at each sensor, and the resulting array data is divided into blocks of J samples and Discrete Fourier transformed to produce $M \le J$ narrowband frequency bins within the design bandwidth $k \in [k_{\mathrm{l}}, k_{\mathrm{l}}]$, where k_{l} and k_{l} are the lower and upper frequencies of the design bandwidth, respectively. The array data in the mth frequency bin is

$$\boldsymbol{z}(k_m) = \sum_{v=1}^{V} \boldsymbol{a}_{r_v}(\theta_v; k_m) s_v(k_m) + \boldsymbol{n}(k_m), \tag{5.1}$$

where $s_v(\cdot)$ is the signal received from the vth source at the origin, $\boldsymbol{n}(\cdot)$ is the uncorrelated noise data and

$$\boldsymbol{a}_r(\theta;k) = \Big[r\frac{e^{-i(kd(r,\theta,z_{-Q})-r)}}{d(r,\theta,z_{-Q})}, \ldots, r\frac{e^{-i(kd(r,\theta,z_Q)-r)}}{d(r,\theta,z_Q)} \Big]^T, \tag{5.2}$$

where

$$d(r,\theta,z) = \sqrt{z^2 + r^2 - 2rz\cos\theta} \tag{5.3}$$

is the distance from the source to a point z in the sensor. The above formulation is valid regardless of whether all the sources are in the farfield or in the nearfield. In the case of farfield sources, $r_v \to \infty$, $v = 1, \ldots, V$ and (5.1) is still valid since

$$\lim_{r\to\infty} \boldsymbol{a}_r(\theta;k) = \left[e^{-ikz_{-Q}\cos\theta}, \ldots, e^{-ikz_Q\cos\theta}\right]^T. \tag{5.4}$$

We can also write (5.1) as

$$\boldsymbol{z}(k_m) = \boldsymbol{A}(k_m)\boldsymbol{s}(k_m) + \boldsymbol{n}(k_m), \quad m = 1, \ldots, M \tag{5.5}$$

where

$$\boldsymbol{A}(k) = \left[\boldsymbol{a}_{r_1}(\theta_1;k_m), \ldots, \boldsymbol{a}_{r_V}(\theta_V;k_m)\right]. \tag{5.6}$$

and $\boldsymbol{s}(k) = [s_1(k), \ldots, s_V(k)]^T$. Equation (5.5) will be useful in analyzing results in this chapter.

5.3 Conventional Broadband Minimum Variance Beamforming

In this section, we outline conventional minimum variance beamforming in the frequency domain. The objective here is to minimize the beamformer output power while maintaining a chosen look direction response.

Applying a set of frequency dependent weights to the received data (5.1), the beamformer output is

$$Z(k_m) = \boldsymbol{w}_m^H \boldsymbol{z}(k_m), \tag{5.7}$$

where $\boldsymbol{w}_m$ is a $2Q+1$ weight vector for the mth frequency bin. Thus, the expected output power of the beamformer is

$$E\{|Z(k_m)|^2\} = \boldsymbol{w}_m^H \boldsymbol{R}(k_m)\, \boldsymbol{w}_m, \tag{5.8}$$

where

$$\boldsymbol{R}(k_m) = E\{\boldsymbol{z}(k_m)\boldsymbol{z}^H(k_m)\}, \tag{5.9}$$

is the data covariance matrix and satisfies $\boldsymbol{R}^H(k_m) = \boldsymbol{R}(k_m)$. We substitute (5.5) in (5.9) to get

$$\boldsymbol{R}(k_m) = \boldsymbol{A}(k_m)\boldsymbol{R}_s(k_m)\boldsymbol{A}^H(k_m) + \boldsymbol{R}_n(k_m) \tag{5.10}$$

where

$$\boldsymbol{R}_s(k) = E\{\boldsymbol{s}(k_m)\boldsymbol{s}^H(k_m)\}, \tag{5.11}$$

is the $V \times V$ source covariance matrix and

$$\boldsymbol{R}_n(k) = E\{\boldsymbol{n}(k_m)\boldsymbol{n}^H(k_m)\},$$

is the $(2Q+1) \times (2Q+1)$ noise covariance matrix.

The spatial response of the beamformer to a source at (r, θ) is

$$b_r(\theta; k_m) = \boldsymbol{w}_m^H \, \boldsymbol{a}_r(\theta; k_m), \tag{5.12}$$

where $\theta \in [0, \pi]$. The broadband minimum variance beamforming problem is formulated mathematically as

$$\begin{aligned} &\min_{\boldsymbol{w}_m} \boldsymbol{w}_m^H \boldsymbol{R}(k_m) \boldsymbol{w}_m \\ &\text{subject to } \boldsymbol{w}_m^H \boldsymbol{a}_{r_1}(\theta_1; k_m) = 1, \end{aligned} \tag{5.13}$$

where (r_1, θ_v) is the location of the desired source and the constraint has been taken as unity without loss of generality. Then the solution to (5.13) is given by [1]

$$\boldsymbol{w}_m^{(\text{opt})} = \frac{\boldsymbol{R}^{-1}(k_m)\boldsymbol{a}_{r_1}(\theta_1; k_m)}{\boldsymbol{a}_{r_1}^H(\theta_1; k_m)\boldsymbol{R}^{-1}(k_m)\boldsymbol{a}_{r_1}^H(\theta_1; k_m)}. \tag{5.14}$$

Since a different weight vector is found for each frequency bin, this method is referred to as the independent multiple narrowband (IMN-MVDR) beamformer [13].

Signal Cancellation

To show the desired signal cancellation in this method, we consider two correlated signals from two identical sources located at (r_1, θ_1) and (r_2, θ_2). The received signals from two sources at the origin of the array are related by

$$s_2(k) = \frac{r_1}{r_2} e^{-ik(r_2 - r_1)} s_1(k). \tag{5.15}$$

The source correlation matrix (5.11) for this case is given by,

$$\boldsymbol{R}_s(k) = E\{s_1(k) s_1^*(k)\} \begin{bmatrix} 1 & \frac{r_1}{r_2} e^{ik(r_2 - r_1)} \\ \frac{r_1}{r_2} e^{-ik(r_2 - r_1)} & \frac{r_1^2}{r_2^2} \end{bmatrix}. \tag{5.16}$$

Observe that $\boldsymbol{R}_s(k)$ is a singular matrix. Singularity of $\boldsymbol{R}_s(k)$ causes rank deficiencies in $\boldsymbol{R}(k_m)$ and in turn the two signals cancel each other[1].

5.4 General Broadband MV Beamforming

5.4.1 Preliminary

It was shown in [13] that the use of a frequency invariant beamformer reduces the computational complexity and increases the rate of convergence of the adaptive parameters. In [3], the same idea was used to reduce the signal cancellation due to coherent interference in minimum variance beamformers. The above work is based on the frequency invariant beamformer structure described in [19], which assumed farfield sources, and is not suitable for nearfield operation. The general beamformer proposed in Chapter 4 has structural properties similar to the beamformer in [19], and, in addition, our beamformer can deal with nearfield sources. Hence we use the frequency invariant version of the beamformer described in Chapter 4 to propose a new MV beamforming method, to overcome the limitations present in [13] and to retain its other capabilities.

[1] See [17, 18] for more detailed treatment of the signal cancellation phenomenon.

5.4.2 Modal Beamformer

Using (4.30) and (4.37), the structure of a broadband frequency invariant beamformer for sources at a radius r_1 from the array origin is given by

$$Z(k) = \sum_{n=0}^{N} A_n \, G_n(r_1; k) \sum_{q=-L}^{L} g_q \, S(z_q; k) \, F_n(z_q; k), \tag{5.17}$$

where $G_n(r, \cdot)$ are the radial focusing filters (4.32) and $F_n(z_q; \cdot)$ are the elementary filters (4.31). The above equation can be written in matrix form:

$$Z(k) = \boldsymbol{b}^H \boldsymbol{C}_{r_1}(k) \, \boldsymbol{z}(k) \tag{5.18}$$

where $\boldsymbol{b} = [A_0, \ldots, A_N]^H$ is a vector of beamshape coefficients,

$$\boldsymbol{C}_{r_1}(k) = \begin{bmatrix} G_0(r_1;k) & 0 & \ldots & 0 \\ 0 & \ddots & & \vdots \\ \vdots & & \ddots & 0 \\ 0 & \ldots & 0 & G_N(r_1;k) \end{bmatrix} \begin{bmatrix} F_0(z_{-Q};k) & \ldots & F_0(z_Q;k) \\ \vdots & \ddots & \vdots \\ F_N(z_{-Q};k) & \ldots & F_N(z_Q;k) \end{bmatrix} \times \begin{bmatrix} g_{-Q} & 0 & \ldots & 0 \\ 0 & \ddots & & \vdots \\ \vdots & & \ddots & 0 \\ 0 & \ldots & 0 & g_Q \end{bmatrix} \tag{5.19}$$

and

$$\boldsymbol{z}(k) = [S(z_{-Q}; k) \cdots S(z_Q; k)]^T$$

represents the array data. The spatial response of the beamformer (5.17) to a source at (r, θ) is given by

$$\begin{aligned} b_r(\theta; k) &= \boldsymbol{b}^H \, \boldsymbol{C}_{r_1}(k) \boldsymbol{a}_r(\theta; k) \\ &\approx b_r(\theta), \;\; \text{if } r = r_1, \, \forall \theta \text{ and } \forall k \in [k_l, k_l], \end{aligned} \tag{5.20}$$

i.e., the response is approximately frequency invariant[2]. Because the beamshape coefficients $\boldsymbol{b}$ are independent of frequency, and the response $b_r(\theta; k)$ is independent

[2]As described in Chapter 4, the behaviour would be exactly frequency invariant were if not for truncation of the aperture and sensor discretization.

of frequency within the design band for $r = r_1$, it follows from (5.20) that

$$\boldsymbol{C}_{r_1}(k)\boldsymbol{a}_{r_1}(\theta;k) \approx \boldsymbol{C}_{r_1}(k_0)\boldsymbol{a}_{r_1}(\theta;k_0) \quad \forall\theta \text{ and } \forall k \in [k_l, k_l], \tag{5.21}$$

where k_0 is a nominal frequency within the bandwidth of interest.

The importance of the above formulation is that the discrete array beamformer (5.18) can be focused to any radius r_1 to give a frequency invariant response at that radius and there is a single set of modal coefficients $\boldsymbol{b}$ that defines the spatial response, i.e., the beampattern shape, over the bandwidth of interest. Thus, the number of adaptation parameters is equal to $N + 1$, the number of modes used. Usually this is much less than that of a conventional adaptive beamformer where the number of adaptation parameters are equal to the product of the number of sensors and number of filter taps per each sensor. Of course, it is the imposition of frequency invariance as a constraint that enables this reduction.

5.4.3 Novel MV Beamforming

We now apply the above beamforming processing (5.18) to the received data (5.1), giving the beamformer output

$$Z(k_m) = \boldsymbol{b}^H \boldsymbol{C}_{r_1}(k_m)\boldsymbol{z}(k_m) \tag{5.22}$$

in the mth frequency bin. The expected output power of the beamformer over all frequency bins is

$$\begin{aligned} E\{|Z|^2\} &= \frac{1}{M}\sum_{m=1}^{M} E\{|Z(k_m)|^2\} \\ &= \boldsymbol{b}\,\overline{\boldsymbol{R}}\,\boldsymbol{b}^H, \end{aligned}$$

where

$$\overline{\boldsymbol{R}} = \frac{1}{M}\sum_{m=1}^{M} \boldsymbol{C}_{r_1}(k_m) E\{\boldsymbol{z}(k_m)\boldsymbol{z}^H(k_m)\}\boldsymbol{C}_{r_1}^H(k_m) \tag{5.23}$$

is the frequency averaged data covariance matrix. The objective here is to find the modal coefficient vector $\boldsymbol{b}$ that minimizes the interference power while passing signals from the desired location (r_1, θ_1) with unity gain for all frequencies within

the design band. This is formulated as

$$\begin{aligned} \min_{\boldsymbol{b}} \ & \boldsymbol{b}^H \overline{\boldsymbol{R}} \boldsymbol{b} \\ \text{subject to} \ & \boldsymbol{D}^H \boldsymbol{b} = \mathbf{1}_{M_1}, \end{aligned} \tag{5.24}$$

where

$$\boldsymbol{D} = [\boldsymbol{C}_{r_1}(k_1)\boldsymbol{a}_{r_1}(\theta_1; k_1), \ldots, \boldsymbol{C}_{r_1}(k_{M_1})\boldsymbol{a}_{r_1}(\theta_1; k_{M_1})]$$

is a constraint matrix and $\mathbf{1}_{M_1}$ is a vector of ones of dimension M_1. Theoretically, a single constraint at the midband frequency should be sufficient as evident from (5.21). However, the array beamformer is only an approximation of the frequency invariant theoretical continuous sensor. Following the idea indicated in [3], we impose a small number of constraints M_1 across the frequency band of interest to reinforce a frequency invariant response.

Equation (5.24) is a well known constrained LMS problem and its optimum solution is given by [1]

$$\boldsymbol{b}_{\text{opt}} = \overline{\boldsymbol{R}}^{-1} \boldsymbol{D} [\boldsymbol{D}^H \overline{\boldsymbol{R}}^{-1} \boldsymbol{D}]^{-1} \mathbf{1}_{M_1}. \tag{5.25}$$

Since we used modal analysis techniques to formulate this beamformer, we will refer it as the modal analysis (MA)-MVDR beamformer.

5.4.4 Analysis of the Covariance Matrix

In this section we investigate the frequency averaged data covariance matrix (5.23) to show that it preserves the directional information of all sources despite the frequency averaging.

Recall that the beamformer (5.17) is an approximation of the broadband continuous (linear) aperture (4.24) derived in Chapter 4. To obtain an approximate analytical expression for the covariance matrix (5.23), we calculate the output of the broadband continuous aperture (5.17) when in the same signal environment described in Section 5.2.2 via

$$\hat{Z}(k) = \int_{-\infty}^{\infty} \rho_{r_1}(z; k) S(z; k) dz \tag{5.26}$$

where

$$\rho_{r_1}(z;k) = \sum_{n=0}^{\infty} A_n \, 2k(-i)^n \, \frac{R_n(\infty,k)}{R_n(r_1,k)} \, j_n(kz), \tag{5.27}$$

and $S(z;k)$ is the Fourier transform of the signal received at a point z on the array. As in the case of the discrete beamformer (5.17), the continuous aperture (5.26) is focused to a radius r_1 in order to have a frequency invariant response for sources at that radius.

For the same signal environment described in Section 5.2.2, we can write

$$S(z;k) = \sum_{v=1}^{V} r_v e^{ikr_v} \, \frac{e^{-ikd(r_v,\theta_v,z)}}{d(r_v,\theta_v,z)} \, s_v(k) + n(z;k), \tag{5.28}$$

where $n(z;k)$ is the sensor noise at z which is assumed to be uncorrelated from point to point on the sensor. From the development of Chapter 2 (see Section 2.6.2), we can write the output of the continuous aperture as,

$$\hat{Z}(k) = \sum_{v=1}^{V} b_{r_v}(\theta_v;k) \, s_v(k) + Z_{\text{noise}}(k), \tag{5.29}$$

where

$$b_r(\theta;k) = \int \rho_{r_1}(z;k) \, re^{ikr} \, \frac{e^{-ikd(r,\theta,z)}}{d(r,\theta_v,z)} \, dz, \tag{5.30}$$

is the spatial response of the continuous aperture to a source at a point (r,θ), and

$$Z_{noise}(k) = \int_{-\infty}^{\infty} \rho_{r_1}(z;k) n(z;k) dz.$$

It can be shown that, when $r_v = r_1$, the spatial response (5.30) is frequency invariant and given by (see (4.16)),

$$b_{r_1}(\theta_v;k) \approx \sum_{n=0}^{\infty} A_n P_n(\cos\theta_1),$$

and generally,

$$b_{r_v}(\theta_v;k) \approx \sum_{n=0}^{\infty} A_n \, \frac{R_n(r_v,k)}{R_n(r_1,k)} \, P_n(\cos\theta_v). \tag{5.31}$$

Now we substitute (5.31) into (5.29) and obtain the output of the continuous aperture to the signal environment described in Section 5.2.2 as

$$\hat{Z}(k) \approx \sum_{v=1}^{V} \sum_{n=0}^{\infty} \frac{R_n(r_v,k)}{R_n(r_1,k)} P_n(\cos\theta_v) s_v(k) + Z_{noise}(k). \tag{5.32}$$

Since the discrete array beamformer (5.22) is an approximation of the continuous sensor, it can be written using (5.32) as

$$Z(k_m) \approx \boldsymbol{b}^H \boldsymbol{T}\boldsymbol{U}(k_m)\boldsymbol{s}(k_m) + \boldsymbol{b}^H \boldsymbol{C}_{r_1}(k_m)\boldsymbol{n}(k_m) \tag{5.33}$$

where the block diagonal matrix

$$\boldsymbol{U}(k) = \mathrm{diag}[\begin{bmatrix} \frac{R_0(r_1,k)}{R_0(r_1,k)} \\ \vdots \\ \frac{R_N(r_1,k)}{R_N(r_1,k)} \end{bmatrix} \cdots, \begin{bmatrix} \frac{R_0(r_V,k)}{R_0(r_1,k)} \\ \vdots \\ \frac{R_N(r_V,k)}{R_N(r_1,k)} \end{bmatrix}],$$

$$\boldsymbol{T} = [\begin{bmatrix} P_0(\theta_1) & 0 & \dots & 0 \\ 0 & \ddots & & \vdots \\ \vdots & & \ddots & 0 \\ 0 & \dots & 0 & P_N(\theta_1) \end{bmatrix}, \cdots \begin{bmatrix} P_0(\theta_V) & 0 & \dots & 0 \\ 0 & \ddots & & \vdots \\ \vdots & & \ddots & 0 \\ 0 & \dots & 0 & P_N(\theta_V) \end{bmatrix}], \tag{5.34}$$

and $\boldsymbol{s}(k) = [s_1(k), \dots, s_V(k)]^T$.

To show the effects of frequency averaging in (5.23), we form an alternative expression for frequency average correlation matrix using (5.33) as

$$\overline{\boldsymbol{R}} \approx \boldsymbol{T}\overline{\boldsymbol{R}}_s\boldsymbol{T}^H + \overline{\boldsymbol{R}}_n, \tag{5.35}$$

where

$$\begin{aligned} \overline{\boldsymbol{R}}_s &= \frac{1}{M}\sum_{m=1}^{M} \boldsymbol{U}(k_m)\boldsymbol{R}_s(k_m)\boldsymbol{U}^H(k_m), \qquad (5.36) \\ \overline{\boldsymbol{R}}_n &= \frac{1}{M}\sum_{m=1}^{M} \boldsymbol{C}_{r_1}(k_m)\boldsymbol{R}_n(k_m)\boldsymbol{C}_{r_1}^H(k_m) \end{aligned}$$

and the source covariance matrix is

$$\boldsymbol{R}_s = E\{\boldsymbol{s}(k_m)\boldsymbol{s}^H(k_m)\}. \tag{5.37}$$

From the above analysis we make the following comments:

1. The directional information of sources is contained in $\boldsymbol{T}$ (5.34), which is independent of frequency. Thus it is factored out in (5.35), when forming the frequency average covariance matrix, and unaffected by the averaging.

2. For correlated signals, the source covariance matrix (5.37) tends to be singular which in turn causes desired signal cancellation in traditional beamformers. By frequency averaging over a sufficiently large bandwidth, we can obtain a non-singular data covariance matrix $\overline{\boldsymbol{R}}$ in our formulation. By using two correlated sources, similar to the analysis given in [17], it is possible to show how the frequency averaging reduces singularity in the data covariance matrix.

3. Frequency averaging in (5.36) involves $\boldsymbol{U}(k)$, which contains radial information of the sources. However, this will not affect the desired signal, since the beamformer is focused to the radius of the desired source.

5.5 Adaptive Algorithm

The constrained minimization problem (5.24) is in the same form as that considered by Frost [1] save that he optimized the array weights whereas we have optimized the modal coefficients. In our case, we use Frost's gradient-based algorithm, which converges in the mean to the optimum solution (5.25), to adapt the modal coefficients.

In summary, the algorithm for our case is given by

$$\boldsymbol{b}(l+1) = \boldsymbol{P}[\boldsymbol{b}(l) - \mu\hat{\boldsymbol{R}}\boldsymbol{b}(l)] + \boldsymbol{F} \tag{5.38}$$

where $\boldsymbol{b}(l)$ is the set of modal coefficients at the lth iteration,

$$\boldsymbol{F} = \boldsymbol{D}(\boldsymbol{D}^H\boldsymbol{D})^{-1}\mathbf{1}_{M_1},$$

the $(N+1)\times(N+1)$ matrix

$$\boldsymbol{P} = \boldsymbol{I}_{N+1} - \boldsymbol{D}(\boldsymbol{D}^H\boldsymbol{D})^{-1}\boldsymbol{D}^H,$$

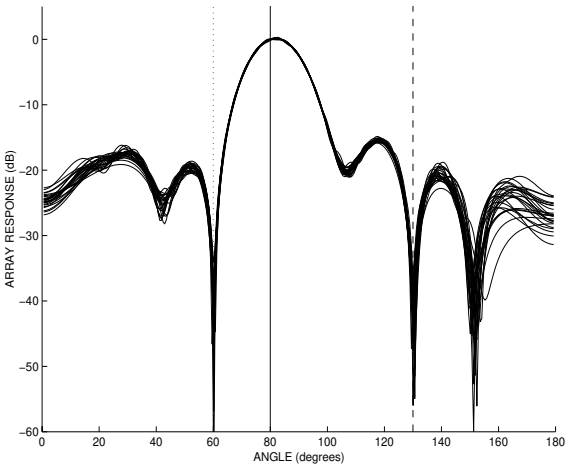

Figure 5.1: Anechoic spatial response of the adapted beamformer at 5m from the array origin at 26 frequencies within the design band of $500 - 3000$ Hz. The solid line indicates the direction of the desired source, while the dashed line indicates an uncorrelated interferer which is 10 times stronger than the desired source, and the dotted line indicates another uncorrelated interfere with same power as the the desired source. All sources are placed at 5m from the array origin.

the initial value of modal coefficients

$$\begin{aligned} \boldsymbol{b}(0) &= \boldsymbol{F}, \\ \hat{\boldsymbol{R}} &= \frac{1}{M}\sum_{m=1}^{M} \boldsymbol{C}_{r_1}(k_m)\boldsymbol{z}(k_m)\boldsymbol{z}^H(k_m)\boldsymbol{C}_{r_1}^H(k_m) \end{aligned} \tag{5.39}$$

is an $(N+1)\times(N+1)$ matrix used to estimate $\overline{\boldsymbol{R}}$ for the lth iteration, and μ is the adaptive step size parameter which controls the convergence characteristics of the algorithm. As noted by Frost, μ is chosen such that $0 < \mu < 1/\sigma_{\max}$, where $\sigma_{\max}$ is the largest eigenvalue of $\boldsymbol{P}\overline{\boldsymbol{R}}\boldsymbol{P}$.

5.6 Examples

We now present an example to show the performance of the adaptive array in a signal environment which consists of nearfield sound sources and their reverberation due to reflections.

The design is suitable for speech with a design bandwidth of $600 - 3000$Hz and a maximum mode index $N = 11$ is used. According to Chapter 4, we determine the number of sensors needed and their location to meet the above bandwidth and mode specification. The resulting non-uniformly spaced double sided linear array

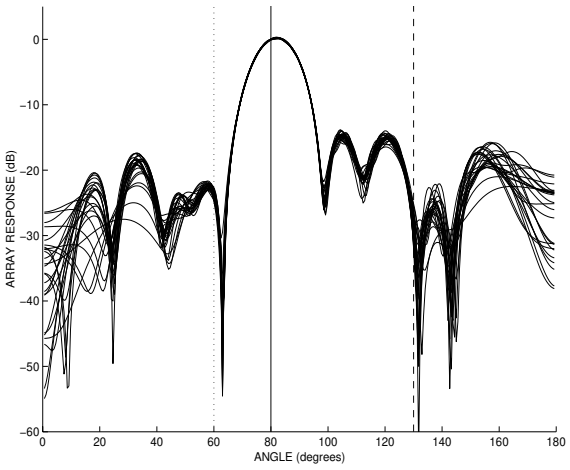

Figure 5.2: Reverberated spatial response of the adapted beamformer at $5m$ from the array origin at 26 frequencies within the design band.

has total of 39 sensors with aperture length of 2.6m.

We consider an anechoic signal environment consisting of a desired source and two uncorrelated interference sources, all 5m away from the array origin, with flat frequency spectra over the bandwidth of interest. The desired signal was at 80°, the first interferer was at 130° and 10 times stronger than the desired signal, and the other interferer was at 60° with the same power as the desired source. White Gaussian noise, uncorrelated from sensor to sensor, was modeled at the input of each sensor such that the SNR of the desired signal at the origin is 30 dB. The received array data $\boldsymbol{z}(k_m)$ was synthesized for 26 frequency bins uniformly spaced within the desired bandwidth, and the adaptive algorithm was used to find the modal coefficients with $M_1 = 3$ frequency constraints. The adaptation step size $\mu = 1 \times 10^{-3}$ was used. Figure 5.1 shows the beampatterns at $r = 5$m produced by the adapted modal coefficients after 4000 data samples. Observe that the beampattern has nulls in the directions of interferers and exhibits little variation with frequency at the focused radius.

Next we consider the performance of the adaptive beamformer in a reverberant rectangular room[3] (7m $\times$ 10m) with reflection coefficient of 0.8 (the array is aligned to the 7m long wall). We used the image-source method [20] to calculate the positions of images (up to the 10th order) of 3 sound sources due to the 4 vertical walls. The adapted beampatterns after 4000 data samples are given in Figure 5.2. Note that, even with the multiplicity of highly correlated reflected signals, the

[3]Here we only consider a 2 dimensional room and thus only reflection by 4 vertical walls are calculated.

beamformer is able maintain a unity gain in the desired direction and attenuates the other two interference sources while preserving its frequency invariant behaviour at the focused radius in the nearfield. Unsurprisingly, the performance is not quite as good as in Figure 5.1.
Comments:

1. Under the above image source modeling, there are 440 correlated interferers (images of the desired source) and 882 uncorrelated interferers (two uncorrelated interferers and their images). Thus, it is impossible to place a null for each interferer. Since signal power received from the interferers are less than that of the original sources, nulls are aligned with the original two uncorrelated interferers.

2. Relative to Figure 5.1, the nulls in Figure 5.2 are misaligned to the angles corresponding to the uncorrelated interferers. This is not an error, but just a property of the optimal solution to which the adaptive beamformer is trying to converge.

5.7 Summary and Contributions

The general broadband adaptive beamforming theory developed in Chapter 4 was used to propose a novel adaptive beamformer. The proposed adaptive beamformer has the capability to overcome desired signal cancellation and to work well for the broadband signal sources in the nearfield of the array.
We itemize some specific contributions made in this chapter:

i. We have extended the general beamforming theory developed in Chapter 4 to propose a novel adaptive beamformer. The frequency invariant nature of the beamforming structure (Chapter 4) is used to combat desired signal cancellation due to correlated interfering signals, and the radial focusing capability is used to deal with the nearfield source signals.

ii. The frequency averaged array data covariance matrix was analyzed to show that the directional information of sources is unaffected by the averaging in our method.

iii. A simulation example is presented to demonstrate the use of the proposed method for microphone array applications in speech acquisition systems.

References

[1] O.L. Frost III, "An algorithm for linearly constrained adaptive array processing," *Proc. IEEE*, vol. 60, pp. 926–936, Aug. 1972.

[2] L.J. Griffiths and C.W. Jim, "An alternative approach to linearly constrained adaptive beamforming," *IEEE Trans. Antennas Propagat.*, vol. AP-30, pp. 27–34, Jan. 1982.

[3] D.B. Ward, "Technique for broadband correlated interference rejection in microphone arrays," *IEEE Trans. Speech and Audio Proc.*, vol. 6, pp. 414–417, July 1998.

[4] T.J. Shan and T. Kailath, "Adaptive beamforming for coherent signals and interference," *IEEE Trans. Acoust. Speech Sig. Proc.*, vol. ASSP-33, pp. 527–536, June 1985.

[5] J.F. Yang and M. Kaveh, "Coherent signal-subspace transformation beamformer," *Proc. IEEE*, vol. 137, pp. 267–275, Aug. 1990.

[6] A. Zeira and B. Friedlander, "Interpolated array minimum variance beamforming for correlated interference rejection," *Proc. IEEE Int. Conf. Acoust., Speech Signal Processing*, pp. 3165–3168, May 1996.

[7] T.S. Lee and T.T. Lin, "Adaptive beamforming with interpolated arrays for multiple coherent interferers," *Signal Processing*, vol. 57, pp. 177–194, 1997.

[8] K. Farrell, R.J. Mammone, and J.L. Flanagan, "Beamforming microphone arrays for speech enhancement," *Proc. IEEE Int. Conf. Acoust., Speech Signal Processing*, pp. 285–288, May 1992.

[9] S. Nordholm, I. Claesson, and B. Bengtsson, "Adaptive array noise suppression of handsfree speaker input in cars," *IEEE Trans. Vehic. Technol.*, vol. 42, pp. 514–518, Nov. 1993.

[10] Y. Kaneda and J. Ohga, "Adaptive microphone array system for noise reduction," *IEEE Trans. Acoust. Speech Sig. Proc.*, vol. ASSP-34, pp. 1391–1400, Dec. 1986.

[11] S. Oh, V. Viswanathan, and P. Papamichalis, "Hands-free voice communication in an automobile with a microphone array," *Proc. IEEE Int. Conf. Acoust., Speech Signal Processing*, pp. 281–284, May 1992.

[12] Y. Grenier, "A microphone array for car environments," *Speech Communication*, vol. 12, pp. 25–39, Mar. 1993.

[13] D.B. Ward, R.A. Kennedy, and R.C. Williamson, "Adaptive broadband beamforming with a dimension-reduction beampattern parameterization," *Int. J. of Adapt. Contr. and Signal Processing*, under review.

[14] A.M. Vural, "A comparative performance study of adaptive array processors," in *Proc. IEEE Int. Conf. Acoust., Speech Signal Processing*, 1977, pp. 695–700.

[15] N.L. Owsley, "Sonar array processing," in *Array Signal Processing*, S. Haykin, Ed., New Jersey, 1985, Prentice Hall.

[16] M.H. Er and A. Cantoni, "Derivative constraints for broadband element space antenna array processors," *IEEE Trans. Acoust. Speech Sig. Proc.*, vol. ASSP-31, pp. 1378–1393, Dec. 1983.

[17] S. Simanapalli and M. Kaveh, "Broadband focusing for partially adaptive beamforming," *IEEE Trans. Aerosp. Electron. Sys.*, vol. 30, pp. 68–79, Jan. 1994.

[18] M. Wax and Y. Anu, "Performance analysis of the minimum variance beamformer," *IEEE Trans. Sig. Proc.*, vol. 44, pp. 938–937, Apr. 1996.

[19] D.B. Ward, R.A. Kennedy, and R.C. Williamson, "Theory and design of broadband sensor arrays with frequency invariant far-field beampatterns," *J. Acoust. Soc. Amer.*, vol. 97, pp. 1023–1034, Feb. 1995.

[20] J.B. Allen and D.A. Berkley, "Image method for efficiently simulating small-room acoustics," *J. Acoust. Soc. Amer.*, vol. 65(4), pp. 943–950, Apr. 1979.

Chapter 6

Other Applications of Modal Analysis

6.1 Introduction

The modal analysis techniques developed in Chapter 2 have already been used to solve beamforming problems in the previous chapters. However, we have claimed that modal analysis is a versatile tool to solve not only beamforming problems but also to address related array processing issues. The reasoning behind this claim is as follows. Any array processing problem involves extracting information from the signal wavefield around the array. The use of modal analysis to represent the wavefield gives structural insights into the problem at hand, which in turn aids in finding a solution. In this chapter we show the application of modal analysis techniques in other areas of array processing. Specifically, we consider isotropic noise modeling and source localization problem to corroborate our claims.

In the first part of this chapter, we consider isotropic noise modeling used for array designs. Historically, isotropic noise is viewed as noise sources uniformly distributed over all directions in the farfield of the array. We consider isotropic noise fields in the nearfield of the array and also diffuse noise fields where noise (point) sources are distributed over the entire space. We use modal techniques to find exact series representations for both nearfield isotropic noise and for diffuse noise fields. The proposed nearfield noise model can be utilized effectively to apply well established farfield array processing algorithms for nearfield applications of sensor arrays. An array gain optimization is used to demonstrate the use of the new noise model.

In the second part of this chapter, we show how to analyze the localization

problem and how to synthesize a solution using modal techniques. We concentrate on the multiple coherent broadband signal environment, where the received signals may be correlated with each other (e.g., due to multipath propagation or deliberate jamming). One of the common approaches to coherent broadband array processing is to use *focusing*[1] *matrices* to align broadband array data to a single frequency and use the frequency averaging to remove the signal correlation. Literally, there are dozens of papers written on these focusing methods. Here, we show how to find alternative but simple solutions for such approaches.

6.2 Spherically Isotropic Noise Modeling

6.2.1 Preliminary

In much of the array processing literature, the observed external noise[2] is assumed to consist of many random waves propagating in all possible directions with equal probability [1]. Such a noise field results in uniform distribution of noise sources over all directions in the farfield of the array, and it is called *farfield spherically isotropic noise*. In many optimal beamformer designs, the noise field is assumed to be known and usually modeled by either white (in time and space) Gaussian noise or farfield spherically isotropic noise.

For nearfield applications of sensor arrays such as teleconferencing, the noise field consists of undesirable nearfield sound sources as well as reverberation caused by the desired and noise sources. Using the *source-image* method [2], we can model reverberation as an infinite set of image point-sources in free space. In an average size room, some or all first-order reflected images will be in the nearfield of the array, while multiply reflected images will tend to be in the farfield. Due to absorption by walls and attenuation with distance, an image generated by a multiply reflected noise source contributes less power compared to first-order reflected images. Thus, the overall noise field can be regarded as nearfield noise sources, with either farfield spherically isotropic noise or white Gaussian noise as a crude approximation. In [3], farfield spherically isotropic noise was used to model the effect of reverberation without considering the effect of nearfield noise sources.

[1] There is a possible confusion by the the use of the term "focusing". Here we use the term "focusing" to denote alignment over frequency as used in the literature. However, the act of focusing usually refers to delay operations used to align the *wavefront* as we used in Chapter 3.

[2] External noise is due to sources other than the desired source. Internal noise is due to sensors and electronics thermal noise.

As an alternative, in this chapter we model the noise field by a source distribution that is uniform over all directions in the nearfield at a fixed distance from the array origin. We call this *nearfield spherically isotropic noise*. This noise model can be utilized effectively to apply any signal processing criterion based on an isotropic type noise correlation (which has traditionally been assumed to be in the farfield) to nearfield applications. In our simulation example in Section 6.2.7 we will show that a design based on this nearfield noise model provides better directional gain than one based on a farfield noise model in a more realistic mixed farfield-nearfield noise field. As motivation for the theoretical development, we consider an array optimization technique formulated for a nearfield array in the following subsection.

6.2.2 Gain optimization for an arbitrary array

The array gain is often used as an indicator of overall array performance. It is defined by

$$G = 4\pi \frac{\text{power received from a desired location } (P_{\text{source}})}{\text{total noise power received } (P_{\text{noise}})} \tag{6.1}$$

Consider an array of $2N+1$ sensors, arbitrarily placed in a bounded region $\Omega \subset \mathbb{R}^3$. Then the normalized response of this narrowband array to a source located outside the region Ω at $\boldsymbol{y}$, is given by

$$b(\boldsymbol{y}) = \sum_{n=-N}^{N} w_n \frac{e^{-ik\|\boldsymbol{y}-\boldsymbol{x}_n\|}}{\|\boldsymbol{y}-\boldsymbol{x}_n\|} y e^{iky}, \tag{6.2}$$

where $\|\cdot\|$ is the vector 2-norm, w_n is the complex gain associated with the sensor positioned at $\boldsymbol{x}_n \in \Omega$, $y = \|\boldsymbol{y}\|$ and k is the wavenumber. Thus, the power received from the desired location $\boldsymbol{y}_{\text{s}}$ of the source is given by

$$P_{\text{source}} = b^*(\boldsymbol{y}_{\text{s}})\, b(\boldsymbol{y}_{\text{s}}),$$

where * denotes complex conjugate. Arranging the weights in an $(2N+1)$-element column vector

$$\boldsymbol{w} = \begin{bmatrix} w_{-N} \\ \vdots \\ w_N \end{bmatrix}$$

and defining a square $((2N+1)\times(2N+1))$ Hermitian matrix

$$\boldsymbol{R}_{\text{source}} = \boldsymbol{a}\boldsymbol{a}^H$$

in terms of the $(2N+1)$ element column vector

$$\boldsymbol{a} = \begin{bmatrix} \dfrac{e^{-ik\|\boldsymbol{y}-\boldsymbol{x}_{-N}\|}}{\|\boldsymbol{y}-\boldsymbol{x}_{-N}\|} \\ \vdots \\ \dfrac{e^{-ik\|\boldsymbol{y}-\boldsymbol{x}_{N}\|}}{\|\boldsymbol{y}-\boldsymbol{x}_{N}\|} \end{bmatrix} ye^{iky},$$

leads to the matrix expression

$$P_{\text{source}} = \boldsymbol{w}^H \boldsymbol{R}_{\text{source}} \boldsymbol{w}.$$

By assuming a *nearfield spherically isotropic noise field*, i.e., having uniformly distributed noise sources on a sphere of radius y, we can write the total noise power received as,

$$P_{\text{noise}} = \int b^*(\boldsymbol{y})\, b(\boldsymbol{y})\, d\hat{\boldsymbol{y}}$$

where $\hat{\boldsymbol{y}} = \boldsymbol{y}/y$ is a unit vector in the direction of $\boldsymbol{y}$ and the integration is over the unit sphere. We define the $((2N+1)\times(2N+1))$ matrix $\boldsymbol{R}_{\text{noise}} = [r_{nm}]$ with elements

$$r_{nm} = \frac{y^2}{4\pi} \int \frac{e^{ik\|\boldsymbol{y}-\boldsymbol{x}_n\|}}{\|\boldsymbol{y}-\boldsymbol{x}_n\|} \frac{e^{-ik\|\boldsymbol{y}-\boldsymbol{x}_m\|}}{\|\boldsymbol{y}-\boldsymbol{x}_m\|} d\hat{\boldsymbol{y}}. \tag{6.3}$$

(Note that $\boldsymbol{R}_{\text{noise}}$ is Hermitian and positive definite). Then,

$$P_{\text{noise}} = 4\pi \boldsymbol{w}^H \boldsymbol{R}_{\text{noise}} \boldsymbol{w},$$

and equation (6.1) becomes a ratio of quadratic forms

$$G = \frac{\boldsymbol{w}^H \boldsymbol{R}_{\text{source}} \boldsymbol{w}}{\boldsymbol{w}^H \boldsymbol{R}_{\text{noise}} \boldsymbol{w}}, \tag{6.4}$$

which is known as *Rayleigh quotient*. The usual goal is to find the weights that maximize G. Equation (6.4) is a well known result for array gain [1, p. 141], [4, p. 164] and $\boldsymbol{R}_{\text{source}}$ and $\boldsymbol{R}_{\text{noise}}$ are commonly known as the source correlation matrix

and noise correlation matrix respectively. The optimum array gain and weights for the special case[3] $\boldsymbol{R}_{\text{source}} = \boldsymbol{a}\boldsymbol{a}^H$ are given by [5]

$$G_{\text{opt}} = \boldsymbol{a}^H \boldsymbol{R}_{\text{noise}}^{-1} \boldsymbol{a} \tag{6.5}$$

and

$$\boldsymbol{w}_{opt} = \boldsymbol{R}_{\text{noise}}^{-1} \boldsymbol{a} \tag{6.6}$$

respectively.

Similar to the above optimization method, most statistically based beamformer problems using conventional criteria require evaluation of the noise correlation matrix. Until now, a farfield isotropic noise model has been used to evaluate the noise correlation matrix. In the next section, we establish an expression of the noise correlation matrix for nearfield isotropic noise, which will enable us to use the above statistically optimum beamforming method in nearfield applications.

6.2.3 Nearfield Isotropic Noise

In this section, we find an exact series representation for the noise correlation r_{nm} (6.3) between two sensors due to a nearfield isotropic noise field.

Let $x_n = \|\boldsymbol{x}_n\|$ and $y = \|\boldsymbol{y}\|$. We write the wavefield at the sensor location $\boldsymbol{x}_n$ due to a source at $\boldsymbol{y}$ using (2.39) as

$$ye^{iky}\frac{e^{ik\|\boldsymbol{y}-\boldsymbol{x}_n\|}}{\|\boldsymbol{y}-\boldsymbol{x}_n\|} = 4\pi ik\sum_{p=0}^{\infty}\sum_{q=-p}^{p} R_p(y,k)Y_{pq}(\hat{\boldsymbol{y}})j_p(kx_n)Y_{pq}^*(\hat{\boldsymbol{x}}_n), \quad y > x_n, \tag{6.7}$$

where $j_p(\cdot)$ is the spherical Bessel function, $R_p(y,k)$ is defined in (2.20) and $Y_{pq}(\cdot)$ is defined in (2.13).

We can now obtain an exact expression for the nearfield isotropic noise correlation matrix as follows: we substitute (6.7) and its conjugate into (6.3), interchange integration and summations, and evaluate the resulting integral using (2.14) to obtain

$$r_{nm} = 4\pi k^2 \sum_{p=0}^{\infty}\sum_{q=-p}^{p} |R_p(y,k)|^2\, Y_{pq}^*(\hat{\boldsymbol{x}}_n)\, Y_{pq}(\hat{\boldsymbol{x}}_m) j_p(kx_n)\, j_p(kx_m), \quad y > x_n. \tag{6.8}$$

Equation (6.8) is a novel result, which gives the noise correlation between a pair

[3] In general, maximization of (6.4) is a *generalized eigenvalue problem.*

of sensors for a noise field generated by uniformly distributed point sources on the surface of a sphere of radius y which encircles the pair of sensors. Another form of (6.8) can be derived using the relationship [6, p. 27]

$$\sum_{q=-p}^{p} Y_{pq}^*(\hat{\boldsymbol{x}}_n) Y_{pq}(\hat{\boldsymbol{x}}_m) = \frac{2p+1}{2\pi} P_p(\cos\gamma_{nm}), \tag{6.9}$$

where $\cos\gamma_{nm} = \hat{\boldsymbol{x}}_n \cdot \hat{\boldsymbol{x}}_m$ is the cosine of the angle between $\hat{\boldsymbol{x}}_n$ and $\hat{\boldsymbol{x}}_m$ and $P_p(\cdot)$ are the Legendre functions. Combining (6.8) and (6.9), we write the correlation between two sensors as

$$r_{nm} = 2k^2 \sum_{p=0}^{\infty} (2p+1) |R_p(y,k)|^2 \, j_p(kx_n) \, j_p(kx_m) P_p(\cos\gamma_{nm}), \quad y > \max\{x_n, x_m\}. \tag{6.10}$$

An attractive feature of (6.10) is that for each term in the series, the dependence on the distance to the noise source y, the angle between two sensors γ_{nm}, and the distance to the two sensors x_n and x_m appear as separate factors.

6.2.4 Linear array

For the simple case of a line array through the origin, γ_{nm} would be equal to either 0 or π depending on the location of the origin, for all pairs of sensors. That is

$$\cos\gamma_{nm} = \mathrm{sgn}(\hat{\boldsymbol{x}}_n \cdot \hat{\boldsymbol{x}}_m)$$

where $\mathrm{sgn}(\cdot)$ is the signum function. Since

$$P_p(-\cos\gamma) = (-1)^p P_p(\cos\gamma)$$

and

$$P_p(1) = 1 \tag{6.11}$$

for all integers p [7, p. 208], the correlation between two sensors for a line array is

$$r_{nm} = 2k^2 \sum_{p=0}^{\infty} (2p+1) \{\mathrm{sgn}(\hat{\boldsymbol{x}}_n \cdot \hat{\boldsymbol{x}}_m)\}^p |R_p(y,k)|^2 j_p(kx_n) j_p(kx_m), \; y > \max\{x_n, x_m\}. \tag{6.12}$$

6.2.5 Farfield isotropic noise

The simplest special case of (6.10) is for farfield isotropic noise, in which case $y \to \infty$. Making use of (2.21)

$$\lim_{y\to\infty} |R_p(y,k)|^2 = \frac{1}{k^2},$$

we find that (6.10) reduces to

$$r_{nm} = 2\sum_{p=0}^{\infty}(2p+1) j_p(kx_n)\, j_p(kx_m)\, P_n(\cos\gamma_{nm}). \tag{6.13}$$

Using [8, p. 366], (6.13) becomes

$$\begin{aligned} r_{nm} &= \frac{2\sin(k\sqrt{x_n^2 + x_m^2 - 2x_n x_m \cos\gamma_{nm}})}{k\sqrt{x_n^2 + x_m^2 - 2x_n x_m \cos\gamma_{nm}}} \\ &= \frac{2\sin(k\|\boldsymbol{x}_n - \boldsymbol{x}_m\|)}{k\|\boldsymbol{x}_n - \boldsymbol{x}_m\|}, \end{aligned} \tag{6.14}$$

which is a well-known result for farfield spherically isotropic noise fields [1, p. 49]. For the simple case of a linear array with uniform half wavelength spacing, the observed noises are uncorrelated between sensors; this fact is readily evident from (6.14). Indeed this is one advantage of the half wavelength sensor spacing chosen for many linear array designs. By comparing with (6.10), one can deduce that such a simple relationship breaks down in the nearfield case.

6.2.6 Diffuse Noise Field

A diffuse sound field consists of waves emanating from point sources uniformly distributed (over distance as well as direction) in $\mathbb{R}^3$. Such fields are used to model the room reverberation in microphone array applications [9]. In this section we will find a closed-form expression for correlation between two sensor elements in a diffuse noise field.

In this case, the total noise power received by the array is

$$P_{\text{noise}} = \int_{\mathbb{R}^3} \left(ye^{-iky}\, b(\boldsymbol{y})\right)^* ye^{-iky}\, b(\boldsymbol{y})\, d\boldsymbol{y}, \tag{6.15}$$

where the integration is over all of $\mathbb{R}^3$. Note that the array response $b(\boldsymbol{y})$ given by (6.2) is in fact a normalized version of the true array response. This normalization

was done by multiplying the true response by ye^{iky} in (6.2). The purpose of this normalization is to have a single expression for both farfield and nearfield array responses. However, if the sources are at different radial distances from the array origin, such a normalization must be removed. Thus, we have compensated for the normalization implicit in (6.2).

By observing (6.15) and (6.2), we can see that the (6.15) does not exist due to singularities at $\boldsymbol{y} = \boldsymbol{x}_q$, for $q = -Q, \ldots, Q$. As was shown in [9], reverberation can be approximately modeled by uniformly distributed point sources outside a sphere of certain radius (say r). The justification in [9] was that speech intelligibility degrades only if reflections are delayed by at least 50ms and noise sources are not usually closer than some minimum distance. Following the same justification we rewrite (6.15) as

$$P_{noise} = \int_{\|y\|>r} \left(ye^{-iky}\, b(\boldsymbol{y})\right)^* ye^{iky}\, b(\boldsymbol{y})\, d\boldsymbol{y}, \tag{6.16}$$

where r is the radius of a suitable sphere centred at the origin, the correlation between two sensor elements is given by

$$r_{nm} = \frac{1}{4\pi} \int_{\|y\|>r} \frac{e^{ik\|\boldsymbol{y}-\boldsymbol{x}_n\|}}{\|\boldsymbol{y}-\boldsymbol{x}_n\|} \frac{e^{-ik\|\boldsymbol{y}-\boldsymbol{x}_m\|}}{\|\boldsymbol{y}-\boldsymbol{x}_m\|} d\boldsymbol{y}. \tag{6.17}$$

As we did in Section 6.2.3, we substitute (6.2) and its conjugate in (6.17) and evaluate the integration over the unit sphere (leaving the radial dependent part of the integration untouched) to get

$$r_{nm} = 4\pi k^2 \sum_{p=0}^{\infty} \sum_{q=-p}^{p} A_p(r,k)\, Y_{pq}^*(\hat{\boldsymbol{x}}_n)\, Y_{pq}(\hat{\boldsymbol{x}}_m) j_p(kx_n)\, j_p(kx_m), \tag{6.18}$$

where

$$A_p(r,k) = \int_r^{\infty} \frac{|R_p(y,k)|^2}{y^2} dy. \tag{6.19}$$

Using (3.21) and (3.19), we write

$$R_p(y,k) = \frac{(i)^{p+1}}{k} \sum_{v=0}^{p} \frac{(p+v)!}{(p-v)!v!} \left(\frac{-i}{2kr}\right)^v. \tag{6.20}$$

Now we substitute the above series expansion in (6.19) and evaluate the integration

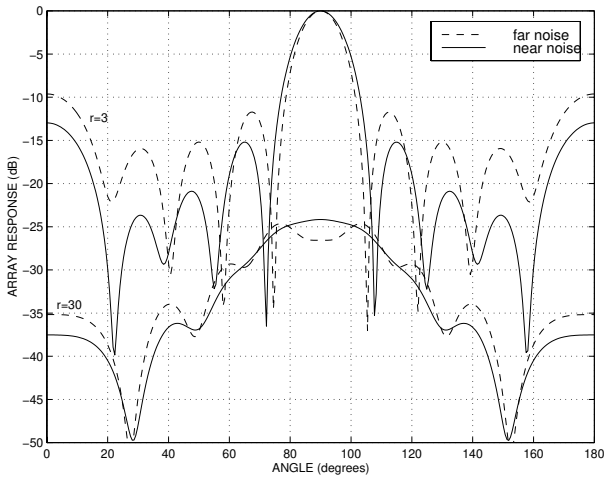

Figure 6.1: Response of the optimum array based on nearfield noise model (solid line) to sources at 3 and 30 wavelengths from the array origin. Also shown is the response of the farfield noise model based array response (dashed line).

to get

$$A_p(r,k) = \frac{1}{k^2 r} \sum_{u=0}^{p} \sum_{v=0}^{p} \frac{(p+v)!}{(p-v)!v!} \frac{(p+u)!}{(p-u)!u!} \frac{(-1)^u}{v+u+1} \left(\frac{i}{2kr}\right)^{v+u}. \tag{6.21}$$

When (6.21) is combined with (6.17), we obtain a closed-form solution for correlation between two sensor elements in a diffuse noise field.

6.2.7 Simulation Example

We now present a design example to demonstrate the use of nearfield isotropic noise modeling for nearfield beamforming. Our demonstration is based on the simple array gain optimization technique outlined in Section 6.2.2. However this noise model can be applied to a wide class of optimization methods in beamforming such as minimum variance (MV), maximum likelihood (ML) and mean square error (MSE).

The design is for a double-sided linear array of 9 sensors with an inter-sensor spacing of $\lambda/2$, where λ is the wavelength. Suppose that the desired source is in the nearfield at 3λ from the array origin, on the broadside of the array. We calculate the optimum weight vector (6.6), with the noise correlation matrix $\boldsymbol{R}_{\text{noise}}$ for nearfield isotropic noise (6.12) at a sphere of radius 2λ. The only requirement that must be satisfied in choosing the radius of the noise sphere is that the sphere should encapsulate the array. In this example, the array aperture is 4λ; thus a

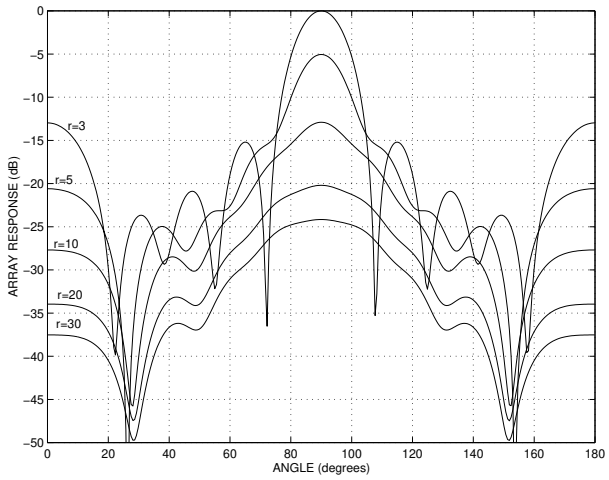

Figure 6.2: Response of the optimum array (nearfield noise model) at 3, 5, 10, 20 and 30 wavelengths from the array origin.

sphere of radius 2λ just encloses the array. Even though the series (6.12) has an infinite number of terms, we approximate it by the first 21 terms for this example. Generally these series expansions are convergent and could be approximated by a finite number of terms depending on the array configuration and the desired operating distance. In this case, 21 terms proved sufficient.

The responses of the resulting array (solid line) to a nearfield source at 3 wavelengths from the array origin and to a farfield source at 30 wavelengths are given in Figure 6.1. Also shown is the response of an optimum array designed using the farfield isotropic noise model (6.14) (dashed). Observe that the nearfield noise model based design provides a better directional array gain in the nearfield and simultaneously provides similar farfield noise rejection when compared with the farfield noise model based design. For both design methods, the power received from a source at 30λ at the look direction is about 25dB less than that of the desired source at 3λ (one would expect only a 10dB difference for a single sensor). The trade-off for using the nearfield noise model is the better directional gain at the expense of slightly wider main lobe width. Figure 6.2 shows the response of the optimum array (designed to operate at 3λ using the nearfield noise model) at different radial distances from the array origin. From this figure, we can note that the nearfield noise, other than in the look direction, and farfield noise in all directions are attenuated with respect to the signal from the desired source. Thus, we can conclude that our design has acceptable performance in a mixed farfield-nearfield noise environment.

6.2.8 Summary

In this section, we have introduced an exact series representation for nearfield-farfield isotropic noise field, which may be useful in sensor array applications in the nearfield. For each term in the series representation, the dependence on the position coordinates of the sensors is factored into components, each of which depends on a single coordinate. This property of the series expansion facilitates the calculation of the correlation matrix for various sensor orientations. While the model has only been demonstrated here for a small line array, it is generally applicable to more complex arrays (2D and 3D). More importantly, this result can be utilized to apply well established farfield array processing algorithms for the nearfield applications.

6.3 Coherent Broadband Source Localization

6.3.1 Preliminary

The problem of detecting and locating multiple broadband sources using an array of sensors has attracted a great deal of attention over the past two decades due to applications in areas such as radar, sonar, communications systems, and speech acquisition systems. In these scenarios, the source signals may be completely correlated, e.g., some of them may be delayed version of others as in severe multipath propagation situations. The study of this problem is termed as *coherent array processing* in the literature. In this section, we briefly review two major approaches to the coherent (farfield) source localization problem which have appeared in the literature, and outline how to simplify them using modal analysis techniques developed in Chapter 2. Unlike in the rest of this thesis, here we only consider sources located in the farfield of the array. This is to show the simplification afforded by modal analysis with respect to existing coherent farfield source localization methods.

6.3.2 Problem formulation

Consider a linear double-sided array of $2Q+1$ sensors. Assume that V unknown broadband signals arrive from directions $\Theta = [\theta_1 \cdots \theta_V]$, where θ_v is the direction of the vth source, measured relative to the array axis. Without loss of generality, we assume that the source signals and noise have finite bandwidth $k \in [k_{\mathrm{l}}, k_{\mathrm{u}}]$, where k_{l} and k_{u} are the lower and upper band edges respectively.

The received signals are discretized at each sensor and the resulting array data is divided into blocks of J samples, and discrete Fourier transformed to produce

$M \leq J$ narrowband frequency bins within the design bandwidth . The array data in the mth frequency bin is

$$\boldsymbol{z}(k_m) = \sum_{v=1}^{V} \boldsymbol{a}(\theta_v; k_m) s_v(k_m) + \boldsymbol{n}(k_m), \tag{6.22}$$

where $s_v(\cdot)$ is the signal received from the vth source at the origin, $\boldsymbol{n}(\cdot)$ is the uncorrelated noise data and

$$\boldsymbol{a}(\theta; k) = \left[e^{-ikz_{-Q}\cos\theta} \cdots e^{-ikz_Q \cos\theta}\right]^T. \tag{6.23}$$

Now (6.22) can be written in matrix form as

$$\boldsymbol{z}(k_m) = \boldsymbol{A}(\Theta; k_m)\boldsymbol{s}(k_m) + \boldsymbol{n}(k_m), \tag{6.24}$$

where

$$\boldsymbol{A}(\Theta; k) = \left[\boldsymbol{a}(\theta_1; k) \cdots \boldsymbol{a}(\theta_V; k)\right], \tag{6.25}$$

and

$$\boldsymbol{s}(k) = \left[s_1(k) \cdots s_V(k)\right]^T.$$

The problem we address in this section is how to determine the direction of arrival (DOA) angles Θ from the array data $\boldsymbol{z}(k_m)$, $m = 1, \ldots, M$.

The correlation matrix of the observed data in the mth frequency bin is defined as

$$\boldsymbol{R}_z(k_m) \triangleq E\{\boldsymbol{z}(k_m)\boldsymbol{z}(k_m)^H\}. \tag{6.26}$$

By substituting (6.24) in (6.26) and assuming that source signals and noise are uncorrelated, we get

$$\boldsymbol{R}_z(k_m) = \boldsymbol{A}(\Theta; k_m)\boldsymbol{R}_s(k_m)\boldsymbol{A}^H(\Theta; k_m) + E\{\boldsymbol{n}(k_m)\boldsymbol{n}(k_m)^H\}, \tag{6.27}$$

where

$$\boldsymbol{R}_s(k_m) \triangleq E\{\boldsymbol{s}(k_m)\boldsymbol{s}^H(k_m)\}, \tag{6.28}$$

is the source correlation matrix.

6.3.3 Focusing Matrices for Coherent Wideband Processing

Wang and Kaveh [10] introduced the use of focusing matrices for the purpose of coherent signal-subspace processing for DOA estimation of farfield wideband sources. These focusing matrices are used for the alignment of the signal subspaces of narrowband components within the bandwidth of the signals, followed by the averaging of narrowband array data covariance matrices into a single covariance matrix, thus achieving a substantial reduction in data. Now, any signal subspace direction finding procedure, (such as MUSIC [11] or its variants), maximum likelihood (ML), or minimum variance (MV), can be applied to this averaged covariance matrix to obtain the desired parameter estimates. We briefly outline the focusing method below.

The first step following the frequency decomposition of the array data vector is to align or focus the signal space at all frequency bins into a common one at a reference frequency by focusing matrices $\boldsymbol{T}(k_m)$ that satisfy

$$\boldsymbol{T}(k_m)\boldsymbol{A}(\Theta; k_m) = \boldsymbol{A}(\Theta; k_0), \quad m = 1, \ldots, M, \tag{6.29}$$

where $k_0 \in [k_l, k_u]$ is some reference frequency and $\boldsymbol{A}(\Theta; k)$ is the direction matrix defined by (6.25). The key problem here is how to find the focusing matrices and it will be solved using the modal representation in the subsequent subsections.

Applying the M focusing matrices to the respective array data vectors (6.24) gives the following focused array data vector,

$$\boldsymbol{T}(k_m)\boldsymbol{z}(k_m) = \boldsymbol{A}(\Theta; k_0)\boldsymbol{s}(k_m) + \boldsymbol{T}(k_m)\boldsymbol{n}(k_m) \quad m = 1, \ldots, M.$$

Then the focused and frequency averaged data covariance matrix is given by

$$\boldsymbol{R} = \sum_{m=1}^{M} \boldsymbol{T}(k_m)\, E\{\boldsymbol{z}(k_m)\boldsymbol{z}^H(k_m)\}\, \boldsymbol{T}^H(k_m). \tag{6.30}$$

We use (6.26), (6.27) and (6.29) to get

$$\boldsymbol{R} = \boldsymbol{A}(\Theta; k_0)\overline{\boldsymbol{R}}_s \boldsymbol{A}^H(\Theta; k_0) + \boldsymbol{R}_{\text{noise}} \tag{6.31}$$

where

$$\overline{\boldsymbol{R}}_s = \sum_{m=1}^{M} \boldsymbol{R}_s(k_m), \tag{6.32}$$

and

$$\boldsymbol{R}_{\text{noise}} = \sum_{m=1}^{M} \boldsymbol{T}(k_m)\, E\{\boldsymbol{n}(k_m)\boldsymbol{n}^H(k_m)\}\, \boldsymbol{T}^H(k_m). \tag{6.33}$$

The focused data covariance matrix (6.31) is now in a form in which almost any narrowband direction finding procedure may be applied. Here, we apply the minimum-variance (MV) method of spatial spectral estimation [12] to the frequency averaged data covariance matrix $\boldsymbol{R}$. The steps used for coherent DOA estimation using focusing matrices are summarized below.

1. Discrete Fourier transform the received signals to obtain the array data vector $\boldsymbol{z}(k_m)$ for $m = 1, \ldots, M$.

2. Calculate an estimate of the frequency-averaged data covariance matrix $\boldsymbol{R}$ as

$$\hat{\boldsymbol{R}} = \sum_{m=1}^{M} \boldsymbol{T}(k_m)\, \boldsymbol{z}(k_m)\boldsymbol{z}^H(k_m)\, \boldsymbol{T}^H(k_m). \tag{6.34}$$

3. Form the MV spectral estimate

$$\hat{Z}(\theta) = \frac{1}{\boldsymbol{a}(\theta; k_0)\hat{\boldsymbol{R}}^{-1}\boldsymbol{a}^H(\theta; k_0)}. \tag{6.35}$$

Several methods of forming focusing matrices have been suggested in the literature. The focusing methods of [10, 13–15] require preliminary DOA estimates in order to construct the focusing matrices. This constitutes a severe disadvantage in practical applications since it leads to biased DOA estimates.

We now use modal analysis techniques to propose novel focusing matrices which do not require preliminary DOA estimates and are completely independent of the signal environment. Here we only consider a linear (possibly nonuniform) array but it may be generalized to arbitrary array configurations.

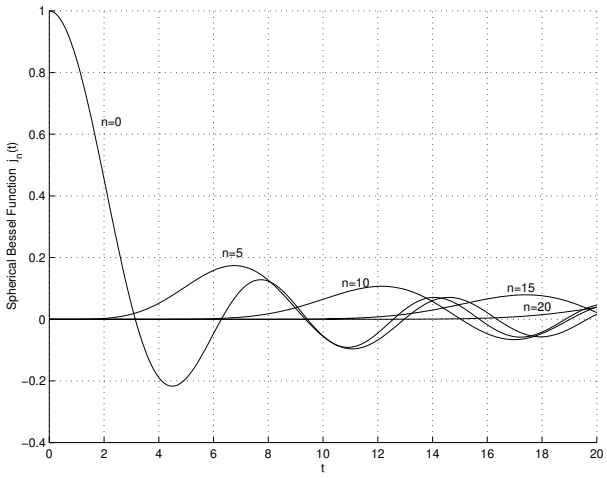

Figure 6.3: Plots of spherical Bessel functions of order $n = 0, 5, 10, 15, 20$.

Using (2.48) we may write

$$e^{-ikz_q \cos\theta} = \sum_{n=0}^{\infty} i^n (2n+1) j_n(kz_q)\, P_n(\cos\theta), \tag{6.36}$$

where $j_n(\cdot)$ is the spherical Bessel function and $P_n(\cdot)$ is the Legendre function. The series expansion (6.36) gives an insight into the spatial wavefield along a linear array. Observe that in each term of the series, the arrival angle θ dependency is separated out from the sensor location z_q and the frequency k. Therefore we may use the above expansion to write the array DOA matrix $\boldsymbol{A}(\Theta; k)$ as a product of two matrices, one depending on DOA angles and the other depending on frequency and sensor locations. Before reaching this step, there are certain hurdles to overcome; for example, expansion (6.36) has an infinite number of terms, thus we can not use it to represent finite-dimensional matrices.

We claim that for a finite aperture array with finite bandwidth signal environment, the series (6.36) can be safely truncated to a by finite number of terms (say N) without generating significant modeling errors. We show this somewhat informally below. A rigorous error analysis is not performed in this thesis but is suggested for future research directions in Chapter 7.

Figure 6.3 shows plots of a few spherical Bessel functions $j_n(\cdot)$ against its argument. We can observe from Figure 6.3 that for a given kz, the function $j_n(kz) \to 0$ as n becomes large. This observation is supported by the following asymptotic

form [16, p. 692]

$$j_n(kz) \approx \frac{(kz)^n}{1 \cdot 3 \cdot 5 \ldots (2n+1)} \quad \text{for } kz \ll n. \tag{6.37}$$

Therefore, we can notice that the factor $(2n+1)j_n(kz_q)$ in (6.36) decays as n grows larger beyond $n = kz_q$. Suppose that the minimum frequency of the signal band is k_l. Then we can truncate (6.36) to N terms if $N > k_l z_Q$, where z_Q is the distance to the Qth sensor (the maximum array dimension). It is difficult to derive an analytical expression for N, but a convenient rule of thumb is $N \sim 2k_l z_Q$.

Now we substitute the first $N+1$ terms of (6.36) into (6.23) and thus write the array steering vector for farfield sources as

$$\boldsymbol{a}(\theta; k) = \boldsymbol{J}(k) \begin{bmatrix} P_0(\cos\theta) \\ \vdots \\ P_N(\cos\theta) \end{bmatrix}, \tag{6.38}$$

where

$$\boldsymbol{J}(k) = \begin{bmatrix} i^0(2 \cdot 0 + 1)\, j_0(kz_{-Q}) & \ldots & i^N(2N+1)\, j_N(kz_{-Q}) \\ \vdots & \ddots & \vdots \\ i^0(2 \cdot 0 + 1)\, j_0(kz_Q) & \ldots & i^N(2N+1)\, j_N(kz_Q) \end{bmatrix}. \tag{6.39}$$

Now we can use (6.38) in (6.25) to write the array DOA matrix for farfield signal environment as

$$\boldsymbol{A}(\Theta; k) = \boldsymbol{J}(k)\boldsymbol{P}(\Theta), \tag{6.40}$$

where the $(N+1) \times V$ matrix

$$\boldsymbol{P}(\Theta) = \begin{bmatrix} P_0(\cos\theta_1) & \ldots & P_0(\cos\theta_V) \\ \vdots & \ddots & \vdots \\ P_N(\cos\theta_1) & \ldots & P_N(\cos\theta_V) \end{bmatrix}. \tag{6.41}$$

The $(2Q+1) \times (N+1)$ matrix $\boldsymbol{J}(k)$ depends on the frequency k and the sensor locations and is independent of the DOA of the signals. Suppose $(2Q+1) > (N+1)$ and $J(k)$ has full rank $N+1$ if the sensor locations are chosen appropriately. With this assumption and using (6.40), we can propose a set of focusing matrices $\boldsymbol{T}(k_m)$

given by

$$\boldsymbol{T}(k_m) = \boldsymbol{J}(k_0)\left[\boldsymbol{J}^H(k_m)\boldsymbol{J}(k_m)\right]^{-1}\boldsymbol{J}^H(k_m) \;\; m = 1, \ldots, M \tag{6.42}$$

which satisfies the focusing requirement (6.29); recall that k_0 is the reference frequency.

The major advantage of the focusing matrices (6.42) over the existing methods is that these matrices do not need preliminary DOA estimates and accurately focus signal arrivals from all directions. Also note that these matrices can be calculated beforehand for a given array geometry and frequency band of interest.

Spatial Resampling Methods

Spatial resampling is another method used to focus the wideband array data to a single frequency so that existing narrowband techniques may be used to estimate the DOA.

The spatial resampling method was first introduced by Krolik and Swinger [17] and is motivated by treating the output of a discrete array as being the result of spatially sampling a continuous linear array. The same concept is also known as an interpolated array [18]. The basic idea of spatial sampling is outlined below.

Suppose we have a separate uniform array with half wavelength spacing for each frequency bin with the same effective array aperture in terms of wavelength. Thus for M frequencies, there are M arrays and the sensor separation of the mth array is $\lambda_m/2$ where $\lambda_m = 2\pi/k_m$. If each array has $2Q+1$ sensors, then the aperture length is the same for all frequencies in terms of corresponding wavelength. Then the mth array steering vector for farfield sources is given by

$$\begin{aligned}\boldsymbol{a}(\theta; k_m) &= [e^{i\pi Q\cos\theta}, \cdots, e^{i\pi\cos\theta}, 1, e^{-i\pi\cos\theta}, \ldots, e^{-i\pi Q\cos\theta}], \\ &= \boldsymbol{a}(\theta), \quad m = 1, \ldots, M.\end{aligned} \tag{6.43}$$

That is the steering vectors of all arrays are equal and hence from (6.25) the DOA matrices of all arrays are the same:

$$\boldsymbol{A}^{(m)}(\Theta; k_m) = \boldsymbol{A}(\Theta), \quad m = 1, \ldots, M, \tag{6.44}$$

where $\boldsymbol{A}^{(m)}(\Theta; k)$ is the DOA matrix of the mth subarray. Hence if we have M arrays for each frequency bin with the same aperture, then their covariance matrices can be averaged over frequency without losing DOA information. The average

covariance matrix can then be used with existing narrowband DOA techniques to estimate DOA angles.

Of course it is not actually practical to have a separate array for each frequency. This problem can be overcome by having a single array and using the received array data to form the array data for M (virtual) arrays by interpolation/extrapolation of the received array data. This is tantamount to constructing a continuous sensor using the received array data and resampling it. There are several methods reported in the literature. In [18] the field of view of the array is divided into several sectors, and a different interpolation matrix is calculated for each sector using a least squares fit. Krolik and Swingler [17] used digital interpolation methods to resample the array data. An alternative technique is explained below.

We will now show how to use the modal techniques to find a transformation matrix to calculate array data for M virtual arrays given the output of a single array. Sensor locations for the real array can be arbitrary on a line, i.e., there is no requirement for it to be a uniformly spaced array. From (6.40) the real array DOA matrix in the mth frequency bin is given by

$$\boldsymbol{A}(\Theta; k_m) = \boldsymbol{J}(k_m)\boldsymbol{P}(\Theta), \tag{6.45}$$

and the DOA matrix of the mth virtual array at frequency k_m would be

$$\boldsymbol{A}^{(m)}(\Theta; k_m) = \boldsymbol{J}^{(m)}(k_m)\boldsymbol{P}(\Theta), \tag{6.46}$$

where from (6.39) with $k_m z_q = q\pi$,

$$\begin{aligned}\boldsymbol{J}^{(m)}(k_m) &= \begin{bmatrix} i^0(2\cdot 0+1)\, j_0(-\pi Q) & \dots & i^N(2N+1)\, j_N(-\pi Q) \\ \vdots & & \vdots \\ i^0(2\cdot 0+1)\, j_0(\pi Q) & \dots & i^N(2N+1)\, j_N(\pi Q) \end{bmatrix} \\ &= \overline{\boldsymbol{J}}, \quad m = 1, \dots, M,\end{aligned} \tag{6.47}$$

and is seems to be a constant matrix, independent of m and k_m. Therefore we can write

$$\begin{aligned}\boldsymbol{A}^{(m)}(\Theta; k_m) &= \overline{\boldsymbol{J}}\boldsymbol{P}(\Theta), \\ &= \boldsymbol{A}(\Theta) \;\; m = 1, \dots, M,\end{aligned} \tag{6.48}$$

which is same for all frequency bins. By manipulating, (6.45) and (6.48), and using

the pseudo inverse of $\boldsymbol{J}(k_m)$ we obtain the least-square solution

$$\boldsymbol{A}^{(m)}(\Theta; k_m) = \boldsymbol{T}(k_m)\boldsymbol{A}(\Theta; k_m), \quad m = 1, \ldots, M, \tag{6.49}$$

where

$$\boldsymbol{T}(k_m) = \overline{\boldsymbol{J}}[\boldsymbol{J}^H(k_m)\boldsymbol{J}(k_m)]^{-1}\boldsymbol{J}^H(k_m), \quad m = 1, \ldots, M, \tag{6.50}$$

are the spatial resampling matrices. Now these spatial resampling matrices (they act as focusing matrices) can be used to align the array data in different frequency bins, so that narrowband DOA techniques can be applied. Similar to the focusing matrices (6.42), these spatial resampling matrices (6.50), do not require preliminary DOA estimation and depend only on the array geometry and the frequency. Also note that the proposed set of resampling matrices is same for the full field of view of the array, unlike in the case of [18].

Modal Space Processing

Observe that the proposed focusing matrices (6.42) and the spatial re-sampling matrices (6.50) have a common (generalized inverse) matrix factor

$$\boldsymbol{G}(k_m) \triangleq [\boldsymbol{J}^H(k_m)\boldsymbol{J}(k_m)]^{-1}\boldsymbol{J}^H(k_m), \quad m = 1, \ldots, M, \tag{6.51}$$

and only differ by the frequency independent factors $\boldsymbol{J}_0(k_0)$ and $\overline{\boldsymbol{J}}$. Also note that from (6.40),

$$\boldsymbol{G}(k_m)\boldsymbol{A}(\Theta; k) = \boldsymbol{P}(\Theta), \quad m = 1, \ldots, M, \tag{6.52}$$

i.e., $\boldsymbol{G}(k_m)$ transforms the array DOA matrix into a frequency invariant DOA matrix. Therefore we can use $\boldsymbol{G}(k_m)$ instead of $\boldsymbol{T}(k_m)$ to align the broadband array data to form a frequency averaged covariance matrix. Intuitively, one can say that the matrices $\boldsymbol{G}(k_m)$ transform the $2Q+1$ array data vector $\boldsymbol{z}(k_m)$ into a $N+1$ *modal data* vector. Now we can estimate the frequency averaged *modal covariance matrix* as

$$\hat{\boldsymbol{R}} = \sum_{m=1}^{M} \boldsymbol{G}(k_m)\, \boldsymbol{z}(k_m)\boldsymbol{z}^H(k_m)\, \boldsymbol{G}^H(k_m). \tag{6.53}$$

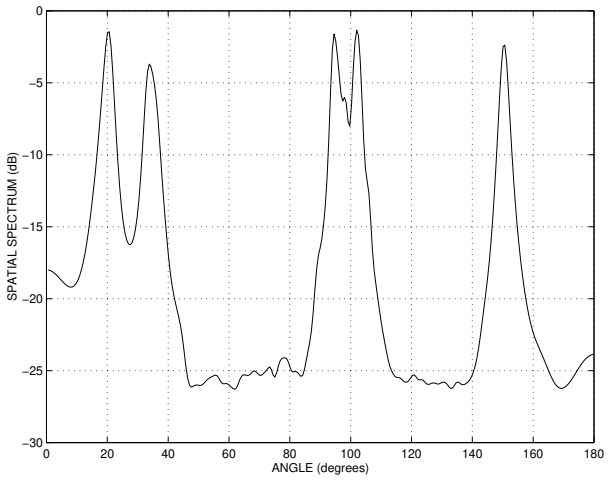

Figure 6.4: The estimated spatial spectrum of the sources in Section 6.3.4.

and the MV spectral estimate

$$\hat{Z}(\theta) = \frac{1}{\left[P_0(\cos\theta) \cdots P_N(\cos\theta)\right] \hat{\boldsymbol{R}}^{-1} \begin{bmatrix} P_0(\cos\theta) \\ \vdots \\ P_N(\cos\theta) \end{bmatrix}}. \tag{6.54}$$

Comments:

1. This method (one can refer it as the *modal space method*) involves less computation compared to the other two methods since the modal space has less dimensions $(N+1)$ than the signal subspace $(2Q+1)$.

2. As for the other two methods, the modal space method does not require preliminary DOA estimates.

3. One can consider the modal space method as a superset of focusing matrices and spatial resampling methods.

6.3.4 Example

In this section, we consider a simple example to show that the proposed modal space processing method can locate broadband coherent sources. Suppose the signal band is $300 - 3000$ Hz and $N = 15$ is sufficient to model the wavefield. We have placed 45 sensors according to Section 4.5, which provides guidelines to design a nonuniformly spaced sensor array for broadband applications.

The signal environment consists of 5 farfield sources at angles $\Theta = [20^\circ, 35^\circ, 95^\circ, 102^\circ, 150^\circ]$ with the sources at 95° and 102° being completely correlated. All sources have the same power of 0 dB SNR at the sensor origin and have flat spectra. The array noise was modeled as zero-mean Gaussian. The DFT of the received array data for 55 frequency bins was modeled assuming their theoretical values.

We calculated the modal covariance matrix (6.53) and then the MV spatial spectrum by (6.54). Figure 6.4 shows the resulting spatial spectrum. Observe that there is a peak corresponding to each of the sources, and it also resolved the two correlated sources which are apart by 7^0. Thus, we can state that the modal space processing can locate coherent broadband sources without preliminary DOA assumptions.

6.3.5 Summary

In this section, we have considered the application of modal analysis techniques to coherent broadband source localization problems. Specifically, we have shown how to formulate focusing and spatial resampling matrices to align received array data to a single frequency. One can use narrowband source localization techniques to estimate DOA once the received array data are aligned. Here, we have only considered a simple example but do not provide more detailed examples or case studies (the reader is referred to [19] for a detailed description of the source localization procedure). Our objective was to illustrate that modal analysis techniques can be used effectively to solve coherent source localization problems. This was achieved by proposing novel focusing matrices, spatial resampling matrices, and a modal space processing technique with clear advantages, over the existing methods.

6.4 Summary and Contributions

In this chapter, the application of modal analysis techniques to the problems of noise modeling and source localization were considered and a number of useful results was established.

We itemize some specific contribution made in this chapter:

i. We established an exact series expansion for the nearfield isotropic noise field which may be useful for array applications in the nearfield.

ii. We showed how to apply the novel representation of the noise field to an optimum linear array design.

iii. A closed-form expression for diffuse noise field was established.

iv. We obtained a novel set of focusing matrices based on modal techniques to align received array data to a single frequency. This result is useful in coherent broadband DOA estimation problems.

v. A set of spatial resampling matrices was established using modal analysis techniques, which is also useful in DOA estimation problems.

References

[1] D.H. Johnson and D.E. Dudgeon, *Array Signal Processing*, Prentice Hall, New Jersey, 1993.

[2] J.B. Allen and D.A. Berkley, "Image method for efficiently simulating small-room acoustics," *J. Acoust. Soc. Amer.*, vol. 65(4), pp. 943–950, Apr. 1979.

[3] J.G. Ryan and R.A. Goubran, "Nearfield beamforming for microphone arrays," *Proc. IEEE Int. Conf. Acoust., Speech Signal Processing*, pp. 363–366, May 1997.

[4] R.J. Mailloux, *Phased Array Antenna Handbook*, Artech House, Boston, 1994.

[5] D.K. Cheng and F.I. Tseng, "Gain optimization for arbitrary arrays," *IEEE Trans. Antennas Propagat.*, vol. AP-13, pp. 973–974, Nov. 1965.

[6] D. Colton and R. Kress, *Inverse Acoustic and Electromagnetic Scattering Theory*, Springer, New York, 1997.

[7] H.B. Dwight, *Tables of Integrals and other Mathematical Data*, Macmillan, New York, 1966.

[8] G.N. Watson, *A Treatise on the Theory of Bessel Functions*, Cambridge University Press, London, 1958.

[9] D.B. Ward and R.C. Williamson, "Beamforming for a source located in the interior of a sensor array," *Fifth International Symposium on Signal Processing and Applications, ISSPA99*, vol. 2, pp. 873–876, Aug. 1999.

[10] H. Wang and M. Kaveh, "Coherent signal-subspace processing for the detection and estimation of angles of arrival of multiple wide-band sources," *IEEE Trans. Acoust. Speech Sig. Proc.*, vol. ASSP-33, no. 4, pp. 823–831, Aug. 1985.

[11] R.O. Schmidt, "Multiple emitter location and signal parameter estimation," *IEEE Trans. Antennas Propagat.*, vol. AP-34, no. 3, pp. 276–280, Mar. 1986.

[12] N.L. Owsley, "Sonar array processing," in *Array Signal Processing*, S. Haykin, Ed., New Jersey, 1985, Prentice Hall.

[13] H. Hung and M. Kaveh, "Focussing matrices for coherent signal-subspace processing," *IEEE Trans. Acoust. Speech Sig. Proc.*, vol. 36, no. 8, pp. 1272–1281, Aug. 1988.

[14] S. Sivanand, J. Yang, and M. Kaveh, "Focussing filters for wideband direction finding," *IEEE Trans. Sig. Proc.*, vol. 39, pp. 437–445, Feb. 1991.

[15] M.A. Doron and A.J. Weiss, "On focusing matrices for wideband array processing," *IEEE Trans. Sig. Proc.*, vol. 40, pp. 1295–1302, June 1992.

[16] E. Skudrzyk, *The Foundations of Acoustics*, Springer-Verlag, New York, 1971.

[17] J. Krolik and D. Swingler, "Focused wide-band array processing by spatial resampling," *IEEE Trans. Acoust. Speech Sig. Proc.*, vol. 38, no. 2, pp. 356–360, Feb. 1990.

[18] B. Friedlander and A.J. Weiss, "Direction finding for wide-band signals using an interpolated array," *IEEE Trans. Sig. Proc.*, vol. 41, no. 4, pp. 1618–1634, Apr. 1993.

[19] S. Haykin, Ed., *Advances in Spectrum Analysis and Array Processing*, Prentice Hall, New Jersey, 1991.

Chapter 7

Conclusions and Future Research

In this chapter, we draw conclusions with respect to the questions[1] posed in this thesis and suggest possible future research directions.

7.1 Conclusions

i. The general broadband nearfield beamforming problem stated in Chapter 1 has been solved in Chapter 4. The proposed beamformer is capable of handling both nearfield and farfield broadband (over a few octaves) sources, and possesses an efficient parameterization with a single parameter to focus the beamformer to a desired operating radius and another set of parameters to control the actual broadband beampattern shape.

ii. A set of analysis tools, called modal analysis techniques has been developed in Chapter 2, which is capable of analyzing and synthesizing wavefields, beampattern specifications, and spatial response of beamformers irrespective whether the sources of interest are in the nearfield or farfield of the beamformer. The usefulness of these tools has been demonstrated by their applications in Chapters 3-6.

iii. The nearfield broadband adaptive beamforming problem has been answered in Chapter 5. The proposed beamformer has the capability to overcome desired signal cancellation and work well for broadband signal sources in the nearfield of the array.

iv. An alternative solution to the nearfield beamforming problem is to transform the desired nearfield beampattern specification to an equivalent farfield

[1] A list of questions is included in Section 1.3.

beampattern and use farfield design techniques. Three such transformation techniques have been developed in Chapter 3 based on modal analysis.

v. An exact series representation for nearfield isotropic noise field has been formulated in Chapter 6, which is useful in sensor array applications in the nearfield. We also have established a closed-form expression for a diffuse noise field.

vi. The broadband coherent source localization problem could be simplified by using modal analysis. A set of focusing matrices (which does not require preliminary location estimates and another single set of spatial re-sampling matrices to cover the entire field of view of the array) has been proposed to eliminate some of the shortcomings of existing coherent source localization methods.

vii. An investigation into the presence of spatial aliasing due to the operation of a linear array in the nearfield is presented in Appendix A. We have found that the received signal from a point source in the nearfield is not bandlimited in spatial frequency and hence the use of half-wavelength spaced arrays introduces undesirable aliasing effects to the array output.

All of the above specific conclusions illustrate the usefulness of modal analysis techniques in solving array signal processing problems. It also shows how a seemingly simple modal representation can have a significant effect on the problems considered in this thesis. *Therefore, we believe that modal analysis techniques will be an integral part of future investigations in many array signal processing problems, especially those requiring operation in the nearfield.*

7.2 Future Directions of Research

Based on the material in this thesis we propose three specific research directions out of many possibilities for future research projects, which could lead to a deeper understanding of broadband beamforming and other areas in array signal processing and provide solutions to related problems.

Modal Analysis: Remove Restrictions

The theory of modal analysis has been well established in this thesis as a useful tool to solve a wide variety of array signal processing problems. However, this theory is

only applicable when all sources are outside the smallest ball centered at the origin that contains the aperture. This somewhat restricts the generality of the modal analysis techniques. Thus, it is natural to extend these techniques to be valid for more general sensor-source geometries, where both sensors and sources are located within the same region.

Modal Analysis: Further Applications

In Chapter 6 we have shown that how one can use modal analysis techniques to model isotropic noise and derive alternative focusing matrices associated with source localization schemes. We believe that there is more to be done in both of these areas. Specifically, we suggest considering the problem of source localization (including nearfield sources) in an arbitrary distributed noise field and seek solutions using modal analysis techniques.

Experimental Tests:

We have not conducted any experimental tests to confirm that the theory developed in this thesis can be successfully implemented in practice. However, we have performed a number of computer simulations to confirm our results. Further, the general theory related to aperture is well corroborated in the literature. Thus, we have no reason to believe that our techniques are not readily applicable. Nevertheless, we suggest here to test our results using a real sensor array; for example a microphone array system can be used to experimentally validate the nearfield beamforming theory proposed in this thesis.

Appendix A

Spatial Aliasing for Nearfield Sensor Arrays

A.1 Introduction

This appendix considers the effect of spatially sampling a spherical wavefront received from a point source in the nearfield of a linear array, along the array axis. It shows that the standard half wavelength sensor spacings rule, which guarantees no aliasing in the operation of farfield arrays, is not sufficient to prevent aliasing in the nearfield. This claim is justified by theoretical considerations and corroborated by simulation results.

A.2 Spatial Aliasing

Consider a linear array aligned to the x axis and a point source at a distance r from the array origin and angle θ measured relative to endfire. Then the signal received at a point x on the array is given by

$$s_{r,\theta}(x) = \frac{e^{-ik\sqrt{r^2+x^2-2rx\cos\theta}}}{\sqrt{r^2+x^2-2rx\cos\theta}}, \tag{A.1}$$

where $k = 2\pi/\lambda$ is the wavenumber and λ is the wavelength of the received signal. If the source of interest is in the farfield of the array, the normalized signal received at a point x on the array is given by

$$s_{\infty,\theta}(x) = \lim_{r\to\infty} s_{r,\theta}(x)\, re^{ikr} = e^{ikx\cos\theta}. \tag{A.2}$$

By using an array, we effectively sample the signal $s_{r,\theta}(x)$ in the spatial domain. To determine the sampling distance, i.e., array spacings, we need to examine the spectral content of the signal $s_{r,\theta}(x)$ with respect to x. Let the Fourier transform of $s(x)$ be

$$S(\xi) = \int_{-\infty}^{\infty} s(x)\, e^{-i\xi x}\, dx \tag{A.3}$$

where ξ is the spatial frequency. Using (A.3), we can write the Fourier transform of (A.2) as

$$S_{\infty,\theta}(\xi) = 2\pi\delta(\xi + k\cos\theta)$$

where $\delta(\cdot)$ is the Dirac delta function. By the usual Nyquist criterion, we need to sample $s_{\infty,\theta}(x)$ with a sampling distance of $d \leq \pi/(k|\cos\theta|) = \lambda/(2|\cos\theta|)$ to avoid spatial aliasing. Since we assume the possible range of $\theta \in [0, \pi]$, it suffices to take $d_{\max} = \lambda/2$. This result, commonly known as the $\lambda/2$ rule, is standard in the array literature [1]. Until now, this rule has been used for designs in both farfield and nearfield (e.g., [2]). We show here that the $\lambda/2$ rule is generally not valid in the nearfield.

The Fourier Transform $S_{r,\theta}(\xi)$ of $s_{r,\theta}(x)$ can be obtained from the results in [3, p. 31]:

$$S_{r,\theta}(\xi) = \begin{cases} j\pi\, e^{ir\xi\cos\theta}\, H_0^{(1)}\big(r\sin\theta\sqrt{k^2-\xi^2}\big), & |\xi| < k \\ 2\, e^{ir\xi\cos\theta}\, K_0\big(r\sin\theta\sqrt{\xi^2-k^2}\big), & |\xi| > k \end{cases}$$

where $H_0^{(1)}(\cdot)$ is the Hankel function of the first kind of order zero and $K_0(\cdot)$ is the modified Bessel function of order zero. Note that there is a singularity at $|\xi| = k$.

A graph of $|S_{r,\theta}(\xi)|$ versus normalized spatial frequency ξ/k for three different sets of values (r, θ) is shown in Figure A.1. From this result, it is evident that the function $s_{r,\theta}(x)$ is not bandlimited if the source is in the nearfield of the array at a smaller angle measured relative to endfire, although it becomes more so as $r \to \infty$ or $\theta \to 90°$. Thus, the use of the $\lambda/2$ rule is not strictly sufficient to ensure no aliasing error, and indeed no sampling distance will entirely eliminate such error.

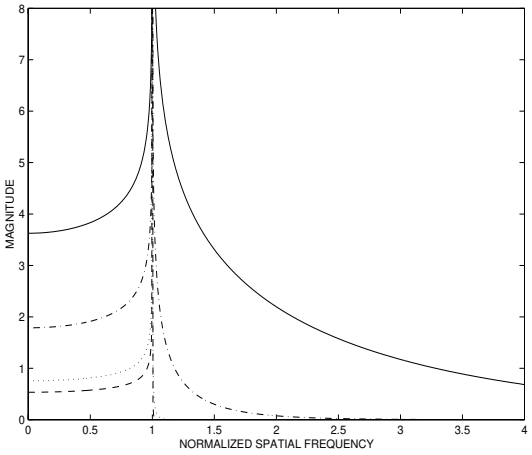

Figure A.1: Magnitude of the Fourier transform $S_{r,\theta}(\xi)$ of the signal $s_{r,\theta}(x)$ plotted against the normalized spatial frequency ξ/k for $r = 3.5\lambda$, $\theta = 1^\circ$ (solid line); $r = 3.5\lambda$, $\theta = 5^\circ$ (dashed dot line); $r = 3.5\lambda$, $\theta = 90^\circ$ (dashed line); and $r = 100\lambda$, $\theta = 1^\circ$ (dotted line).

A.3 Nearfield Rule of Thumb

To explain the above behaviour, we now examine $S_{r,\theta}(\xi)$ when $\xi > k$ for different values of r and θ. Since $K_0(z) \approx -\ln(z)$ for $z \to 0$ and $K_0(z) \approx \sqrt{\pi/(2z)}e^{-z}$ for large $z > 1$ [4, p. 203], $|S_{r,\theta}(\xi)|$ decays rapidly as the argument of $K_0(\cdot)$ (i.e., $r\sin\theta\sqrt{\xi^2 - k^2}$) increases. Suppose there exists positive numbers M and z_0 such that $|S_{r,\theta}(\xi)| < M$ for $r\sin\theta\sqrt{\xi^2 - k^2} > z_0$ for a given r and θ. Then for a suitably small M we can assert that $S_{r,\theta}(\xi)$ is approximately bandlimited by

$$\xi_0 = \sqrt{k^2 + \frac{z_0^2}{r^2\sin^2\theta}}, \tag{A.4}$$

and a sampling distance of π/ξ_0 or less reduces the aliasing to an acceptable level. It is difficult to find an analytic expression for z_0 in terms of M or quantify an acceptable level of aliasing. But a convenient rule of thumb is $z_0 \approx 1$.

Note that when $r \to \infty$, $\xi_0 \to k$; hence $S_{r,\theta}(\xi)$ is bandlimited by k for this case. For the case of $\theta = 90^\circ$, $\xi_0 = \sqrt{k^2 + 1/r^2} \approx k$ for all practical values of r in the nearfield. For example if $r = 3\lambda = 6\pi/k$ then $\xi_0 = k\sqrt{1 + 1/36\pi^2} \approx k$. Hence, for angles close to 90°, $S_{r,\theta}(\xi)$ is bandlimited by k even for nearfield signals. However, nearfield signals from small angles are not spatially bandlimited which can be gleaned from (A.4).

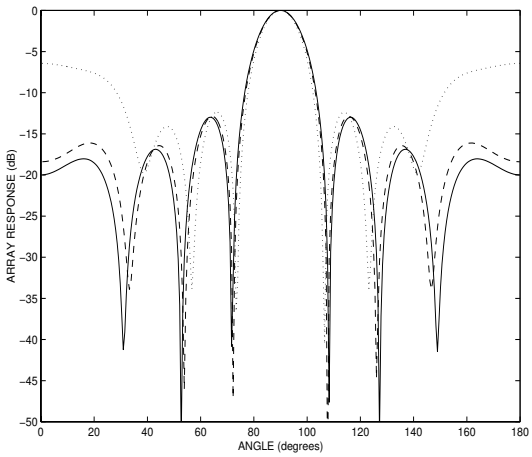

Figure A.2: Magnitude of the array response of a $\lambda/2$-spaced 7-sensor array (dotted line), $\lambda/4$ spaced 13 sensor array (dashed line); and $\lambda/6$-spaced 37-sensor array (solid line) to a nearfield source at 3.5λ from the array origin. The aperture length of each of three arrays is equal to 3λ.

A.4 Simulations and Conclusion

To conclude, we show the effect of spatial aliasing due to sampling a signal from a nearfield source at 3.5λ from an array origin, where λ is the wavelength of the signal. Figure A.2 shows the magnitude response of three arrays with different sensor spacings of $\lambda/2$, $\lambda/4$ and $\lambda/6$, to the above source as a function of θ. For comparison purposes, we make all three arrays to have equal aperture length, thus they have 7, 13 and 19 elements, respectively. The effect of aliasing is clearly evident from the response of the $\lambda/2$ spaced array, however there is little or no effect of aliasing present in the response of the $\lambda/6$-spaced array. This result is in agreement with (A.4) which gives sensor spacing of $\lambda/5.6$ to avoid aliasing for the case of $r = 3.5\lambda$ and $\theta = 1^\circ$ degrees.

Thus, we can conclude that the received signal from a point source in the nearfield is not bandlimited in spatial frequency and hence the use of standard half wavelengths spaced arrays introduces undesirable aliasing effects to the array output. The use of finer sensor spacings can overcome limitations imposed by aliasing.

References

[1] J.L. Flanagan, "Beamwidth and useable bandwidth of delay-steered microphone arrays," *AT&T Technical Journal*, vol. 64, pp. 983–995, Apr. 1985.

[2] Y. Grenier, "A microphone array for car environments," *Speech Communication*, vol. 12, pp. 25–39, Mar. 1993.

[3] A. Erdelyi, Ed., *Tables of Integral Transforms*, vol. II, McGraw-Hill, New York, 1954.

[4] N.W. McLachlan, *Bessel Functions for Engineers*, Oxford University Press, London, 1961.